Partitioning Water Vapor Fluxes by the Use of Their Water Stable Isotopologues: From the Lab to the Field

Maria Elisabeth Quade

Energie & Umwelt / Energy & Environment
Band / Volume 469
ISBN 978-3-95806-417-1

Mitglied der Helmholtz-Gemeinschaft

JÜLICH
Forschungszentrum

Schriften des Forschungszentrums Jülich
Reihe Energie & Umwelt / Energy & Environment Band / Volume 469

Forschungszentrum Jülich GmbH
Institut für Bio- und Geowissenschaften
Agrosphäre (IBG-3)

Partitioning Water Vapor Fluxes by the Use of Their Water Stable Isotopologues: From the Lab to the Field

Maria Elisabeth Quade

Schriften des Forschungszentrums Jülich
Reihe Energie & Umwelt / Energy & Environment Band / Volume 469

ISSN 1866-1793 ISBN 978-3-95806-417-1

Bibliografische Information der Deutschen Nationalbibliothek.
Die Deutsche Nationalbibliothek verzeichnet diese Publikation in der Deutschen Nationalbibliografie; detaillierte Bibliografische Daten sind im Internet über http://dnb.d-nb.de abrufbar.

Herausgeber und Vertrieb: Forschungszentrum Jülich GmbH
Zentralbibliothek, Verlag
52425 Jülich
Tel.: +49 2461 61-5368
Fax: +49 2461 61-6103
zb-publikation@fz-juelich.de
www.fz-juelich.de/zb

Umschlaggestaltung: Grafische Medien, Forschungszentrum Jülich GmbH

Druck: Grafische Medien, Forschungszentrum Jülich GmbH

Schriften des Forschungszentrums Jülich
Reihe Energie & Umwelt / Energy & Environment, Band / Volume 469

D 5 (Diss. Bonn, Univ., 2019)

ISSN 1866-1793
ISBN 978-3-95806-417-1

Vollständig frei verfügbar über das Publikationsportal des Forschungszentrums Jülich (JuSER) unter www.fz-juelich.de/zb/openaccess.

Abstract

Water stable isotopes are powerful tracers for partitioning of the terrestrial ecosystem water vapor fluxes into process-based components, i.e. evapotranspiration (*ET*) into soil evaporation (*E*) and plant transpiration (*T*). The isotopic methodology for *ET* partitioning is based on the fact that *E* and *T* have distinct water stable isotopic compositions, which in turn are due to each flux being differently affected by isotopic kinetic effects. To use stable isotopologues of water in *ET* partitioning studies, a good knowledge of the isotopic (equilibrium and kinetic) fractionation effects is crucial. While the temperature-dependent equilibrium fractionation factor is well characterized (Majoube 1971), the kinetic fractionation factor (α_K), relevant, e.g., during soil evaporation, needs further investigation.

In order to address this knowledge gap, we conducted a series of three different long-term bare soil evaporation experiments (differing in soil-water availability and aerodynamic conditions) to obtain α_K values from the collected isotopic data and the inversion of a well-known resistance-to-transfer model (i.e., the Craig and Gordon (1965) model). The isotopic composition of the soil water (δ_s) vapor was monitored non-destructively by using gas-permeable tubing (Rothfuss et al. 2013). The Craig and Gordon (1965) model was used in two different approaches. The first approach uses the Keeling (1958) plot to obtain values for the isotopic composition of the evaporation (δ_E). The second approach uses the slope of the linear regression between $\delta_s{}^2H$ and $\delta_s{}^{18}O$. Results showed that the largest source uncertainty in the computation of α_K stemmed from the uncertainty associated with the δ_E values modeled with the Keeling (1958) plot method. In the second approach α_K values were within the theoretical range proposed by Dongmann et al. (1974) and Mathieu and Bariac (1996), which pointed to the prevalence of the turbulent transport of water vapor under saturated and unsaturated soil conditions.

A variety of studies use different measurement techniques to estimate the isotopic composition of *ET* (δ_{ET}), *T* (δ_T) and δ_E for *ET* partitioning at the field scale. Here, especially the long-term monitoring of δ_E and δ_T is challenging. For this, non-destructive soil water stable isotopic monitoring using gas-permeable material is a promising tool. We tested the method of Rothfuss et al. (2013) to measure δ_s in an ET partitioning field campaign during one growing season of sugar beet (*Beta vulgaris*). To evaluate this method, the estimates of the transpiration fraction (*T/ET*) obtained from non-destructive soil profiles (P) were compared to the destructive soil sampling (S). In addition, the isotope-based approach was compared to *T/ET* estimates obtained from the combination of micro-lysimeter and eddy covariance (EC) measurements. Results showed discrepancies between the δ_E values obtained from S and P, which are in line with recent findings for different sampling methods (Orlowski et al. 2016a, Orlowski et al. 2018). However, the mean absolute deviations found between isotope-based and lysimeter-based *T/ET* estimates were more than three times higher than the differences between S and P. This underlines the great potential of gas-permeable tubing for long-term monitoring in the field and calls for further investigation of the isotopic offsets between direct measurement and extraction methods.

The long-term monitoring of δ_E by using gas-permeable material is only one challenge for *ET* partitioning studies. To provide sub daily estimates of *T/ET*, the long-term monitoring of δ_{ET} and δ_T should be improved. Therefore, a review of the current and past literature was written about the progress and challenges of isotope-based ET partitioning. In total, we reviewed 31 studies and analyzed which methods provide the most promising approach for the long-term monitoring of δ_{ET}, δ_T and δ_E. Next to gas-permeable material for the determination of δ_E, we encourage the development of experimental setups allowing for the determination of *ET* isotopic fluxes by combining EC measurements and high-frequency laser spectroscopy. The use of the gas-permeable material has also a great potential to measure δ_T. Albeit up to now only one study (Volkmann et al. 2016) showed that in-situ monitoring of δ_T in tree xylem is possible, this approach should be further developed for medium-sized plants (e.g. maize) and, in the longer term, thin-stem (cereal) plants.

Zusammenfassung

Stabile Wasserisotope sind leistungsstarke Tracer zur Partitionierung der terrestrischen Ökosystemflüsse in ihre Einzelkomponenten wie zum Beispiel Evapotranspiration (*ET*) in Bodenverdunstung (*E*) und Pflanzentranspiration (*T*). Diese Methode ist anwendbar aufgrund der Tatsache, dass der Wasserdampf aus *E* und *T* eine unterschiedliche Isotopenzusammensetzung hat. Die Unterschiede in der Isotopenzusammensetzung werden durch die sogenannte Isotopenfraktionierung verursacht. Um stabile Wasserisotope in *ET*-Partitionierungsstudien zu verwenden, ist ein gutes physikalisches Verständnis dieser Isotopenfraktionierung (Gleichgewichts- und kinetische Fraktionierung) notwendig. Während die temperaturabhängige Gleichgewichtsfraktionierung (α_{eq}) bereits gut charakterisiert ist (Majoube 1971), ist die genaue Berechnung der kinetischen Isotopenfraktionierung (α_K) immer noch eine große Herausforderung.

Zur Charakterisierung von α_K wurden drei unterschiedliche Langzeit-Bodensäulen-Experimente durchgeführt, die sich in der Wasserverfügbarkeit und in den aerodynamischen Bedingungen unterschieden. Dabei wurde die Isotopenzusammensetzung des Bodenwassers nicht-destruktiv durch die Verwendung von mikroporösen gaspermeablen Schläuchen gemessen (Rothfuss et al. 2013). Mit den Daten dieser drei Experimente wurde das Craig and Gordon (1965)-Modell mit zwei unterschiedlichen Ansätzen getestet. Der erste Ansatz bestimmte die Isotopen-zusammensetzung von *E* (δ_E) mittels des Keeling-Plots (Keeling (1958), um mit diesen Werten α_K zu berechnen. Im zweiten Ansatz wurde die Steigung der linearen Regressionslinie zwischen $\delta_s{}^2H$ und $\delta_s{}^{18}O$ verwendet, um α_K-Werte zu fitten. Die Ergebnisse zeigen, dass besonders der Keeling (1958)-Plot für die Berechnung von δ_E unter den gegebenen Laborbedingungen schwierig umzusetzen war. Mit dem zweiten Ansatz konnten α_K-Werte innerhalb des theoretischen Bereichs nach Dongmann et al. (1974) und Mathieu and Bariac (1996) berechnet werden, was auf eine Dominanz des turbulenten Wasserdampftransportes unter gesättigten und ungesättigten Bodenbedingungen hinweist.

Eine Vielzahl von *ET*-Partitionierungsstudien verwendet unterschiedliche Messmethoden zur Bestimmung der Isotopenzusammensetzung von *ET* (δ_{ET}), *T* (δ_T) und δ_E. Besonders die kontinuierliche Langzeit-Messung von δ_E und δ_T ist eine große Herausforderung. Die nicht-destruktive Messung mit Hilfe von gaspermeablem Material ist dabei der vielversprechendste Ansatz. Deshalb testeten wir die Methode von Rothfuss et al. (2013) zur Messung der Isotopenzusammensetzung des Bodenwassers in einer *ET*-Partitionierungsfeldkampagne auf einem Zuckerrübenfeld (*Beta vulgaris*). Um die Ergebnisse zu bewerten, wurde das Transpirationsverhältnis (*T/ET*) mit Hilfe nicht-destruktiver Bodenprofile (P) und mit destruktiver Probennahme (S) bestimmt. Zusätzlich wurde *T/ET* auch mit der Kombination von Eddy-Kovarianz (EC) mit Mikro-Lysimeter-Messungen bestimmt. Die Ergebnisse zeigen Unterschiede zwischen S und P, welche mit aktuellen Erkenntnissen über unterschiedliche Messmethoden (Orlowski et al. 2016a, Orlowski et al. 2018) übereinstimmen. Die gefundenen Unterschiede zwischen den Isotopen- und Lysimeter-basierten *T/ET* Schätzungen waren mehr als dreimal größer. Dies zeigt das große

Potenzial der gaspermeablen Schläuche für *ET*-Partitionierungsstudien im Feld. Dafür sollte die Methode allerdings noch weiterentwickelt werden und die Unterschiede zu den anderen Mess- und Extraktionsmethoden genauer quantifiziert werden.

Die Verwendung des gaspermeablen Materials für die Langzeit-Messung von δ_E ist lediglich eine Herausforderung innerhalb der *ET*-Partitionierungsstudien. Um eine tägliche oder stündliche Auflösung von *T/ET* Schätzungen zu ermöglichen, muss auch die Langzeit-Messung von δ_{ET} und δ_T verbessert werden. Dafür wurde ein Review über die aktuellen Fortschritte und Herausforderungen von Isotopen-basierten *ET*-Partitionierungsstudien verfasst. Insgesamt wurden 31 Studien analysiert, um herauszufinden, welches die vielversprechendste Methode für die Langzeit-Messung von δ_{ET}, δ_T und δ_E ist. Neben der bereits erwähnten nicht-destruktiven Methode, welche gaspermeables Material zur Bestimmung von δ_E verwendet, schlagen wir eine Kombination von EC und High-Flow-Laserspektroskopie als den vielversprechendsten Ansatz zur Bestimmung von δ_{ET} vor. Auch wenn die Messgeräte teuer sind und noch weiterentwickelt werden müssen, kann diese Investition einen großen Fortschritt in der Langzeit-Messung von δ_{ET} bedeuten. Die Verwendung des gaspermeablen Materials besitzt auch großes Potential für δ_T-Messungen. Bisher hat nur eine Studie (Volkmann et al. 2016) gezeigt, dass die In-situ-Messung von δ_T in Bäumen möglich ist. Dieser Ansatz sollte weiterentwickelt werden, damit dieser auch für Messungen von mittelgroßen Pflanzen wie zum Beispiel Mais und längerfristig für dünnstielige (Getreide-) Pflanzen verwendet werden kann.

List of publications included in this thesis

Quade, M. Brüggemann, N. Graf, A. Vanderborght, J. Vereecken, H. and Rothfuss, Y. 2018: Investigation of Kinetic Isotopic Fractionation of Water during Bare Soil Evaporation, Water Resources Research 54, 6909-6928, https://doi.org/10.1029/2018WR023159

Quade, M. Klosterhalfen, A. Graf, A. Brüggemann, N. Hermes, N. Vereecken, H. and Rothfuss, Y 2019: In-situ Monitoring of Soil Water Isotopic Composition for Partitioning of Evapotranspiration During One Growing Season of Sugar Beet (*Beta vulgaris*), Agricultural Forest Meteorology 266-267,53-64, https://doi.org/10.1016/j.agrformet.2018.12.002

Quade, M. Dubbert, M. Brüggemann, N. Graf, A. Vereecken, H. and Rothfuss, Y.: Progress and Challenges of Isotope Based Source Partitioning of Evapotranspiration (in preparation)

Table of Content

List of Abbreviations and Variables

C	mole fraction of water ($5.56 \cdot 10^4$ mol m^{-3})
C_a^v	atmospheric water vapor isotopic concentration [kg m^{-3}]
C_a	water vapor concentration of the laboratory background air [kg m^{-3}]
C_b	water vapor concentration of the background air [kg m^{-3}]
C_{col}	water vapor concentration inside the soil column [kg m^{-3}]
C_E	water vapor concentration of evaporation [kg m^{-3}]
C_{ET}	water vapor concentration of evapotranspiration [kg m^{-3}]
CH	canopy height [m]
C_s^v	surface water vapor isotopic concentration [kg m^{-3}]
$C_{\omega\chi_a}(f)df$	cospectral density of fluctuations in the vertical wind velocity and water vapor mixing ratios at the frequency f [Hz].
D_i	molecular diffusivities of either i = ^2H or ^{18}O
DoE	day of experiment
D_w	molecular diffusivities of either ^1H or ^{18}O
E	evaporation
EC	eddy covariance
EF	evaporation front
E_i	surface isotopic flux
ET	evapotranspiration
F_{ET}	water vapor flux [mmol m^{-2} s^{-1}]
g	leaf stomatal conductance [mol m^{-2} s^{-1}]
g_t	total stomatal conductance [mol m^{-2} s^{-1}]
h	relative humidity [expressed in %]
ISS	isotopic steady state
K	eddy diffusivity of water vapor [m^2 s^{-1}]
L	effective anatomical dimension [m]
LAI	leaf area index [m^2 m^{-2}]
L_E	latent heat flux of E [W m^2]
L_{ET}	latent heat flux of ET [W m^2]
LMWL	local meteoric water line
LRS	linear regression slope
M_a	molecular weight of dry air [kg mol^{-1}]
M_i	molar mass of the isotope [g mol^{-1}]
MR_a	water vapor mixing ratio of the laboratory background air [kg m^{-3}]
MR_{col}	water vapor mixing ratio inside the soil column [kg m^{-3}]
M_w	molar mass of water [g mol^{-1}]
m_w	molar weight of water ($1.8*10^{-2}$ kg)
n	exponent for the aerodynamic regime [-]
N_i	amount of either ^2H or ^{18}O
N_j	amount of either ^1H or ^{16}O
NSS	non-steady state
Pe	Péclet number
P	soil profiles
P_{sat}	saturated vapor pressure [Pa]
p_w	pressure of the liquid water phase [hPa]
R	universal gas constant (8.3144 J mol^{-1} K^{-1})
r_a	aerodynamic resistance [s m^{-1}]
r_b	boundary layer resistance [s m^{-1}]
r_i	resistance of the isotopic species [s m^{-1}]
RMSE	root mean square error
r_s	the leaf stomatal resistance [s m^{-1}]
R_{std}	atom ratio of the international standard [-]
R_x	atom ratio of Ni and Nj [-]
S	soil samples
S	storage term [Δ(mol(H_2O) mol(dry air)$^{-1}$)) Δ(m)$^{-1}$]
S_E	slope of the evaporation line
T	transpiration
T/ET	transpiration fraction [expressed in %]
T_a	atmospheric temperature [°C]
T_{EF}	soil temperature at the evaporation front [°C]
T_{rate}	transpiration rate [mmol m^{-2} s^{-1}]
T_s	soil surface temperature [K]
T_{soil}	soil temperature [°C]
V_m	mesophyll water volume [mol m^{-3}]
W	water concentration within the leaf [mol m^{-2} leaf]
w_i	humidity in the stomatal cavity [mol(H_2O) mol(air)$^{-1}$]
w_{in}	incoming mole fraction of water [mol(H_2O) mol(air)$^{-1}$]

w_{out}	outgoing mole fraction of water [mol(H_2O) mol(air)$^{-1}$]
α_K^i	isotopic kinetic fractionation factor [-]
α_{eq}	equilibrium fractionation factor
δ	isotopic composition [expressed in ‰]
δ_a	isotopic composition of the atmospheric water vapor [expressed in ‰]
δ_a^V	isotopic composition of the atmospheric water vapor [expressed in ‰]
δ_C	Craig and Gordon steady-state isotopic ratio at the evaporation site
δ_E	isotopic composition of the evaporated water vapor [expressed in ‰]
δ_{EF}^V	isotopic composition of the soil water at the evaporation front in the vapor phase [expressed in ‰]
δ_{ET}	isotopic composition of water vapor from evapotranspiration [expressed in ‰]
δ_{in}	isotopic composition of the incoming water vapor [expressed in ‰]
δ_l	isotopic composition of the liquid evaporating water body [expressed in ‰]
δ_L	isotopic composition of the leaf water [expressed in ‰]
δ_s^l	isotopic composition of the liquid soil water [expressed in ‰]
$\delta_{s_{init}}^l$	initial soil liquid water isotopic concentration [expressed in ‰]
δ_s^v	isotopic composition of the soil water vapor [expressed in ‰]
δ_{source}	isotopic concentration of the root zone source water [expressed in ‰]
δ_{st1}^l	isotopic concentration of the liquid water in standard 1 [expressed in ‰]
δ_{st2}^l	isotopic concentration of the liquid water in standard 2 [expressed in ‰]
δ_{out}	isotopic composition of the outgoing water vapor [expressed in ‰]
δ_T	isotopic composition of the transpired water vapor [expressed in ‰]
δ_x	isotopic concentration of the xylem water [expressed in ‰]
$\Delta_{L,b}$	isotopic enrichment of the bulk leaf water
$\Delta_{L,e}$	evaporative isotopic enrichment in leaves
$\Delta_{L,s}$	isotopic fractionation enrichment that occurs within the leaf
Δ_v	isotopic enrichment of the atmospheric water vapor
Δ_z	height difference [m]
Δ_ε	kinetic isotopic effect [-]
$\Delta_{\chi a}$	changes in the mixing ratio of the water vapor [mol(H_2O) mol(dry air)$^{-1}$]
ε_{eq}	equilibrium enrichment [-]
θ_{res}	residual soil water content [m^3 m^{-3}]
θ_s	soil volumetric water content [m^3 m^{-3}]
θ_{sat}	saturated soil water content [m^3 m^{-3}]
ρ	volumetric mass of water [g cm^{-3}]
ρ_a	density of dry air [kg m^{-3}]
ρ_w	density of water (1000 kg m^{-3})
$\sigma^2_{T/ET}$	standard error of *T/ET*
$\sigma^2_{\delta_E}$	standard error of δ_E
$\sigma^2_{\delta_{ET}}$	standard error of δ_{ET}
$\sigma^2_{\delta_T}$	standard error of δ_T
ω	vertical wind speed [m s^{-1}]

List of Figures

Figure 3.4
(a) Oxygen isotopic composition of the evapotranspiration flux ($\delta_{ET}{}^{18}O$ in ‰), determined with the Keeling plot approach (results with $R^2 > 0.6$ are shown); (b) oxygen isotopic composition of the transpiration flux ($\delta_T{}^{18}O$ in ‰) inferred from that of the water extracted from the plant xylem sap ($\delta_x{}^{18}O$ in ‰) and assuming isotopic steady-state conditions ($\delta_T{}^{18}O = \delta_x{}^{18}O$); (c) oxygen isotopic composition of the evaporation flux ($\delta_E{}^{18}O$ in ‰) calculated with Equation (3.3) on the basis of either destructive (sampling of soil down to 5 cm depth, red symbols) or non-destructive (monitoring system with the tubing profiles, blue symbols) determination of δ_s^1; (d) transpiration fraction (*T/ET*) calculated with Equation (3.1) on the basis of destructive (red) and non-destructive determination of δ_s^1 (blue). Grey shaded areas indicate values outside the theoretical range, and blue shaded areas represent nighttime periods.

Figure 3.5
Latent heat flux (W m^{-2}) of evapotranspiration measured by the eddy covariance station (L_{ET}(EC), black line) and partitioning results for the latent heat flux of evaporation obtained from single measurements with micro-lysimeters (L_E(lysimeter), black squares), from the soil samples (L_E(S), red dots) and soil profiles (L_E(P), blue triangles) for (a) δ^2H and (b) $\delta^{18}O$**.** Blue shaded areas represent the nighttime period. L_E(S) and L_E(P) were calculated on basis of isotope-derived *T*/*ET* ratios and L_{ET}(EC) using the following relationship: $L_E = 1 - T/ET * L_{ET}$.

Figure 3.6
Relative differences in transpiration fraction (*T/ET*) derived from (a) soil samples (S) (δ^2H-estimates – $\delta^{18}O$-estimates), (b) soil profiles (P) (δ^2H-estimates – $\delta^{18}O$-estimates), (c) δ^2H-estimates (S – P), and (d) $\delta^{18}O$-estimates (S – P). Blue shaded areas represent nighttime periods.

Figure 4.1
Results of the literature review (a): Evolution of the number of citations per year (blue bars) and cumulative number of publications (1990-2018, black line); (b): percentage of methods for determination of δ_E (c): percentage of methods which were used to determine δ_T; (d): percentage of methods which were used to determine δ_{ET}.

Figure 4.2
Exemplary Keeling (1958) plot.

Figure A1
Water vapor mixing ratio (in ppmV) and isotopic composition (δ^2H and $\delta^{18}O$ in ‰) of the water vapor sampled on Day of Experiment 14 from the ambient air “atm”, both standards (“STD1” and “STD2”) and soil depths (“soil”), the numbers representing the depth/high regarded to the soil surface

Figure B1
Linear regression line (Keeling plot) of δ^2H (left) and $\delta^{18}O$ (right) against the inverse MR on Day of Experiment 73, values for the y-Intercept (I), the coefficient of determination (R^2) and the p-value are reported.

Figure D1
Observed (blue points) and fitted (black lines) relationships between the hydrogen (panels a-b) and oxygen (panels c-d) isotopic compositions of the water vapor sampled from the soil standards 1 (panels a-c) and 2 (panels b-d) (δ^v_{st1} and δ^v_{st2}) with water vapor mixing ratio (MR).

List of Tables

Chapter 1

1.1 Introduction

The continental water reservoirs at and near the earth surface are constantly in motion. Water vapor which evaporates from the soil and is transpired by plants forms clouds in the atmosphere. The clouds release the water vapor in form of precipitation back to the surface. Here the water evaporates again, or is extracted and transpired by plants, or else moves through the soil to replenish groundwater. Atmospheric water vapor is also a key contributor to the greenhouse effect which makes quantitative measurements of the single sources and sinks important for improving meteorological and hydrological forecasting models. But measurements of the raw contributions of the two major sources, namely soil evaporation (E) and plant transpiration (T) are still a major challenge within eco-hydrological studies. Often the net flux, namely evapotranspiration (ET), is measured via eddy covariance (EC) stations. Disentangling the ET flux into E and T can be done by source partitioning methods. These methods are divided into correlation-based modelling approaches using existing EC measurements (Scanlon and Kustas 2010) and a variety of instrumental approaches (Kool et al. 2014). The latter are limited to a smaller field scale and range from soil-flux chamber measurements (Raz-Yaseef et al. 2010, Yaseef et al. 2010) over micro-lysimeter measurements (Kelliher et al. 1992) to atmospheric profile measurements (Ney and Graf 2018).

Another method for the source partitioning of ET is based on the analysis of the flux composition (δ) in the heavier water stable isotopologues $^{1}H^{2}H^{16}O$ and $^{1}H_{2}{}^{18}O$ defined as (Coplen 2011):

$$\delta_{\mathrm{x}}\,[‰] = \left(\frac{R_{\mathrm{x}}}{R_{\mathrm{std}}} - 1\right) \tag{1.1}$$

with $R_{\mathrm{x}} = N_{\mathrm{i}}/N_{\mathrm{j}}$ the atom ratio of either $N_{\mathrm{i}} = {}^{2}H$ (rare) and $N_{\mathrm{j}} = {}^{1}H$ (abundant) or $N_{\mathrm{i}} = {}^{18}O$ and $N_{\mathrm{j}} = {}^{16}O$. R_{std} is the atom ratio of the international standard (Standard Mean Ocean Water, SMOW) provided by the International Atomic Energy Agency. The heavier isotopes have different physical properties during phase change which leads to differences in their δ-value within the compartments of the ecosystem. These effects are summarized under the term isotopic fractionation processes.

The isotopic composition of the evaporated water vapor (δ_{E}) is always affected by these fractionation effects, resulting in a lower δ_{E} value compared to the measured isotopic composition of the total water vapor from evapotranspiration (δ_{ET}). Plants transpire often at isotopic steady state, which is associated which no fractionation effects and therefore a higher value of the isotopic composition of the transpired water vapor (δ_{T}). In the atmosphere above the soil-plant continuum the measured δ-value represents a mixture of both sources. Single measurements of δ_{E}, δ_{T} and δ_{ET} allow for a relative quantification of the so-called transpiration fraction (T/ET) via a simple linear mixing model:

$$\delta_{ET} = (1 - x)\delta_E + x\delta_T \quad (1.2)$$

where x is defined as T/ET.

To measure or estimate δ_E, δ_T and δ_{ET} a variety of different methods exists. For the estimation of δ_{ET} the Keeling (1958) plot approach is the most common method. This approach was first developed to estimate the contribution of CO_2 sources (Keeling 1958, Keeling 1961). Later this approach was used for the estimation of δ_{ET} of ecosystems (Brunel et al. 1992, Yakir and Wang 1996). The basic assumptions behind this method are (i) the measured atmospheric water vapor and isotopic composition reflects the mixture of the atmospheric background water vapor and the emitted sources E and T; (ii) mixing is fully turbulent and no loss of water vapor occurs by e.g. condensation; (iii) there are no more than two sources contributing to ET, which must have distinct isotopic composition values (Yakir and Sternberg 2000). Therefore, measurements of the atmospheric water vapor concentration as well as its isotopic compositions within and above the ecosystem are necessary. During the first studies (e.g. Wang and Yakir 2000, Yepez et al. 2003) atmospheric water vapor was sampled via a cryogenic trapping system and finally analyzed in the laboratory with an isotope ratio mass spectrometer. Later, the development of field-deployable tunable diode laser spectrometers made in-situ monitoring of the atmospheric water vapor possible, and rapidly increased the number of isotope-based ET partitioning studies (Lee et al. 2007, Xu et al. 2008, Rothfuss et al. 2010, Wang et al. 2010, Wenninger et al. 2010).

The in-situ determination of δ_E is currently under development. During the first studies (e.g. Walker and Brunel 1990, Wang and Yakir 2000, Ferretti et al. 2003) traditional destructive soil sampling was conducted to obtain measurements of the soil water. The soil water was extracted in the laboratory and finally δ_E was calculated by the use of the Craig and Gordon (1965) model. For a correct estimation of δ_E, the isotopic composition of the liquid soil water from the evaporation front (EF) is needed; but determining the exact location of the EF is difficult even by sampling soil profiles with an auger. Additionally, this method has disadvantages, e.g. disturbance of the ecosystem or limitations of the water extraction method (Orlowski et al. 2016a, Orlowski et al. 2016b). Recently developed methods like soil water probes (Volkmann and Weiler 2014, Gaj et al. 2016) or gas-permeable tubing (Rothfuss et al. 2013) enabled non-destructive in-situ monitoring of soil water vapor. These methods have great potential for the long-term monitoring at many meteorological measurement sites, but a detailed evaluation is still required.

In-situ measurements of δ_T are the most challenging task for further studies. To simplify this task, a number of studies (e.g. Brunel et al. 1992, Zhang et al. 2011, Aouade et al. 2016) used the steady-state assumption, excluding isotopic fractionation during the transpiration process. Under these conditions δ_T

is equal to the source water used by the plant which can be obtained by destructive sampling of xylem or stem tissue and subsequent water extraction.

As previously mentioned, water extraction methods may alter isotopic results. Alternative such as custom made chambers (e.g. Wang et al. 2013, Good et al. 2014, Lu et al. 2017) allow the on-line assessment of δ_T via a mass-balance approach. However, chambers have their own drawbacks, e.g. increased temperature and relative humidity compared to the outside temperature. Volkmann et al. (2016) recently developed an in-situ method for the monitoring of δ_T of tree xylem by the use of a "xylem water isotope probe" with a gas-permeable head. This method was able to obtain direct, continuous and high-resolution measurements of the tree xylem. Further development and application to smaller plants, e.g. maize and, on longer term, thin-stem (cereals) plants, should be the focus of future studies.

1.1 The Craig and Gordon (1965) model

The Craig and Gordon (1965) model describes the enrichment process of an evaporating water body (Figure 1). It assumes that the surface isotopic flux E_i is proportional to the difference of isotopic concentration between the atmosphere C_a^V and the soil surface C_s^V, and inversely proportional to the isotopic resistance r_i to vapor flow (Braud et al. 2005a):

$$E_i = \frac{C_s^V - C_a^V}{r_i} \quad (1.3)$$

where V refers to the water vapor phase. Barnes and Allison (1983) proposed an equation for the isotopic resistance:

$$r_i = r_a \alpha_K^i \quad (1.4)$$

where r_a is the aerodynamic resistance to vapor transfer, and α_K^i the isotopic kinetic fractionation factor.

The isotopic concentration can be approximated by (Braud et al. 2005a):

$$C_i = \frac{M_i}{M_w} R_i \rho \quad (1.5)$$

with M_i, M_w the molar mass of isotopes and water, R_i the isotopic ratio and ρ the volumetric mass of water. Combining Equation 1.5 and 1.3 leads to:

$$E_i = \rho_{sat} \frac{M_i}{M_w} \frac{h_s R_s^V - h_a R_a^V}{r_a \alpha_K^i} \quad (1.6)$$

with $h = \rho/\rho_{sat}$ the relative humidity.

Similarly, the evaporation flux E can be expressed as:

$$E = \frac{\rho_s - \rho_a}{r_a} = \rho_{sat}\frac{h_s - h_a}{r} \quad (1.7)$$

By (i) dividing left and right hand-terms of Equations 1.6 and 1.7 together, (ii) defining the isotopic ratio of the evaporation as $R_E = E_i/E$ (R_E), (iii) converting isotopic ratios into isotopic compositions (δ, Equation 1.1), and (iv) by considering $h_s \approx 1$, the equation for the isotopic composition of the evaporated water vapor is obtained:

$$\delta_E = \frac{1}{\alpha_K^1(1-h_a)}\left(\delta_{EF}^V + 1 - \left(\delta_a^V + 1\right)h_a\right) - 1 \quad (1.8)$$

where δ_E, δ_{EF}^V and δ_a^V are the isotopic composition values of the evaporation (E), soil water at the evaporation front (EF) and atmosphere (a). δ_{EF}^V is obtained from δ_{EF}^L, the isotopic composition of the soil liquid water and the vapor-liquid thermodynamic equilibrium fractionation factor α_{eq}:

$$\alpha_{eq} = \frac{R_{EF}^L}{R_{EF}^V} = \frac{\delta_{EF}^L + 1}{\delta_{EF}^V + 1} \quad (1.9)$$

Combining Equation 1.8 and 1.9 leads to:

$$\delta_E = \frac{1}{\alpha_K^i(1-h_a)}\left(\frac{\delta_{EF}^L + 1}{\alpha_{eq}} - (\delta_a + 1)h_a\right) - 1. \quad (1.10)$$

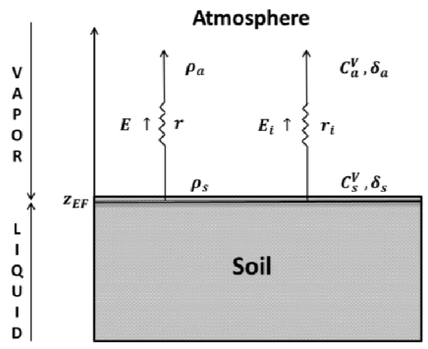

Figure 1.1
Scheme of the evaporation process from liquid soil water to water vapor at the evaporation front z_{EF}.

This equation is commonly used to determine the isotopic composition of the evaporated water vapor in the specific context of *ET* partitioning.

The equilibrium fractionation effect is well characterized by Majoube (1971) and describes the change in the isotopic composition depending on the surface temperature (T_s):

$$\alpha_{eq}(T_S) = exp\left(-\left(\frac{A}{T_s^2} + \frac{B}{T_s^2} + C\right)\right) \quad (1.11)$$

with the empirical constants A = 1137, B= –0.4156 and C = –0.0020667 for ^{18}O and A = 24844, B = –76.25 and C = 0.05261 for ^{2}H.

The kinetic fractionation factor is defined as the ratio of the transport resistances from the evaporating water surface to the ambient air. The lighter isotopes need less energy for the phase transition. In case of a fully saturated water vapor layer (i.e. relative humidity = 100%) above the water surface, the liquid and vapor phases are at isotopic thermodynamic equilibrium (i.e. absence of kinetic fractionation). This situation usually occurs during precipitation formation in clouds. In most cases the air layer is non-saturated (i.e. relative humidity < 100%) and the kinetic fractionation process will lead to an isotopic enrichment of the evaporating water surface. Craig and Gordon (1965) experimentally determined α_K^i as inversely proportional to the ratio of the molecular diffusivities (D) of the most abundant (w) to the rare (i) isotopes. Later Dongmann et al. (1974) proposed the following expression:

$$\alpha_K^i = \left(\frac{D_w}{D_i}\right)^n \quad (1.12)$$

The exponent n is dimensionless and accounts for the aerodynamic regime above the liquid-vapor interface. Dongmann et al. (1974) proposed that n = 0.5 under fully turbulent conditions and n = 1 under fully diffusive conditions (n = 2/3 under laminar flow conditions). Other authors (e.g. Barnes and Allison 1983, Mathieu and Bariac 1996) give other definitions of n (e.g. constant or soil water content depending). The right choice of the exponent n is still under debate and will be discussed in detail in Chapter 2.

The schematic manner of the evaporation process can be described in a dual isotopic coordinate system (Figure 1.2). The linear regression of δ^2H vs. $\delta^{18}O$ from global precipitation water describes the equilibrium fractionation process. This line is defined as the global meteoric water line (GMWL, Craig 1961) by the following equation (Rozanski et al. 1993):

$$\delta^2H = 8.2\ \delta^{18}O + 11.3 \quad (1.13)$$

This equation describes a global relationship. A similar equation can be obtained from the linear regression of δ^2H and δ^{18}O from precipitation water at one site over a longer period (>3 years). This line is defined as the local meteoric water line (LMWL). An example for the LMWL at the research center Jülich is shown in Figure 1.2. This line describes the spatiotemporal variation of the isotopic composition of precipitation, which is related to several processes, e.g. latitude effects, altitude effects and continental effects (Sprenger et al. 2016).

The linear regression of δ^2H and δ^{18}O from liquid soil water defines a line, the so called "evaporation line" with the slope S_E (Gat 1971):

$$S_E = \frac{[h(\delta_a - \delta_l) + \varepsilon_{eq} + \Delta\varepsilon]_{2_H}}{[h(\delta_a - \delta_l) + \varepsilon_{eq} + \Delta\varepsilon]_{18_O}} \quad (1.14)$$

were δ_l is the liquid isotopic composition of the evaporating water body (e.g. soil or rain water), ε_{eq} is the equilibrium enrichment ($\varepsilon_{eq} = 1 - \alpha_{eq}$) and $\Delta\varepsilon$ is the kinetic isotopic effect (Gat 1996):

$$\Delta\varepsilon = (1 - h)\left(\frac{D_w}{D_i} - 1\right)n \quad (1.15)$$

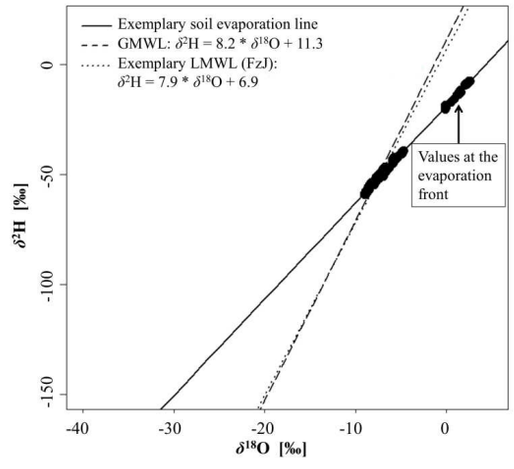

Figure 1.2
Exemplary evaporation line (black solid line) from the isotopic composition of the liquid soil water (black dots), the global meteoric water line (GMWL, Craig 1961, Rozanski et al. 1993) and an exemplary local meteoric water line (LMWL, Andreas Lücke, personal communication, 2018) from the Research Center Jülich (Forschungszentrum Jülich).

S_E usually has a value between 2 and 6.5 (Sprenger et al. 2016). This is caused by the fact, that during the evaporation process the remaining water becomes stronger enriched in the oxygen isotopes compared to the hydrogen isotopes due to the kinetic fractionation effect. An exemplary soil evaporation line is shown in Figure 1.2. The values at the evaporation front are usually more enriched compared to the deeper soil layers and form a separate cluster.

1.2 Objectives and outline of the thesis

The aim of this thesis is to improve the understanding of water vapor ecosystem fluxes by the use of stable isotopologues and to evaluate current measurement techniques. The main focus was on the use of gas-permeable tubing for non-destructive long-term monitoring of the isotopic composition of soil water vapor. This thesis was divided into three work packages resulting in three publications. Two publications are published in scientific journals and one is prepared for submission (see section: List of publications included in this thesis).

The first publication addresses the problem of the poorly characterized kinetic fractionation effect and is presented in Chapter 2. Here we present the results of three soil column laboratory experiments, where different soil-water availability and aerodynamic conditions could be simulated, to quantify α_K during the bare soil evaporation process. For this, the Craig and Gordon (1965) model was tested using two different approaches. First, the Keeling (1958) plot method was used to obtain values for δ_E and α_K could be determined via Equation 1.10. In a second approach, α_K was obtained from the slope of the evaporation line in a dual isotopic coordinate system by combining Equation 1.14 and 1.15. For both methods δ_s^l was monitored non-destructively by sampling the soil water vapor with microporous gas-permeable tubing and online analysis with a laser spectrometer (Rothfuss et al. 2013).

The second publication is presented in Chapter 3 and presents the application of the method of Rothfuss et al. (2013) in the field for the first time. This method allowed for the non-destructive monitoring of δ^2H and $\delta^{18}O$ of soil water during a field *ET* partitioning campaign in sugar beet. To evaluate the method, *T/ET* estimates obtained from the non-destructive method were compared to the commonly used destructive sampling and subsequent cryogenic vacuum extraction of soil water. Finally, isotope-based *T/ET* estimates were compared to those obtained from a combination of micro-lysimeter and EC measurements to prove their reliability.

The last publication is presented in Chapter 4 and provides a review on the progress and challenges of isotope-based measurement techniques used in *ET* partitioning studies. In total, 31 studies were analyzed (found, and further progress monitored, by entering search term ((“evapotranspiration” or

"transpiration" or "evaporation") and partition* and isotop*) into the ISI Web of Science search engine www.webofknowledge.com) to assess which method provides the most promising approach for the long-term monitoring of δ_{ET}, δ_T and δ_E in the field. The measurement technique and theory for δ_{ET}, δ_T and δ_E are described in subchapters before the actual progress and challenges is discussed. Additionally, a detailed tabular overview of the 31 studies is provided.

Chapter 2

Investigation of Kinetic Isotopic Fractionation of Water during Bare Soil Evaporation

Based on the journal article:

Quade, M. Brüggemann, N. Graf, A. Vanderborght, J. Vereecken, H. and Rothfuss, Y. 2018: Investigation of Kinetic Isotopic Fractionation of Water during Bare Soil Evaporation, Water Resources Research 54, 6909-6928, https://doi.org/10.1029/2018WR023159

2.1 Introduction

Kinetic isotopic effects during evaporation (E) greatly impact the stable isotopic composition (δ) of environmental water pools (e.g., soil, plant, surface waters, groundwater, and atmospheric water vapor) and fluxes (e.g., evaporation and plant transpiration) (Horita et al. 2008, Sprenger et al. 2016, Xiao et al. 2017). A better understanding of the implications of these effects, in addition to the well characterized equilibrium effects (Majoube 1971, Lin and Horita 2016), is required for using the isotopologues $^{1}H^{2}H^{16}O$ and $^{1}H_{2}{}^{18}O$ as tracers of processes in the water cycle.

The kinetic fractionation factor (α_K) introduced in the Craig and Gordon (1965) model is theoretically defined as the ratio of the transport resistances from the evaporating water surface to the ambient air of $^{1}H^{2}H^{16}O$ or $^{1}H_{2}{}^{18}O$ to that of the most abundant isotopologue $^{1}H_{2}{}^{16}O$. The same authors first experimentally determined α_K to be inversely proportional to the ratio of the molecular diffusivities of $^{1}H_{2}{}^{16}O$ and of either $^{1}H^{2}H^{16}O$ or $^{1}H_{2}{}^{18}O$. Dongmann et al. (1974) proposed the following expression, assuming that (i) turbulent transport was a non-fractionating process and (ii) molecular diffusion resistances were inversely proportional to the *nth* power of the corresponding diffusivities (D):

$$\alpha_K = \left(\frac{D_w}{D_i}\right)^n \tag{2.1}$$

where w stands for $^{1}H_{2}{}^{16}O$ and i for either $^{1}H^{2}H^{16}O$ or $^{1}H_{2}{}^{18}O$. The dimensionless exponent n accounts for the aerodynamic regime above the liquid–vapor interface (i.e., where the relative humidity is 100%). While the diffusivity ratio is considered constant in Eq. (2.1), n ranges from 0.5 (fully turbulent) to 1 (fully diffusive), with a value of 2/3 corresponding to laminar flow conditions (Dongmann et al. 1974). From two independent methods (i.e., evaporation of water under laminar flow conditions and water vapor transport through a diffusion tube), Merlivat (1978) determined the ratio of diffusivities D_w/D_i to be equal to 1.0251 and 1.0285 for $^{1}H^{2}H^{16}O$ and $^{1}H_{2}{}^{18}O$. These results disagree with those obtained from the kinetic theory of gases (i.e., 1.0168 and 1.0323) and were then explained to be due to different collision diameters of $^{1}H_{2}{}^{16}O$, $^{1}H^{2}H^{16}O$, and $^{1}H_{2}{}^{18}O$. It was only much later that Cappa et al. (2003) reconciled these observed differences with the kinetic theory by invoking water surface cooling during evaporation, as measured by Fang and Ward (1999), that plays a crucial role in fractionation of evaporating water. More recently, Luz et al. (2009) conducted evaporation experiments in air, argon, and helium, over 10 to 70 degrees temperature range, and found results similar to those of Merlivat (1978). Their experiments confirmed that these discrepancies could not be due to different collision diameters of the three isotopologues.

Even though the values to be used for D_w/D_i seem to have reached a certain consensus in the isotopic community (currently, the most widely used are those of Merlivat (1978), see review of Horita et al. (2008)), the value for n can only be either an educated guess by the user (depending on the aerodynamic

conditions prevailing between the evaporation front and the free atmosphere) or deduced quantitatively from atmospheric measurements (e.g., wind velocity) and the application of an evaporation model (e.g., Merlivat and Jouzel 1979).

Rothfuss et al. (2012) suggested that n should vary in time for an evaporating soil even if atmospheric conditions remained the same: the non-saturated air layer developing at the soil surface enhances purely diffusive transport of water vapor and its isotopologues towards the free atmosphere, leading to a progressive increase of n.

Unfortunately, direct laboratory or in situ measurements of kinetic fractionation factors during soil evaporation by applying the Craig and Gordon (1965) model (Braud et al. 2009a, Braud et al. 2009b, Rothfuss et al. 2012, Dubbert et al. 2013), suffer from the following two issues:

(i) The isotopic composition of the net evaporation flux (δ_E, expressed in ‰ on the VSMOW scale, Gonfiantini (1978) has to be disentangled from the isotopic composition of the background atmosphere (δ_a). This is now facilitated by the emergence of laser absorption spectrometry applied to chamber measurements (Dubbert et al. 2013, Dubbert et al. 2014, Dubbert et al. 2017) or the 'Keeling plot' approach (Keeling 1958, Iannone et al. 2010, Good et al. 2014). Under controlled conditions in the laboratory (Braud et al. 2009b, Rothfuss et al. 2010, Rothfuss et al. 2012), δ_E can then directly be measured, while environmental conditions simulated in such climatic chambers may not be encountered in nature;

(ii) The time-consuming and labor-intensive methods frequently used for the determination of soil liquid water isotopic composition $\left(\delta_s^l\right)$, i.e., destructive sampling and vacuum distillation or direct equilibration methods (Araguás-Araguás et al. 1995, Garvelmann et al. 2012, Orlowski et al. 2013) do not allow frequent measurements of soil water isotopic composition. However, Rothfuss et al. (2013), Volkmann and Weiler (2014) and Gaj et al. (2016) recently developed non-destructive methods for monitoring δ_s^l online with high precision and accuracy via measurements of the soil water vapor isotopic composition $\left(\delta_s^v\right)$ considering thermodynamic equilibrium at the sampling depth. The method of Rothfuss et al. (2013) was further applied in the laboratory (Gangi et al. 2015, Rothfuss et al. 2015).

Rothfuss et al. (2015) also showed that α_K could be determined using a simplified formula for the slope of the "evaporation line" (i.e., the linear regression of $\delta^{18}O$ versus δ^2H of the soil liquid water in a dual isotope space) derived from the Craig and Gordon (1965) model and first proposed by Gat (1971). This method (referred to as "G71") has the advantage over the Craig and Gordon (1965) model (referred to as "CG65") that it only relies on measurements of δ_a, δ_s^l and not on measurements of δ_E.

In this study, we determined α_K by applying both CG65 and G71 formulas in an inverse mode during a soil evaporation experiment conducted in the laboratory. The abovementioned limitations of the isotopic methodology were overcome with (i) a Keeling plot technique for the determination of δ_E and (ii) by using the method of Rothfuss et al. (2013) for the non-destructive determination of δ_s^v.

2.2 Material and methods

2.2.1 Soil measurements

The evaporation experiment was carried out using the setup of Gangi et al. (2015) which consists of a 0.127 m^3 PVC tube (0.48 m in diameter, 0.70 m height) sealed at the bottom (Figure 2.1a) and coated with insulating sheets (Armaflex™, 0.05 m wall thickness, Armacell International S.A., Luxembourg). Three connecting ports were available at six different depths (i.e., –0.01, –0.03, –0.07, –0.15, –0.30, and –0.57 m): one inlet for the carrier gas, i.e., synthetic dry air (20.5 % O_2 in N_2 with approx. 20–30 ppmv water vapor, Air Liquide, Germany), one sample air outlet, and one duct for a combined soil volumetric water content (θ_s) and temperature (T_s) probe (SMT-100, truebner GmbH, Neustadt, Germany; precision for soil water content and temperature was 3% and 0.2°C, respectively). Each gas inlet and outlet were connected to a 0.3 m long piece of microporous polypropylene tubing (Accurel® PP V8/2HF, Membrana GmbH, Germany). The tubing is water-tight, yet gas-permeable (pore size of 0.2 µm) and allows the sampling of soil water vapor and the measurement of δ_s^l in a non-destructive manner with high precision and accuracy as detailed in Rothfuss et al. (2013).

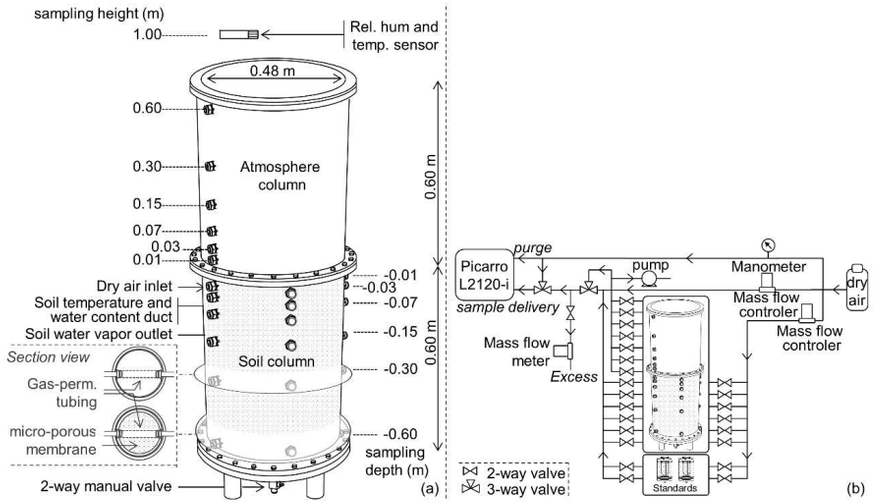

Figure 2.1
Experimental setup: (a) PVC soil monolith with system for applying water suction at the bottom, atmosphere column, and available measurements; (b) experimental setup for sampling water vapor at the different soil depths, from the two soil water standards, and from the atmosphere.

The soil column was filled with a silt loam soil (20.1 % sand, 65 % silt, 14.9 % clay) sieved to 2 mm grain size and dried at 110°C for 24 hours. The soil column was saturated with water of known isotopic composition from the bottom through a perforated acrylic glass plate covered with a water-permeable nylon membrane (ecoTech Umwelt-Messsysteme GmbH, Bonn, Germany) by applying slight overpressure from an external tank.

Two soil water isotopic standards were prepared using the same setup as Rothfuss et al. (2013), consisting of a 2.57 l volume airtight acrylic glass cylinder. These two vessels were filled and packed with the same silt loam soil and saturated with one of the two standard waters of isotopic composition δ^{l}_{st1} (δ^2H = –1.5 ‰, δ^{18}O = 7.2 ‰) and δ^{l}_{st2} (δ^2H = –103.2 ‰, δ^{18}O = –21.3 ‰), respectively. The saturated soil water volumetric content (θ_{sat}) value was determined from the ratio of the volume of water needed for saturation and the volume of the soil water isotopic standards and was equal to 0.45 $m^3\ m^{-3}$. The residual water content value was θ_{res} = 0.00 $m^3\ m^{-3}$ (Lutz Weihermüller, personal communication)

2.2.2 Atmospheric measurements

A second PVC tube of the same dimensions and open at both ends was installed gastight on top of the tube with the soil monolith. Atmospheric water vapor could be sampled at six different heights above the soil surface (0.01, 0.03, 0.07, 0.15, 0.30, and 0.57 m) inside the air column. In addition, the surrounding atmospheric water vapor was sampled at 1.00 m above the soil surface, i.e., outside of the column's volume. Air relative humidity (h, %) and temperature (T_a, °C) were monitored at the same height with a RFT-2 sensor (Meter Group, Munich, Germany; precision of relative humidity and temperature measurements was 2 % and 0.1°C, respectively).

2.2.3 Sampling protocol

δ_s^l was determined from δ_s^v measurements three times a day at each depth of the soil column according to the method developed and described by Rothfuss et al. (2013). 85 ml min^{-1} of dry synthetic air was directed through the permeable tubing for 30 min. The sampled soil water vapor was diluted with dry synthetic air (Figure 2.1b) in order to (i) reach a water vapor mixing ratio ranging between 10,000 and 15,000 ppmv and (ii) to generate an excess flow upstream of the cavity ring-down laser spectrometer (L2120-*i*, Picarro, Inc., Santa Clara, CA, USA) to avoid any contamination of sample air with ambient air. A 30 min sampling duration was required to reach steady state values for both $\delta^2H_S^v$ and $\delta^{18}O_S^v$ for a period of at least 10 min. These last 10 min (corresponding to approx. 385 observations) were used to compute the δ_s^v mean value. Computed mean values with standard deviations >2 ‰ and >0.5 ‰ for $\delta^2H_S^v$ and $\delta^{18}O_S^v$, respectively, were not taken into account in the analysis as they pointed to, e.g., condensation in the tubing system. Water vapor mixing ratio dependencies of the laser spectrometer isotopic composition readings (Schmidt et al., 2010) were accounted for by computing the theoretical δ_s^v values at 10,000 ppmv. Finally, the corresponding δ_s^l values were calculated at the measured soil temperature (Rothfuss et al. 2013):

$^1H^2H^{16}O$: $$\delta_s^l = 104.96 - 1.0342 \cdot T_s + 1.0724 \cdot \delta_s^v \quad (2.2a)$$

$^1H^1H^{18}O$: $$\delta_s^l = 11.45 - 0.0795 \cdot T_s + 1.0012 \cdot \delta_s^v \quad (2.2b)$$

where T_S is the soil temperature in °C.

δ_a was measured three times a day at each available height above the soil surface. Air was sampled at a rate of 200 ml min^{-1} for 15 min. This flow rate was chosen to minimize (i) memory effects due to the volume of the tubing system between air intake and the laser spectrometer and (ii) disturbance inside the air column. The threshold flow rate value below which sampling from one of the three lowest

atmospheric layers (i.e., centered at 0.01, 0.03, and 0.07 m above the soil surface) did not impact the other (or the other two) was estimated at 241 ml min^{-1}. This threshold value corresponded to the volume of a cylindrical air layer with 0.02 m height (3619 ml) divided by the sampling duration (15 min). The last three minutes (corresponding to approx. 115 observations) were used to compute the mean value of the isotopic composition of atmospheric water vapor (δ_a) which was, as for δ_s^v, corrected for water vapor mixing ratio dependency. δ_a and δ_s^l values were finally corrected for a potential laser analyzer drift using the isotopic compositions δ_{st1}^l and δ_{st2}^l of the two water standards as anchor points.

Water vapor of the atmosphere column, of both soil standards, and from the different tubing sections in the soil column were sampled sequentially in the following order: standard1 – standard2 – soil (–0.60 m) – atmosphere (0.01 m) – soil (–0.03 m) – atmosphere (0.30 m) – soil (–0.15 m) – atmosphere (0.60 m) – soil (–0.30 m) – atmosphere (0.03 m) – soil (–0.07 m) – atmosphere (0.15 m) – soil (–0.01 m) – atmosphere (0.07 m) – atmosphere (1.00 m) – standard1 – standard2. This order was chosen to avoid consecutive sampling of neighbor atmospheric heights and soil depths. The 5.75 hour-long sampling sequence was completed by 2.25 hours of sampling the atmosphere at 1.00 m and the whole was repeated three times per day (i.e., to add up to a 24 hour-long daily sampling period).

2.2.4 Determination of δ_E and δ_{EF} for the computation of α_K from the Craig and Gordon model

Using the classical approach of Rideal-Langmuir (Sverdrup 1952), Craig and Gordon (1965) modeled the evaporation of $^1H^2H^{16}O$ and $^1H_2{}^{18}O$ from a free surface water body through a series of consecutive layers as the ratio of isotopic composition differences and transport resistances. When we apply this model to soil pore water we derive the following expression for the isotopic kinetic fractionation factor α_K:

$$\alpha_K = \frac{\frac{(\delta_{EF}+1)}{\alpha_{eq}} - h\prime(\delta_a+1)}{(1-h\prime)(\delta_E+1)} \quad (2.3)$$

where δ_{EF} is the isotopic composition of the soil liquid water at the evaporation front (e.g., the surface under fully saturated conditions) and δ_a is the vapor isotopic composition of the laboratory air measured at 1 m height above the soil column. α_{eq} is the isotopic equilibrium fractionation factor between soil liquid and vapor at the soil temperature T_S (Majoube 1971) and h' is the relative humidity of the air normalized to the saturated vapor pressure (P_{sat} [Pa]) (Soderberg et al. 2012) at the temperature of the evaporation front T_{EF}:

$$h' = h\frac{P_{sat}(T_a)}{P_{sat}(T_{EF})} \quad (2.4)$$

where h [%] is the relative humidity in the laboratory.

δ_E was determined with a Keeling plot approach (Keeling 1958) considering the moisture inside the air column (of volumetric concentration C_{col} [kg m^{-3}] and isotopic composition δ_{col}) as a mixture of evaporated soil moisture (of concentration C_E [kg m^{-3}] and isotopic composition δ_{E}) and laboratory air moisture (of concentration C_{a} [kg m^{-3}] and isotopic composition δ_{a}, measured at 1 m height above the soil surface):

$$\delta_{\mathrm{col}} = \frac{1}{C_{\mathrm{col}}}[C_{\mathrm{a}}(\delta_{\mathrm{a}} - \delta_E)] + \delta_E \qquad (2.5a)$$

The laser spectrometer measures water vapor mixing ratios (MR, -, usually expressed in ppmv) rather than concentrations. Assuming that $C_{\mathrm{a}}/C_{\mathrm{col}} \cong MR_{\mathrm{a}}/MR_{\mathrm{col}}$, where MR_{a} and MR_{col} are the water vapor mixing ratios measured in the ambient laboratory air (a) and in the atmospheric column (col), Eq. (5a) becomes:

$$\delta_{\mathrm{col}} \cong \frac{1}{MR_{\mathrm{col}}}[MR_{\mathrm{a}}(\delta_{\mathrm{a}} - \delta_E)] + \delta_E \qquad (2.5b)$$

δ_E was determined from the y-intercept of the linear regression between δ_{col} and $1/MR_{\mathrm{col}}$. Only significant linear relationships with a p-value lower than 0.05 were used (an exemplary Keeling plot is shown in Fig. B1 of Appendix B).

Another approach to calculate α_{K} used the slope of the so-called "evaporation line" (S_E) proposed by Gat (1971):

$$S_E = \frac{\left[h\left(\delta_a - \delta^l_{s_{init}}\right) + \varepsilon_{eq} + \Delta\varepsilon\right]_{2_H}}{\left[h\left(\delta_a - \delta^l_{s_{init}}\right) + \varepsilon_{eq} + \Delta\varepsilon\right]_{18_O}} \qquad (2.6)$$

where $\delta^{\mathrm{l}}_{\mathrm{s_{init}}}$ is the initial soil liquid water isotopic composition (e.g., before water vapor is removed from the soil via evaporation). $\varepsilon_{\mathrm{eq}}$ is the equilibrium enrichment, i.e., the deviation of α_{eq} from unity. $\Delta\varepsilon$ is the kinetic isotopic effect which is associated with the $^{1}H^{2}H^{16}O$ and $^{1}H_{2}{}^{18}O$ vapor transport. Under the assumptions that (i) the turbulent transport is a non-fractionating process and that (ii) the ratio of the molecular resistance to the total resistance equals one, $\Delta\varepsilon$ is defined as (Gat 1996):

$$\Delta\varepsilon = (1 - h)\left(\frac{D_w}{D_i} - 1\right)n \qquad (2.7)$$

Rearranging Equations (2.6) and (2.7) gives the following expression for n:

$$n = \frac{\left[h\left(\delta_a - \delta^l_{s_{init}}\right) + \varepsilon_{eq}\right]_{2_H} - S_E\left[h\left(\delta_a - \delta^l_{s_{init}}\right) + \varepsilon_{eq}\right]_{18_O}}{(1-h)\left(S_E\left(\frac{D_w}{D_{18_O}} - 1\right) - \left(\frac{D_w}{D_{2_H}} - 1\right)\right)} \quad (2.8)$$

Mathieu and Bariac (1996) proposed a formulation incorporating the soil surface water content (θ_{EF}, in $m^3\ m^{-3}$) to simulate the evolution of n. The latter is modeled to range from $n_a = 0.5$, i.e., soil is saturated at the evaporation front and evaporation is atmosphere controlled ($\theta_{EF} = \theta_{sat} = 0.45\ m^3\ m^{-3}$), to $n_S = 1$, i.e., soil water content at the evaporation front reaches the residual value and evaporation is soil-controlled ($\theta_{EF} = \theta_{res} = 0.00\ m^3\ m^{-3}$):

$$n = \frac{(\theta_{EF} - \theta_{res})n_a + (\theta_{sat} - \theta_{EF})n_s}{\theta_{sat} - \theta_{res}} \quad (2.9)$$

Due to the fact that the computation of α_K with the different methods relies on simultaneous measurements of δ_{EF}, δ_a, and δ_E, synchronous values for all three variables were determined from the measured values by linear interpolation for time points 04:00, 12:00, and 20:00 hours each day and used for the calculation of α_K. The time gap between the actual measurements and interpolated data ranged between 0.25 and 4 hrs.

In this study, α_K was (i) calculated with the Craig and Gordon (1965) model (Equation (2.3), method "CG65") and (ii) determined from S_E values measured at a daily temporal step (Equations (2.1) and (2.8), method "G71"). For the latter method values of diffusivity ratios D_w/D_i were taken from Merlivat (1978). The α_K estimates derived from CG65 and G71 were compared to those of Mathieu and Bariac (1996) (Eq. 9) by calculating the model-to-data fit (root mean square error – RMSE). The proportion of α_K estimates falling into the theoretical range (corresponding to $0.5<n<1$) of Dongmann et al. (1974) was determined by calculating the hit rate (Doswell et al. 1990). Note that α_K values outside the theoretical range but for which either α_K +1standard error or α_k –1 standard error fell into the theoretical range was counted as a hit. The error associated with the calculation of α_K was determined by taking into account the effect of all variable and parameter uncertainties, i.e., by propagation of errors, and is detailed in Appendix C.

Table 2.1
Overview on equations used in this study to calculate the kinetic fractionation factor with their corresponding references.

Reference	α_K	n
Dongmann et al. (1974)	$\alpha_K = \left(\frac{D_w}{D_i}\right)^n$	n = 0.5 (fully turbulent) n = 2/3 (laminar) n = 1 (fully diffusive)
Mathieu and Bariac (1996)	$\alpha_K = \left(\frac{D_w}{D_i}\right)^n$	$n = \frac{(\theta_{EF} - \theta_{res})n_a + (\theta_{sat} - \theta_{EF})n_s}{\theta_{sat} - \theta_{res}}$
Gat (1971) (G71)	$\alpha_K = \left(\frac{D_w}{D_i}\right)^n$	$n = \frac{\left[h(\delta_a - \delta^l_{s_{init}}) + \varepsilon_{eq}\right]_{2_H} - S_E\left[h(\delta_a - \delta^l_{s_{init}}) + \varepsilon_{eq}\right]_{18_O}}{(1-h)\left(S_E\left(\frac{D_w}{D_{18_O}} - 1\right) - \left(\frac{D_w}{D_{2_H}} - 1\right)\right)}$
Craig and Gordon (1965) (CG65)	$\alpha_K = \frac{\frac{(\delta_{EF}+1)}{\alpha_{eq}} - h'(\delta_a + 1)}{(1-h')(\delta_E + 1)}$	-

2.2.5 Sensitivity of α_K to aerodynamic conditions

The sensitivity of α_K to (i) the aerodynamic conditions prevailing in the laboratory and to (ii) the development of a dry soil surface layer was investigated during three successive experiments, lasting 40 days each. In a first experiment (E1), the soil column was initially saturated with water (θ = 0.45 m^3 m^{-3} across all depths). In a second experiment (E2), water was withdrawn from the bottom after re-saturation of the soil column until water content reached 0.25 m^3 m^{-3} at the soil surface. Subsequently, in a third experiment (E3) water was withdrawn from the bottom after re-saturation until θ = 0.34 m^3 m^{-3} was reached at the soil surface. Additionally, the relative humidity and isotopic composition of the laboratory air were artificially increased by evaporating 1 L of ^{2}H-enriched water over three days. The isotopic composition of the ^{2}H-enriched water solution was linearly extrapolated at δ^2H = 4469370.0 ±611811.0 ‰ and δ^{18}O = 2507.9 ±327.0 ‰ from a series of dilution experiments with the standard 1 liquid water (i.e., of isotopic composition δ^l_{st1}).

2.3 Results

2.3.1 Atmosphere column

Figure 2.2a shows the evolution of the laboratory air temperature and relative humidity during all three experiments. Figure 2.2a underlines the semi-controlled conditions prevailing during the experiments, i.e., both T_a and h fluctuated on a daily basis in response to outside weather conditions. The mean T_a (resp. h) value during E1, E2, and E3 was 19.6 ±0.9°C (37.9 ±5.3%), 21.8 ±1.3°C (45.4 ±4.6%), and 20.2 ±0.9°C (52.1 ±3.25%), respectively. E1 was started on 22 February 2017 (Day of Experiment, DoE 1) and ran until 2 April 2017 (DoE 40). Here we observed the lowest mean T_a and h values compared to E2 and E3. E2 was conducted in the late spring/early summer (from 3 May 2017 to 11 June 2017) which was characterized by rapidly changing weather conditions (until DoE 92) and by dry and hot conditions (from DoE 92 to 110). Highest values for h were observed during E3, which was carried out from 30 August 2017 to 8 October 2017.

The isotopic composition of the atmospheric water vapor (δ^2H_a and $\delta^{18}O_a$) inside the atmosphere column and at 1 m above the soil surface almost exclusively varied during E1 and E2 due to changing weather conditions outside the laboratory (Fig. 2.2b and c). In E2 from DoE 86 to DoE 87, strong fluctuations of δ^2H_a and $\delta^{18}O_a$ occurred due to a late spring storm. Following the labeling pulse, δ^2H_a ($\delta^{18}O_a$) increased from –130.0 ±1.3 ‰ (–17.4 ±0.2 ‰) on DoE 211 to –7.2 ±1.4 ‰ on DoE 213 (–16.1 ±0.3 ‰ on DoE 215) at height 0.01 m (E3). Note that water vapor mixing ratio and isotopic compositions data at height 0.01 m in the atmospheric column was not available during E1 due to technical problems.

2.3.2 $\delta^{18}O$-δ^2H relationship for laboratory air water vapor and soil liquid water

Figure 2.3 displays the isotopic composition results for laboratory air water vapor (blue symbols) and soil liquid water (red symbols) in dual isotopic ($\delta^{18}O$, δ^2H) plots. The slope values of the linear regression (LRS) fitted to the atmospheric data were 6.1, 7.0, and 6.2 for E1, E2, and E3 (excluding the data during the ^2H labeling period; black dots), respectively, which was significantly lower than the slope of the local meteoric water line (black dashed line; Andreas Lücke, personal communication). This was certainly due to the fact that a significant portion of the laboratory air humidity was provided by the evaporation of soil water (characterized by lower LRS slopes due to kinetic effects). Similar results were observed by Rothfuss et al. (2015).

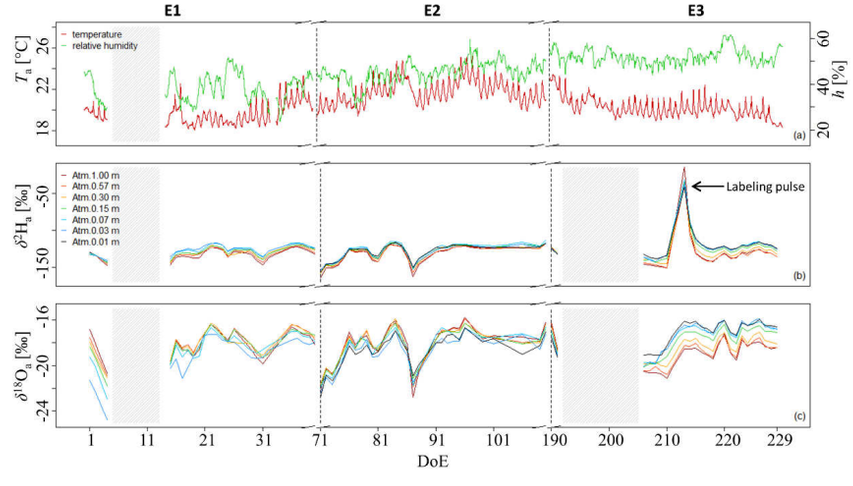

Figure 2.2
(a): Time series of temperature (T_a, °C) and relative humidity (h, %) of the ambient air in the laboratory (sampled one meter above the soil surface, i.e., outside the atmosphere column); (b): time series of the hydrogen (δ^2H_a, ‰) and (c) oxygen ($\delta^{18}O_a$, ‰) stable isotopic compositions of the water vapor across heights within the atmosphere column for experiments E1 to E3. Grey shaded stripes indicate missing data due to encountered technical problems.

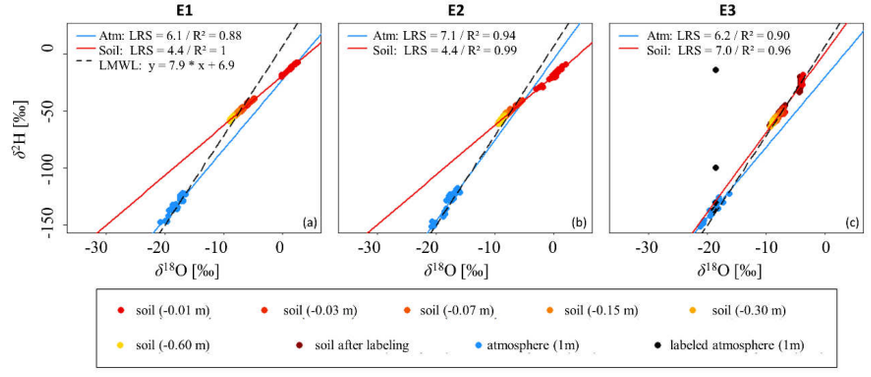

Figure 2.3
Measurements of the laboratory air water vapor isotopic composition (blue symbols) 1 m above the soil surface and soil liquid water isotopic composition (red: –0.01 m; dark orange: –0.03 m; orange: –0.07 m; light orange: –0.15 m; dark yellow: –0.30 m; yellow: –0.60 m) from all depths along with their respective linear regression lines (atmosphere: blue solid line; soil: red solid line) in dual isotopic plots for experiment (a) E1, (b) E2, and (c) E3. Data collected in the period following the ^2H labeling pulse (black symbols) were excluded from the regression for E3 (c). Linear regression slopes (LRS) and coefficients of determination (R^2) as well as the equation for the local meteoric water line (LMWL) are reported (black dotted line).

The slope of the $\delta^{18}O$-$\delta^{2}H$ relationship for soil liquid water remained unchanged during E1 and E2 (LRS ≈ 4.4, with R^2≈1, p-value = 0.00) and within the expected theoretical range (Sprenger et al. 2016). The labeling of the laboratory air moisture in E3 had a remarkable influence on the water isotopic composition of the upmost soil layer. As a consequence, the LRS slope was significantly higher (7.0, R^2 = 0.96, p-value=0.00), which highlighted the influence of the laboratory air water vapor on the isotopic composition of the soil water within the column.

2.3.3 Soil and atmospheric profiles

Figure 2.4 shows the vertical profiles of laboratory air mixing ratio (*MR*) (Fig. 2.4a), soil water content (Fig. 2.4d) and isotopic compositions (Fig. 2.4b-c,e-f) measured during E1. Water vapor *MR* was nearly constant across sampling heights above 0.03 m. Water vapor *MR* and isotopic composition profiles shifted during the course of the experiment towards higher values. The hydrogen (oxygen) isotopic composition of the water vapor in the atmosphere column $\delta^{2}H_{col}$ ($\delta^{18}O_{col}$) below 0.03 m was higher (lower) than that of the laboratory air. The direct influence of fractionating evaporation on the water vapor isotopic compositions could be measured near the soil surface only (i.e., at 0.01, 0.03 and 0.07 m heights). The differences between δ_{col} heights at 1 m and 0.01 m were greater at the beginning of the experiment when there was a water film on the soil surface which was evaporating freely.

Figure 2.4d-f illustrates the soil water content (θ) profiles and the corresponding soil liquid water $\delta^{2}H$ and $\delta^{18}O$ during E1. The soil surface water content (i.e., measured at –0.1 m, θ_{surf}) was stable throughout E1 and decreased slightly from 0.45 $m^3\ m^{-3}$ (saturated initial conditions) to 0.42 $m^3\ m^{-3}$ (DoE 40). During the first 30 days, only the first 0.05 m of soil was impacted by evaporation, i.e., soil water content value decreased from 0.45 (DoE 1) to 0.42 $m^3\ m^{-3}$ (DoE 30), while θ remained nearly constant in soil layers below 0.30 m. During the last 10 days of E1, the soil dried faster at 0.30 m depth compared to the other soil layers. The mean evaporation rate computed by mass balance from the temporal changes of the θ profiles over the 40 days of experiment was 0.41 mm d^{-1}. Soil liquid water (Fig. 2.4e and 2.4f) became isotopically enriched at the surface relative to the deeper layers, with $\delta^{2}H_s^l$ ($\delta^{18}O_s^l$) increasing from –47.0 ±1.6 ‰ (–6.2 ±0.2 ‰) to –8.9 ±1.5 ‰ (2.2 ±0.2 ‰) at –0.01 m.

During E2 the water vapor *MR* and isotopic composition (Fig. 2.5a-c) profiles behaved similarly as during E1. Due to the drier soil (compared to E1) the observed gradient in *MR* between the column atmosphere at 0.01 m and the ambient laboratory air at 1.00 m was significantly smaller. The soil dried almost uniformly (Fig. 2.5d) across the profile from 0.25 to 0.22 $m^3\ m^{-3}$. The calculated mean evaporation rate (0.59 mm d^{-1}) was significantly higher than during E1 although the soil was much drier (Fig. 2.2). This can be explained by a greater vapor pressure deficit (due to higher temperature and comparable relative humidity) of the laboratory air and by the existence of capillary rise. Maximum

depth gradients of soil liquid water isotopic composition ($\Delta(\delta^2H_s^l)/\Delta z$, where z stands for soil depth) were observed in the upmost soil layer (0.01 m), indicating that the evaporation front was located at the soil surface (Rothfuss et al., 2015). At depth 0.01 m, $\delta^2H_s^l$ ($\delta^{18}O_s^l$) ranged between –30.9 ±1.5 ‰ (–2.9 ±0.2 ‰) and –9.6 ±1.6 ‰ (1.4 ±0.2 ‰).

During E3, water vapor *MR* in the laboratory was slightly higher compared to during E1 and E2 (Fig. 2.6a). The ^2H labeling pulse led to an enrichment of the atmosphere column water vapor of –12.9 ‰ (at height 1 m) on DoE 213. Afterwards, the δ^2H_a profiles returned to their normal range (–149.7 ‰ < δ^2H_a < –122.3 ‰ at 1 m height) before labeling. In E3, the soil dried almost uniformly across depths from 0.38 to 0.32 $m^3\ m^{-3}$ (Fig. 2.6d) with a mean evaporation rate of 1.14 mm d^{-1}. $\delta^2H_s^l$(–0.01 m) varied from –53.4 ±1.5 ‰ (DoE 190) to –18.7 ±1.6 ‰ (DoE 206) (maximum value observed after the ^2H labeling pulse) and decreased to –33.1 ±1.7 ‰ (DoE 229). $\delta^{18}O_s^l$ increased from –7.4 ±0.2 ‰ at the beginning of the experiment to –4.1 ±0.2 ‰ at DoE 229.

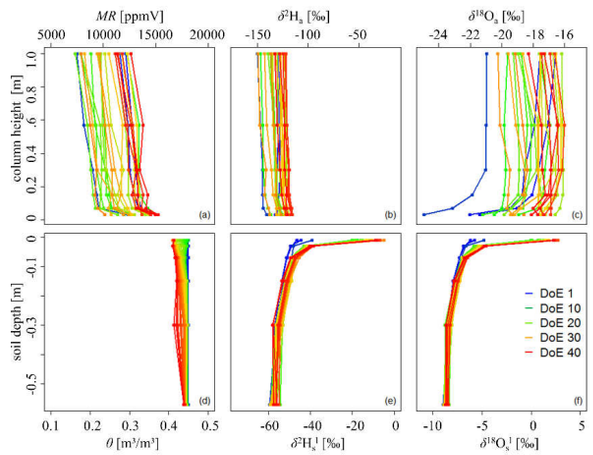

Figure 2.4

Experiment 1 (day of experiment – DoE 1 to 40): profiles of (a) water vapor mixing ratio (*MR*) and (b) hydrogen and (c) oxygen isotopic compositions (δ^2H_a and $\delta^{18}O_a$) in the atmosphere column across heights. Profiles of (d) soil water volumetric content (θ, $m^3\ m^{-3}$) and (e) hydrogen and (f) oxygen isotopic compositions (δ^2H_s and $\delta^{18}O_s$) across depths.

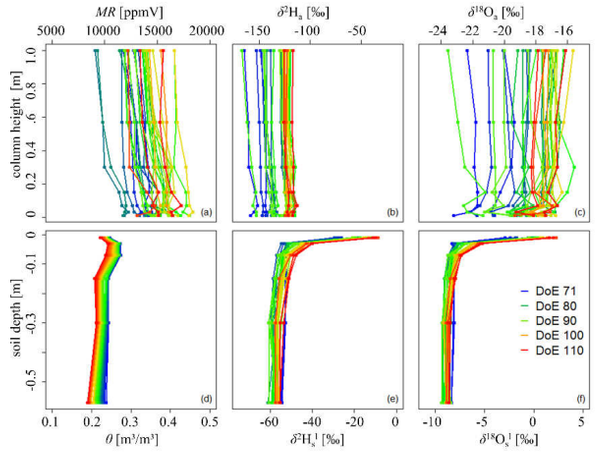

Figure 2.5
Experiment 2 (day of experiment – DoE 71 to 110): profiles of (a) water vapor mixing ratio (*MR*) and (b) hydrogen and (c) oxygen isotopic compositions (δ^2H_a and $\delta^{18}O_a$) in the atmosphere column across heights. Profiles of (d) soil water volumetric content (θ, $m^3\ m^{-3}$) and (e) hydrogen and (f) oxygen isotopic compositions (δ^2H_s and $\delta^{18}O_s$) across depths.

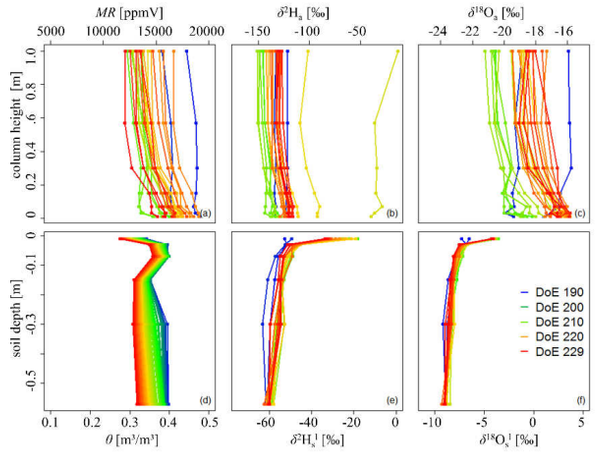

Figure 2.6
Experiment 3 (day of experiment – DoE 190 to 229): profiles of (a) water vapor mixing ratio (*MR*) and (b) hydrogen and (c) oxygen isotopic compositions (δ^2H_a and $\delta^{18}O_a$) in the atmosphere column across heights. Profiles of (d) soil water volumetric content (θ, $m^3\ m^{-3}$) and (e) hydrogen and (f) oxygen isotopic compositions (δ^2H_s and $\delta^{18}O_s$) across depths.

2.3.4 Isotopic composition of evaporation and kinetic fractionation factor

As a consequence of the progressive water isotopic enrichment in the upper soil layers (Fig. 2.7a and b), δ^2H_E increased with time from –149.7 ±2.9 ‰ to –82.2 ±8.2 ‰ during the first 40 days of experiment, whereas $\delta^{18}O_E$ increased from –40.9 ±3.0 ‰ to –26.2 ±2.8 ‰ in the same time. α_K mean values (Table 2.2) obtained with the CG65 method were 1.0375 ±0.0049 and 1.0238 ±0.0034 for $^1H^2H^{16}O$ and $^1H_2{}^{18}O$, respectively. Only 4% of the calculated α_K^{2H}, but 100% of the α_K^{18O}values were within the theoretical range given by Dongmann et al. (1974). By using the G71 method, the mean α_K^{2H} value was equal to 1.0132 ±0.0011, while the mean α_K^{18O} value was 1.0149 ±0.0012, with a hit rate of 96 % (92 % for α_K^{2H}). A trend in both data as simulated by the model of Mathieu and Bariac (1996) was not visible. As a measure of model-to-data fit, the root mean square error (RMSE) was estimated at 0.0247 for α_K^{2H} and 0.0096 for α_K^{18O} (CG65), and 0.0009 for α_K^{2H} and to 0.0011 for α_K^{18O} (G71), respectively.

During E2 (Fig. 2.8), water in the upper soil layers was initially isotopically enriched compared to that of the deeper soil layers, and the enrichment increased continuously. δ_E showed no significant (upward) trend during the course of experiment and was on average –88.6 ±8.2 ‰ (δ^2H_E) and –24.2 ±2.2 ‰ ($\delta^{18}O_E$). The observed decrease of δ^2H_a and $\delta^{18}O_a$ between DoE 85 and 87 translated into an increase of the computed values of δ^2H_E and $\delta^{18}O_E$, and ultimately to a decrease of $\alpha_K{}^2H$ and $\alpha_K{}^{18}O$ estimates. Mean α_K values were 1.0386 ±0.005 and 1.0232 ±0.0052 for $^1H^2H^{16}O$ and $^1H_2{}^{18}O$, respectively, when using CG65. The hit rate for α_K^{2H} ($\alpha_K{}^{18}O$) values was 3% (100%) and the RMSEs were 0.0208 (0.0055) for α_K^{2H} (α_K^{18O}). By using the G71 method, the mean α_K^{2H} and α_K^{18O} values were 1.0132 ±0.0015 and 1.0149 ±0.0017, respectively. 84 % and 90 % of the values were within the theoretical range, and the RMSEs were 0.0054 and 0.0061 for $^1H^2H^{16}O$ and $^1H_2{}^{18}O$, respectively. During E2, the isotopic kinetic fractionation factor increased with a slope of 0.0001 d^{-1} for both isotopologues using the G71 method, while in the case of using the CG65 no systematic increase was observed.

In E3 (Fig. 2.9), δ^2H_E ($\delta^{18}O_E$) increased from –155.5 ±7.0 ‰ (–37.2 ±5.0 ‰) on DoE 190 to –47.6 ±3.3 ‰ (–5.7 ±0.6 ‰) on DoE 210. The ^2H labeling pulse on DoE 211 caused two depleted values for δ^2H_E (i.e., –166.6 ±39.0 ‰ on DoE 212 and –149.1 ±40.9 ‰ on DoE 213). Before and after this peak, the δ^2H_E ($\delta^{18}O_E$) mean value was –60.9 ±7.0 ‰ (–9.1 ±1.1‰). The mean α_K^{2H} was 0.9887 ±0.0336 and was affected by the rapid change in δ^2H_E and δ^2H_a shortly following the labeling pulse (DoE 212) and reached a minimum value of 0.87 ±0.01. α_K^{18O} was not significantly impacted by the labeling pulse using the CG65 model, yielding a mean value of 1.0011 ±0.0051. The associated hit rate was 15% for $\alpha_K{}^2H$ values and 8% for $\alpha_K{}^{18}O$ values. When using the G71 method, α_K^{2H} and α_K^{18O} values were affected by the

labeling pulse. α_K^{2H} (α_K^{18O}) values increased up to 1.0391 ±0.002 (1.044 ±0.002) on DoE 212 with mean values of 1.0078 ±0.0077 for α_K^{2H} values and 1.0089 ±0.0086 for α_K^{18O} values. The hit rate of α_K^{2H} and α_K^{18o} values decreased to 4%. The RMSE for α_K^{2H} (α_K^{18O}) values was 0.0434 (0.0187) when considering CG65, whereas the RMSE for α_K^{2H} (α_K^{18O}) values decreased to 0.0061 (0.0061) when considering G71.

Table 2.2
Mean kinetic fractionation factor (α_K) values, hit rate (%), i.e., the proportion of α_K estimate lying within the theoretical range ($1.0125<\alpha_K^{2H}<1.0251$ and $1.0141<\alpha_K^{18O}<1.0285$) and goodness of fit (RMSE) between α_K estimates and simulated values using the model of Mathieu and Bariac (1996). "CG65" and "G71" refer to the two different methods of calculation of α_K values.

	E1		**E2**		**E3**	
	α_K^{2H}	α_K^{18O}	α_K^{2H}	α_K^{18O}	α_K^{2H}	α_K^{18O}
CG65						
mean value (±1sd) [-]	1.0375 ±0.0049	1.0238 ±0.0034	1.0386 ±0.005	1.0232 ±0.0052	0.9887 ±0.0336	1.0011 ±0.0051
hit rate [%]	4	100	3	100	15	8
RMSE [-]	0.0247	0.0096	0.0208	0.0055	0.0434	0.0187
G71						
mean value (±1sd) [-]	1.0132 ±0.0011	1.0149 ±0.0012	1.0132 ±0.0015	1.0149 ±0.0012	1.0078 ±0.0077	1.0089 ±0.0086
hit rate [%]	96	92	84	90	4	4
RMSE [-]	0.0009	0.0011	0.0054	0.0061	0.0061	0.0061
Mathieu and Bariac (1996)						
mean value (±1sd) [-]	1.0129 ± 0.0003	1.0146 ± 0.0003	1.0185 ±0.0003	1.0209 ±0.0003	1.0152 ± 0.0005	1.0173 ± 0.0006

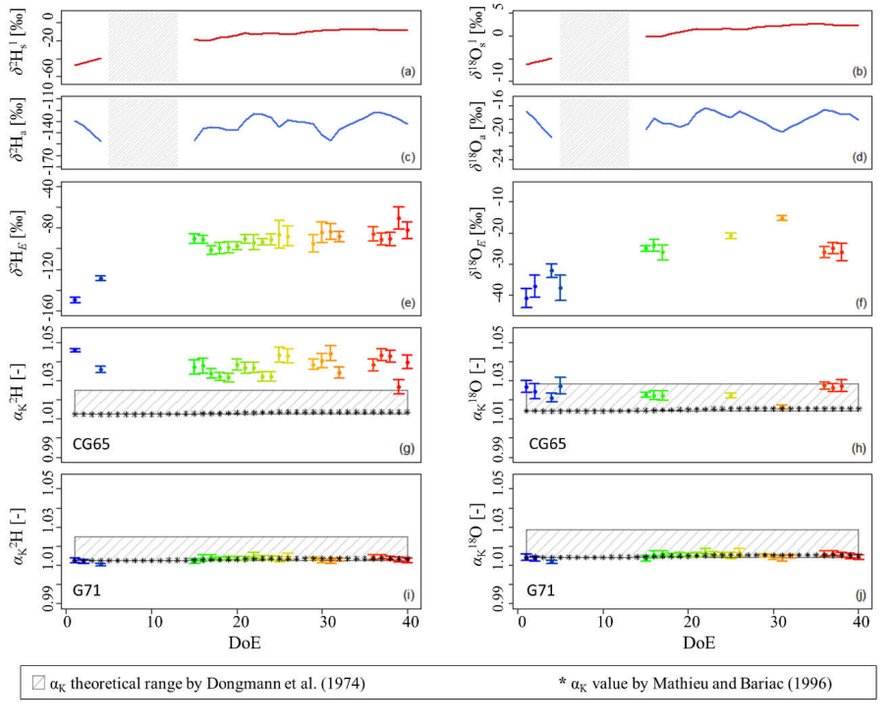

Figure 2.7

Experiment 1: Isotopic composition of the soil liquid water ($\delta^2H_S^l$ and $\delta^{18}O_S^l$, in ‰) at depth 0.01 m (a-b), of the laboratory air water vapor (δ^2H_a and $\delta^{18}O_a$ in ‰) at 1 m above the soil surface (c-d), of the evaporated water vapor (δ^2H_E and $\delta^{18}O_E$ in ‰, e-f) calculated with the Keeling plot method (only results with a p-value lower than 0.05 are shown); α_K results by using the inverse Craig and Gordon (1965) model (method "CG65", g-h); α_K results obtained from the value of the slope of the "evaporation line" given by Gat (1971) (method "G71", i-j). Theoretical ranges of α_K values are represented by the grey shaded horizontal stripes, and results of the model of Mathieu and Bariac (1996) are displayed for comparison (black stars).

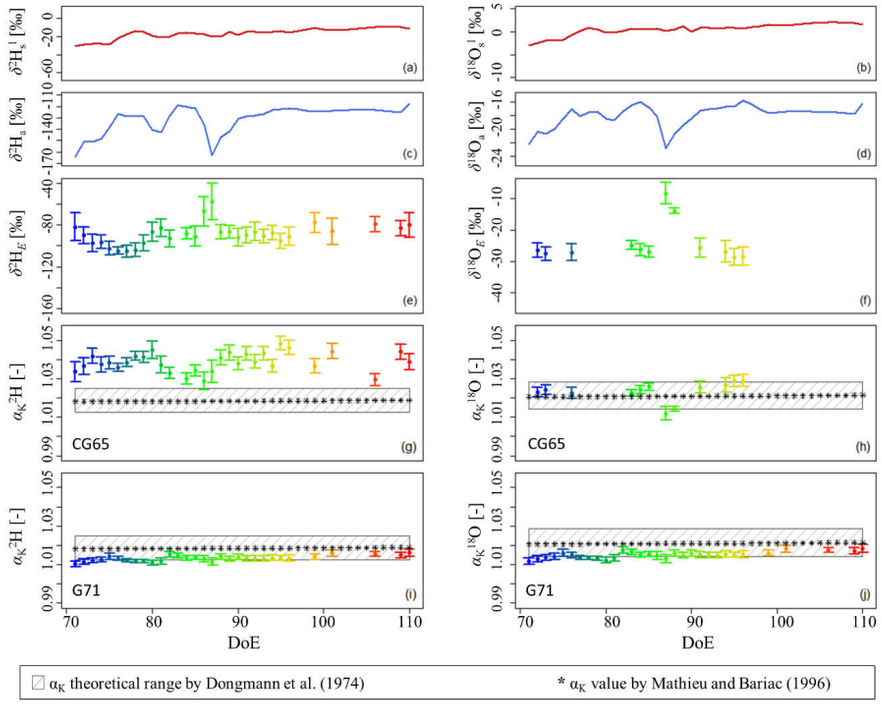

Figure 2.8

Experiment 2: Isotopic compositions of the soil liquid water ($\delta^2H_S^l$ and $\delta^{18}O_S^l$, in ‰) at depth 0.01 m (a-b), of the laboratory air water vapor (δ^2H_a and $\delta^{18}O_a$ in ‰) at 1 m above the soil surface (c-d), of the evaporated water vapor (δ^2H_E and $\delta^{18}O_E$ in ‰, e-f) calculated with the Keeling plot method (only results with a p-value lower than 0.05 are shown); α_K results by using the inverse Craig and Gordon (1965) model (method "CG65", g-h); α_K results obtained from the value of the slope of the "evaporation line" given by Gat (1971) (method "G71", i-j). Theoretical ranges of α_K values are represented by the grey shaded horizontal stripes and results of the model of Mathieu and Bariac (1996) are displayed for comparison (black stars).

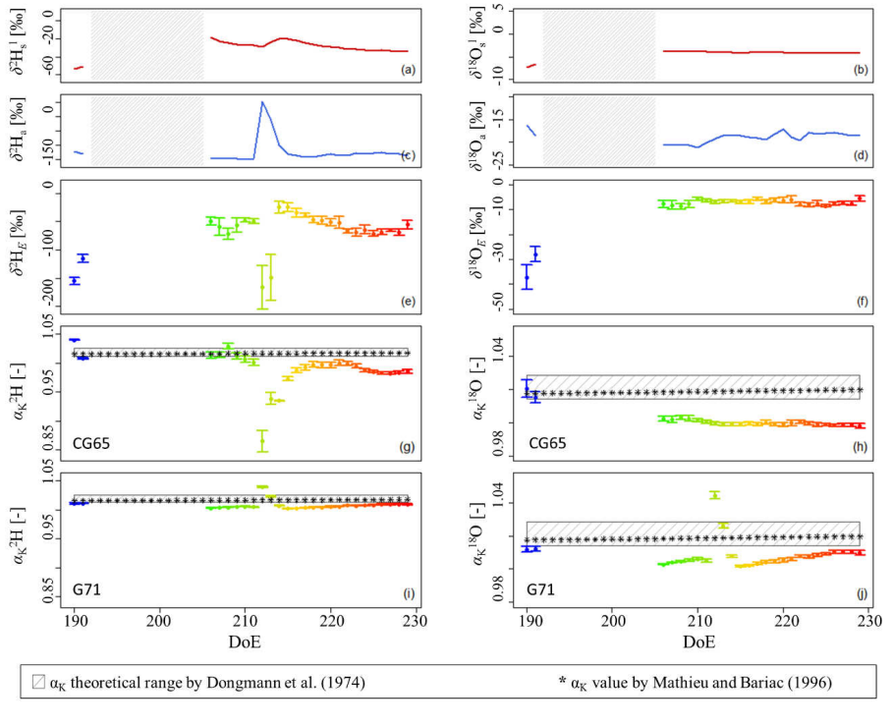

Figure 2.9

Experiment 3: Isotopic compositions of the soil liquid water ($\delta^2H_S^l$ and $\delta^{18}O_S^l$, in ‰) at depth 0.01 m (a-b), of the laboratory air water vapor (δ^2H_a and $\delta^{18}O_a$ in ‰) at 1 m above the soil surface (c-d), of the evaporated water vapor (δ^2H_E and $\delta^{18}O_E$ in ‰, e-f) calculated with the Keeling plot method (only results with a p-value lower than 0.05 are shown); α_K results by using the inverse Craig and Gordon (1965) model (method "CG65", g-h); α_K results obtained from the value of the slope of the "evaporation line" given by Gat (1971) (method "G71", i-j). Theoretical ranges of α_K values are represented by the grey shaded horizontal stripes and results of the model of Mathieu and Bariac (1996) are displayed for comparison (black stars). Note for 9c-j: y-axes scales differ from Figs 2.7 and 2.8.

2.4 Discussion

The coupling between soil gas-permeable tubing and laser-based spectroscopy allowed measuring δ_s^l profiles in a non-destructive manner during a series of experiments differing in the soil water and atmospheric forcing status. We estimated α_K values by using the Craig and Gordon (1965) model in an inverse mode (method CG65). α_K values could also be determined from the approximation of the slope of the evaporation line (Gat 1971), also based originally on the Craig and Gordon (1965) model (method G71). The main difference between these two approaches is the requirement or not of δ_E as input variable. δ_E was determined via a Keeling plot approach (Keeling 1958) as the y-intercept of the linear regression of δ_{col} versus $1/MR_{col}$. δ_E is therefore statistically the more accurate (i) the greater the $1/MR_{col}$ and δ_{col} vertical gradients are, but also (ii) the higher the MR_{col} values are measured directly above the evaporation front (i.e., at 0.01 m height). Mean values of the differences $MR_{col}(0.01) - MR_{col}(1.00)$, $\delta^2H_{col}(0.01) - \delta^2H_{col}(1.00)$, and $\delta^{18}O_{col}(0.01) - \delta^{18}O_{col}(1.00)$ were equal to 3 045 ppmv, 6.9 ‰, and –1.6 ‰ during experiment E1 and equal to 1 988 ppmv, 3.6 ‰, and –0.5 ‰ during E2. We assumed no occurrence of water vapor condensation in the atmosphere column, which is a prerequisite for using the Keeling plot approach. This was the case under the laboratory conditions, where no measureable temperature gradient existed between the atmosphere column and the free laboratory air. This approach also assumes no change of δ_a during the sampling sequence (from 0.01 to 1.00 m). Mean changes of δ_a during one sampling sequence were 2.8 ± 2.1 ‰ (3.3 ± 3.2 ‰) for $\delta_a{}^2H$ ($\delta_a{}^{18}O$) and 0.4 ± 0.3 ‰ (0.6 ± 0.5 ‰) during E1 and E2. A too strong increase (or decrease) of δ_a which resulted in a keeling plot linear regression with a p-value > 0.05 was systematically excluded from the analyses. Finally, the column air should be perfectly mixed at each sampling height in the atmosphere column, i.e., no lateral isotopic gradients should exist. Only then is δ_{col} a representative value of the water vapor in the sampled air layer inside the atmosphere column. This last assumption could unfortunately not be verified during the experiments as it would have required several intake lines at each height.

One limitation of the experimental setup was the sequential sampling of water vapor across heights in the atmosphere column. This reduced the temporal resolution of the δ_{col} profile, with a temporal gap between sampling at 0.01 m (closest to the surface) and at 1.00 m (laboratory "free air") of six hours. As the computation of α_K values following the CG65 method theoretically requires the simultaneous determination of the isotopic composition of soil water and of evaporated water vapor, $\delta_s^l$and δ_{col} measurements across depths and heights were linearly interpolated in time to provide three daily profiles (i.e., at 04:00, 12:00, and 20:00 hours). While it was reasonable to assume that change of δ_s^l at a given depth was a linear function of time, this might be questionable for changes of δ_{col}, even if the conditions in the atmosphere column remained close to laminar throughout the experiments. Together with the

limited temporal resolution, this could have affected the representativeness of δ_E estimates and ultimately those of α_K values using the CG65 method.

Oerter et al. (2017) showed that both soil (gravimetric) water content and clay (gravimetric) content should be taken into account for the calculation of δ_s^l on basis of δ_s^v. However, in the present study, only a temperature correction was applied. On the one hand, the clay content value was the same across soil layers in the column as well as in the two soil standards. Therefore, the effect of clay particles on the isotopic composition of the equilibrated soil pore water vapor could be neglected. On the other hand, E1, E2, and E3 were run under different conditions of soil water availability for evaporation, which would require a soil water content correction. However, we can safely assume that the soil water content effect on the value of δ_s^v was not visible during the series of experiments. The value of δ_s^l measured at 0.60 m depth was constant for all experiments, even though the soil water content was not, i.e., varied between 0.21 and 0.45 $m^3\ m^{-3}$.

A systematic bias was observed between $\alpha_K^{^2H}$ and $\alpha_K^{^{18}O}$ estimates during E1 and E2 obtained with the CG65 method. While $\alpha_K^{^{18}O}$ was in general within its theoretical range (1.0141-1.0285, corresponding to 0.5<n<1), $\alpha_K^{^2H}$ values were almost always higher than 1.0251 (corresponding to the maximum value n=1, see Table 2). These differences could be explained by potential underestimation/overestimation of δ^2H_E. The precise characterization of the local gradients of δ_{col} (especially close to the soil surface), on which the determination of δ_E depends, was enabled by finding the optimal combination of sampling duration and intake flow rate. On the one hand, greater sampling duration and flow rate values ensure minimizing memory effects from previous sampling. On the other hand, they might lead to overlapped sampling, e.g., sampling of water vapor at 0.01 and 0.03 m simultaneously from the 0.01 m column intake line. Duration and flow rate were set to 15 min and 200 ml min^{-1}, respectively, during all experiments, which corresponded to a sampled air layer of 0.016 m height in the atmosphere column, i.e., lower than 0.02 m, which is the difference between the lowest and second lowest air column sampling height. This means, that there was theoretically no overlapped sampling at 0.01 m, where the vertical resolution was the greatest. Despite these settings, $\alpha_K^{^2H}$ results might have been, at least partly, influenced by a stronger memory effect of the δ^2H_{col} measurements of the laser spectrometer than for $\delta^{18}O_{col}$ measurements (Schmidt et al. 2010).

Results of both methods were compared to those of the model of Mathieu and Bariac (1996), which conceptualizes the exponent n simply as the mean between the end-member values n_a (=0.5) and n_s (=1.0), weighted by the absolute deviation of the soil water content measured at the evaporation front (θ_{EF}) from residual and saturated water contents (θ_{res} and θ_{sat}, see Eq. (9)), respectively. This model assumes therefore that only fully turbulent conditions occur when the soil is saturated ($\theta_{EF} = \theta_{sat}$, leading to n =

n_a), which is not necessarily the case, i.e., laminar flow boundary conditions can exist in such cases. The model of Mathieu and Bariac (1996) also considers that, when the soil is at its driest at the evaporation front (θ_{EF}=θ_{res}, leading to n=n_s), molecular diffusion entirely controls water vapor transport to the atmosphere. This assumption might also not be justified as it does not take into account the thickness of the evaporation front nor the aerodynamic conditions in the free atmosphere above.

Contrary to CG65 and G71, the model of Mathieu and Bariac (1996) predicted for all experiments steady monotonic increases of n (and therefore of α_K values) as a consequence of marginal (E1 and E2) or slow (E3) decreases of θ_{EF} with time. θ_{EF} was measured at high temporal resolution and accuracy. The determination of θ_{res} = 0.00 m^3 m^{-3} and θ_{sat} = 0.45 m^3 m^{-3} was not straightforward and, in the present study, depended on how well the soil was sieved, homogenized, and finally repacked in the column. The overall uncertainty of the calculation of α_K values using CG65 obtained from the error propagation calculations was 2.9 ‰ (2.4 ‰), 3.6 ‰ (2.6 ‰) and 4.4 ‰ (1.4 ‰) for $\boldsymbol{\alpha_K^{2H}}$ ($\boldsymbol{\alpha_K^{18O}}$) during E1, E2 and E3. This is approximately two times higher than the estimates of the G71 method (1.1 ‰, 1.4 ‰ and 0.8 ‰ for $\boldsymbol{\alpha_K^{2H}}$ and 1.3 ‰, 1.5 ‰ and 0.9 ‰ for $\boldsymbol{\alpha_K^{18O}}$ during E1, E2 and E3, respectively). Figures 2.7, 2.8, and 2.9 illustrate these observations well.

The value of n obtained from G71 was by nature less sensitive to the uncertainties associated with isotopic input variables (i.e., $\delta^l_{s_{init}}$ and δ_a, ε, and $\Delta\varepsilon$) as it was determined on basis of a ratio of $\delta^{18}O$ and δ^2H data (Eq. (6), Table 1)**.** Since n evolution was determined in a dual isotopic space it was therefore common for both isotopologues. As a consequence, for example on DoE 213 (experiment E3) the rapid change in δ^2H_E led to sudden variations of α_K^{2H} as well as of α_K^{18O}. G71 results were, in contrast to CG65 results, always within theoretical ranges. They also matched well the values of the model of Mathieu and Bariac (1996) during E1 (RMSE = 0.0009) and reasonably well during E2 (0.0054<RMSE<0.0061). For the latter experiment, G71 α_K estimates ($1.0103 < \alpha_K^{2H} < 1.0161$ and $1.0117 < \alpha_K^{18O} < 1.0183$) systematically plotted below those of the Mathieu and Bariac (1996) model ($1.018 < \alpha_K^{2H} < 1.0189$ and $1.0204 < \alpha_K^{18O} < 1.0215$), which would still indicate that turbulent transport of water vapor prevailed, even though soil water content was significantly lower. CG65 estimates of α_K^{18O} were greater than those by the model of Mathieu and Bariac (1996) during E1 and E2, and suggest, again contrary to G71 results, a more predominant role of molecular diffusion in the transport of water vapor.

Although relative humidity in the atmosphere has no impact on the value of α_K, it partly controls δ_s^l via the kinetic isotopic effect term introduced in Eq. (7). The primary objective of experiment E3 was to significantly increase the relative humidity of the laboratory free air to observe its effect on the soil water isotopic enrichment. Even though relative humidity was significantly higher during E3 (52.1 ±3.3%) than during E1 (37.9 ±5.3%) and E2 (45.4 ±4.6%), the impact on both soil hydrogen and oxygen water

isotopic surface enrichments was not clear before the intrusion of the enriched atmospheric water vapor occurred. In contrast, the labeling pulse in E3 was shortly (1 day) followed by the intrusion of laboratory air water vapor into the first centimeters of the soil. The maximum δ^2H_s value was observed on DoE 215, i.e., 3 days after the isotopic composition of the laboratory air reached its maximum value (Fig. 2.9). This illustrates how conditions in the atmosphere column contrasted with the well-mixed aerodynamic conditions inside the laboratory. The response time of the isotopic composition of soil to the isotopic composition of the atmosphere had clear effects on both methods for determining α_K values. CG65 and G71 systematically underestimated MB96 results after the labeling pulse during E3 (to the exception of the DoE 212-213 period for G71). Possible reason for this was the non-attainment of thermodynamic equilibrium conditions in the soil pore space at the evaporation front (EF) upon invasion of the enriched column air water vapor in the upper soil layers. This could have led to errors in the determination of δ_{EF} values, and, ultimately in those of δ_E and α_K.

Only a handful of studies aimed at estimating and/or modeling α_K values during bare soil evaporation. Braud et al. (2009a) could retrieve $\boldsymbol{\alpha_K^{18_O}}$ values by using the CG65 method as upper boundary condition for their soil-vegetation-atmosphere model SiSPAT-Isotope during a series of long-term drying experiments in the laboratory. For this, they precisely calibrated the soil water transport module of SiSPAT-Isotope. They simulated a general decreasing trend for $\boldsymbol{\alpha_K^{18_O}}$ with highest (~1.020<$\boldsymbol{\alpha_K^{18_O}}$<~1.030) values at soil water saturation and lowest values – sometimes even lower than 1.000 – (0.980<$\boldsymbol{\alpha_K^{18_O}}$<1.020), when the evaporation front was located the furthest away from the soil surface. This is inconsistent with both the general belief that *n* should increase with increasing thickness of the soil surface dry layer and decreasing soil water content (Barnes and Allison 1983), and the model of Mathieu and Bariac (1996). Rothfuss et al. (2012) determined values for $\boldsymbol{\alpha_K^{18_O}}$ under strictly controlled conditions in a climatic chamber, assuming isotopic steady-state evaporation from their soil monolith. They calibrated SiSPAT-Isotope using multiple objective functions and found $\boldsymbol{\alpha_K^{18_O}}$ to range between 1.021 and 1.033. Rothfuss et al. (2015) used the G71 method for determination of both $\boldsymbol{\alpha_K^{18_O}}$ and $\boldsymbol{\alpha_K^{2_H}}$ with help of novel online laser spectroscopy and non-destructive monitoring of $\boldsymbol{\delta_s^l}$. They also found an overall decreasing trend for both kinetic fractionation factors, corresponding to *n* values ranging from 0.95 to 0.6. The authors could partly reconcile their results with theory by considering that relative humidity value at the evaporation front was no longer equal to 100 %. Soderberg et al. (2012) pointed out the need to account in the Craig and Gordon (1965) model for the effect of very low soil water tension (pF>5) on the value of the relative humidity at the evaporation front following the Kelvin equation (Gee et al. 1992). In the present study during E2 where soil was the driest, soil water tension minimum value was calculated with the van Genuchten-mualem model (Mualem 1976, van Genuchten 1980) on basis of

the minimum recorded volumetric water content value and the soil retention curve parameters (Lutz Weihermüller, personal communication). It was estimated to range between 2077 and 2611 hPa, which corresponded to a pF value between 3.32 and 3.42 Therefore, soil water tension was not considered to have an impact on the value of α_K computed with the CG65 method via its impact on the isotopic kinetic effect $\Delta\boldsymbol{\varepsilon}$.

When determining δ_E by using the Craig and Gordon (1965) model in a forward mode for, e.g., evapotranspiration (ET) partitioning in the field, G71 should be used together with the model of Mathieu and Bariac (1996) as independent assessment for setting the value of α_K correctly. Sensitivity of the isotopic partitioning of ET to α_K values should be done, if applicable, in light of the potential discrepancies between results of the two methods. For this purpose, $\boldsymbol{\delta}_{\mathbf{s}}^{\mathbf{l}}$ measurements should not be restricted to the upper few centimeters of soil (where evaporation takes place), but rather be conducted throughout the entire soil profile to be able to compute slopes of the evaporation line. Measurements of $\boldsymbol{\delta}_{\mathbf{s}}^{\mathbf{l}}$ should finally be performed at high temporal resolution to evaluate α_K dynamics.

2.5 Conclusion

In this study, we were able to monitor soil and atmospheric isotopic composition profiles non-destructivly at a high temporal and vertical resolution during a series of bare soil evaporation experiments differing in soil water content and atmospheric forcing. In combination with meteorological measurements and by using a Keeling plot approach, we could determine the isotopic composition of the evaporated water vapor and finally compute the hydrogen and oxygen kinetic fractionation factors from the Craig and Gordon (1965) model with two different inverse modeling approaches on a daily basis.

Our results show that the application of the Keeling plot approach (Keeling 1958) in the laboratory remains highly challenging, with direct consequences for the isotopic composition of evaporated water vapor and its uncertainty using the CG65 approach. This was particularly true for the computation of the hydrogen kinetic fractionation factor, as measurements of δ^2H seemed to suffer from greater analytical memory effects than those of δ^{18}O. The determination of α_K values from the computation of the slope of the so-called “evaporation line” in a dual isotope space (G71) was independent from information on δ_E, and as such provided the best model-to-data fit with the simple two-end member formulation of Mathieu and Bariac (1996) during the first experiment. The discrepancy in results between G71 and the model of Mathieu and Bariac (1996) indicated, e.g., that turbulent transport of water vapor would have still played a preponderant role in the removal of moisture by evaporation during the second experiment, even at a soil water content much below saturation.

Our series of experiments call for further investigation of the temporal dynamics of α_K values with novel non-invasive and/or non-destructive isotopic monitoring tools. They also underline the need for repetitive and thorough determination of soil water isotopic composition profiles in the field for determination of α_K values using both the G71 model and the Mathieu and Bariac (1996) model approaches. This should be useful for providing δ_E estimates in the context of the partitioning of evapotranspiration into soil evaporation and plant transpiration.

Chapter 3

In-situ Monitoring of Soil Water Isotopic Composition for Partitioning of Evapotranspiration during One Growing Season of Sugar Beet (*Beta vulgaris*)

Based on a journal article submitted as:

Quade, M. Klosterhalfen, A. Graf, A. Brüggemann, N. Hermes, N. Vereecken, H. and Rothfuss, Y 2019: In-situ Monitoring of Soil Water Isotopic Composition for Partitioning of Evapotranspiration During One Growing Season of Sugar Beet (*Beta vulgaris*), Agricultural Forest Meteorology 266-267,53-64, https://doi.org/10.1016/j.agrformet.2018.12.002

3.1 Introduction

A process-based understanding of the atmospheric water cycle is crucial for improving meteorological and hydrological forecasting models. However, usually only the total flux of H_2O, evapotranspiration (*ET*), is measured, while land-surface models are able to compute its component fluxes, evaporation (*E*) and transpiration (*T*). There is an ongoing debate on the value of the transpiration fraction (*T*/*ET*) across ecosystems and spatial/temporal scales. The study of Jasechko et al. (2013) reported the largest contribution of *T* to *ET* (up to 90 %) on the global scale to date, while others found smaller contributions, e.g., values between 35-80 % (Coenders-Gerrits et al. 2014, Good et al. 2015, Wei et al. 2017).

Evapotranspiration is commonly measured with the eddy covariance (EC) technique, and a global network of EC flux measurement sites was established in the last few decades. Partitioning *ET* into its component fluxes (*E* and *T*) can be done by source partitioning methods (Kool et al. 2014), which include (i) correlation-based modelling approaches applied to the available EC measurements (Scanlon and Kustas 2010) or a combination of EC measurements with additional (ii) instrumental approaches, e.g. soil-flux chamber measurements (Raz-Yaseef et al. 2010, Lu et al. 2017), sap-flow measurements (e.g., heat dissipation method; Granier 1987, Hölttä et al. 2015), micro-lysimeter measurements (Kelliher et al. 1992) or atmospheric profile measurements (Ney and Graf 2018). Correlation-based modelling approaches are able to partition the ET flux continuously on a sub-daily timescale (Good et al. 2014, Scanlon and Kustas 2010, 2012, Wang et al. 2016), but their partitioning performance depends on input estimations, meteorological conditions and study site characteristics and thus can be unclear, and these modelling approaches are not widely established yet. It has been shown by Klosterhalfen et al. (2019) that more research is needed to distinguish situations where these methods yield reliable estimates from those where large errors can occur. Additional instrumental approaches usually measure the net *E* or *T* flux independently (see review ofKool et al. 2014). Closed bare soil flux chamber measurements provide the net *E* flux, but during the chamber measurement non-natural conditions are introduced, primarily by increasing vapor pressure and decreasing incoming solar radiation, which adds to the uncertainty of the *E* flux measurement (Dubbert et al. 2013). Micro-lysimeter measurements also provide the *E* flux. They are generally considered to be a reliable and simple method, but are time-consuming, have a small sample size compared to the field scale, and cannot be used for a long time period or during rain events without further modifications, because over time micro-lysimeters would diverge from the general field conditions (Boast and Robertson 1982, Shawcroft and Gardner 1983, Evett et al. 1995, Kool et al. 2014). Newly developed methods like high-resolution profile measurements, as described by Ney and Graf (2018), provide detailed information about the ecosystem, but are up to now not usable for long-term automated measurements.

Another approach to *ET* partitioning is estimating the relative transpiration fraction (*T/ET*) on the basis of water stable isotopic data (see review and opinion papers of Sutanto et al. 2014, Xiao et al. 2018). This approach consists of measuring the hydrogen and oxygen stable isotopic compositions (δ^2H and δ^{18}O) of the single components *ET*, *E* and *T*, and solving the following two end-member mixing model for *x*:

$$\delta_{ET} = (1 - x)\delta_E + x\delta_T \quad (3.1)$$

with $\delta_{ET}, \delta_E, \delta_T$, and x being the isotopic compositions of *ET*, *E*, *T*, and the *T*/*ET* flux ratio. Equation (3.1) assumes that only two sources contribute to *ET*, and therefore, it cannot be applied in case of another identified source (e.g., leaf surface evaporation of morning dew). The accuracy of the isotopic partitioning method also depends on how significantly different δ_{ET}, δ_E and δ_T values are (Rothfuss et al. 2010).

The δ_{ET} value can be determined statistically from measurements of the atmospheric water vapor concentration and isotopic composition using, e.g., the Keeling plot (Keeling 1958) and the flux-gradient (Lee et al. 2007) approaches, chamber measurements (Dubbert et al. 2013, Wang et al. 2013) or EC measurements (Griffis et al. 2010, Good et al. 2012). The most common approach is the Keeling plot method, which assumes that turbulent mixing is the only process that causes upward transport of water vapor and that the isotopic composition of the background (i.e., local) water vapor as well as δ_{ET} do not change over time during measurements.

The isotopic composition of *T* (δ_T) can be determined (i) destructively by assuming isotopic steady state (δ_T is equal to the isotopic composition of the leaf input water, i.e., the xylem sap – δ_x) (Rothfuss et al. 2010, Zhang et al. 2011), or (ii) by considering isotopic transient state ($\delta_T \neq \delta_x$). In the latter case, δ_T can be determined either destructively (Dubbert et al. 2013, Dubbert et al. 2017) or non-destructively with closed or dynamic plant or leaf chambers (Wang et al. 2010, Dubbert et al. 2013, Good et al. 2014).

δ_E is usually indirectly calculated on the basis of measurements of the isotopic composition of soil liquid water (δ_s^l) at the evaporating front and by use of the Craig and Gordon (1965) model (Good et al. 2014). In the vast majority of partitioning studies, δ_s^l is determined by destructive sampling of surface soil, subsequent cryogenic extraction and isotopic analysis of soil water in the laboratory (Lee et al. 2010, Zhang et al. 2011, Aouade et al. 2016). This method is time-consuming, and new evidence shows that soil physicochemical properties affect the isotopic composition of the extracted soil water (Orlowski et al. 2016a, Orlowski et al. 2018). Rothfuss et al. (2013), Volkmann and Weiler (2014), Gaj et al. (2016), Oerter et al. (2017) presented a series of methods where soil water vapor can be sampled non-

destructively with gas-permeable membranes or tubing. Theoretically, this allows for long-term on-line monitoring of δ_s^l and δ_E in the field. Although the monitoring method of Rothfuss et al. (2013) was successfully applied in the laboratory to pure quartz sand (Gangi et al. 2015, Rothfuss et al. 2015) and silt loam (Quade et al. 2018), it has so far not been tested in the field for *ET* partitioning purposes.

In the present study, the non-destructive on-line method of Rothfuss et al. (2013) was evaluated in the field during one growing season of sugar beet (*Beta vulgaris*) to test its suitability for long-term monitoring of soil water isotopic composition under field conditions and for calculating *T/ET* values. *T/ET* values calculated on the basis of estimates of δ_E, either determined from destructive sampling or with the non-destructive monitoring method, were compared against each other. Additionally, the isotope-based *T/ET* values were compared to those obtained from in-situ measurements of *E* and *ET* (latent heat flux) determined with the combined EC and micro-lysimeter measurements to evaluate their reliability.

3.2 Material and methods

3.2.1 Study site

Measurements were conducted at the TERENO (www.tereno.net) research site Selhausen (50°52'09''N, 6°27'01''E) in North Rhine-Westphalia, Germany. It is an agricultural field located in the northern part of the Rur river catchment. The site is equipped with an EC station (EC_SE_001 in the TERENO online data portal http://teodoor.icg.kfa-juelich.de, DE-RuS on www.icos-ri.eu). The soil is classified as a silt loam with particle size distribution 20.1 % sand, 65 % silt, and 14.9 % clay. The field has an area of approximately 10 ha, with an extension of 400 m in WSW-ENE direction and 200 m (east end) to 300 m (west end) perpendicular to it. All measurements were carried out in the center of the field, at a distance of at least 100 m (and 200 m in the main wind direction WSW) to the edge. Apart from a tree row at the west end of the field, the surrounding is occupied with similar fields growing either the same crop (sugar beet), barley or wheat. The post-processing of the EC measurements at a height of 2.43 m above the ground is operationally combined with modelling the footprint following Kormann and Meixner (2001).

The lysimeter, atmospheric, and soil water isotopic measurements were conducted on three different dates (D) corresponding to different canopy heights (CH, in m) and leaf area indices (LAI, in $m^2\ m^{-2}$):

D1: 29 May 2017 10:30-13:00 UTC (CH=0.18, LAI=0.7)

D2: 13 July 2017 08:30-11:00 UTC (CH=0.40, LAI=2.3)

D3: 21-22 August 2017 10:30-13:30 UTC (CH=0.45, LAI=6.7).

During this period (D1-D3), the average temperature was 18.6 ± 4.4 °C; rain events occurred at 36 of 86 days with a total amount of 207.8 mm. The contribution of the field to the EC flux signal was 93 % on average and always greater than 84 % during the day. During the night between August 21 and 22, modelled footprint contributions were lower due to stable atmospheric stratification, being 81 % on average and down to 28 % in two cases where the footprint model was probably affected by poor EC data quality.

Apart from the latent heat flux (Sect. 2.5), the following meteorological and soil measurements of the station were used in this study: Air temperature (T_a, in °C) and relative humidity (h, expressed in %) were measured at a height of 2.5 m above ground with a HMP45C sensor (Vaisala, Helsinki, Finland). Soil temperature (T_s, in °C) and volumetric water content (θ_s, in $m^3\ m^{-3}$) were measured at depths –0.01 m, –0.05 m and –0.10 m with combined soil moisture and temperature sensors (SMT-100, Truebner GmbH, Neustadt, Germany).

3.2.2 Isotopic monitoring set-up and measurement protocol

$\delta^{18}O$ and $\delta^{2}H$ were measured with a cavity ring-down spectrometer (L2120-*i*, Picarro Inc., Santa Clara CA, USA). The analyzer was placed in a self-designed air-conditioned box (0.9 x 0.9 x 1.5 m) together with the necessary equipment, i.e., one dry synthetic air gas bottle (20.5 % O_2 in N_2 with approx. 20–30 ppmv water vapor; Air Liquide, Germany) and an automated unit of analog/digital modules (ICP-DAS Europe GmbH, Germany) for data acquisition and operating the mass flow controllers (GF40, Brooks Instrument GmbH, Germany) and magnetic valves (type 6011, Bürkert GmbH & Co. KG, Germany). Atmospheric profiles were measured by sequential sampling at five different heights (0.01, 0.20, 0.45, 1.00, and 1.50 m). The water vapor mixing ratio (MR, defined as the ratio of absolute volumetric concentrations of water vapor and dry air) and isotopic composition (δ_a) were measured sequentially over 30 min across heights (i.e., 6 min for each height). Sampling duration per sampling height was chosen in order to minimize natural temporal variations of MR and δ_a over the course of the measuring sequence. In addition, air was actively pumped (PK T01 310, Pfeiffer Vacuum GmbH, Germany) upstream of the laser spectrometer at a flow rate of 3 l min^{-1} to maximize the response time (Figure 3.1). At each sampling height, the last 3 min (approx. 98 observations) of measurements were used to compute the δ_a mean value of the respective sampling period.

Profiles of δ_s^l were monitored by using gas-permeable microporous polypropylene tubing (Accurel® PP V8/2HF, Membrana GmbH, Germany, 0.16 cm wall thickness, 0.55 cm i.d., 0.86 cm o.d.). The

characteristics of this tubing material was discussed in detail by Rothfuss et al. (2013). At three different depths (–0.01, –0.05, and –0.1 m), 0.2 m long pieces of tubing were installed between two crop rows shortly after sowing of the sugar beet. Dry synthetic air was directed into the gas-permeable tubing at a flow rate of 85 ml min^{-1} for 30 min. The sampled soil water vapor was diluted with dry synthetic air to ensure an excess flow before the laser spectrometer analyzer and to avoid any contamination with ambient air (Fig. 3.1). The part of the tubing system conducting soil water vapor was heated with heating wire (Thermo Tronic, Dennerle GmbH, Vinningen, Germany; wire length 2 m, total heating power 40 W) and coated with an insulated tubing (Armaflex, Armacell International S.A., Luxembourg; 0.05 m wall thickness) to avoid condensation due to temperature changes. For each soil depth, the laser spectrometer data of the last 10 min of the 30 min sampling duration (corresponding to approx. 385 observations) were used to compute the mean value soil water vapor isotopic composition (δ_s^v).

δ_s^v and δ_a values with standard deviations greater than 2 ‰ for δ^2H and 0.5 ‰ for $\delta^{18}O$ (i.e., indicating problems during sampling, e.g., condensation) were discarded from the analysis. Subsequently, δ_s^v and δ_a values were referenced to a MR value of 10,000 ppmv (see Appendix D for details on the method) to account for the WMVR dependency of the laser analyzer (Schmidt et al. 2010). These corrected δ_s^v values were then used to compute the corresponding δ_s^l at the measured soil temperature T_s [°C] (Rothfuss et al. 2013):

$^1H^2H^{16}O$: $$\delta_s^l = 104.96 - 1.0342 \cdot T_s + 1.0724 \cdot \delta_s^v \quad (3.2a)$$

$^1H^1H^{18}O$: $$\delta_s^l = 11.45 - 0.0795 \cdot T_s + 1.0012 \cdot \delta_s^v \quad (3.2b)$$

The obtained δ_s^l values were finally corrected against measurements of two internal standards before and after the series of measurements in the field each day. For this, two acrylic glass vessels (2.57 l volume), each equipped with 0.15 m gas-permeable tubing, were filled with the soil from the test site (sieved at 2 mm and dried at 110 °C for 24 hours). Finally, the soil was saturated with either one of two standard waters of isotopic composition δ_{st1}^l (δ^2H = –1.5 ‰; $\delta^{18}O$ = +7.2 ‰) and δ_{st2}^l (δ^2H = –103.2 ‰; $\delta^{18}O$ = –21.3 ‰). Soil water vapor was sampled for 30 min at a flow rate of 85 ml min^{-1} and different dilution rates to obtain MR values between 5,300 and 24,100 ppmv.

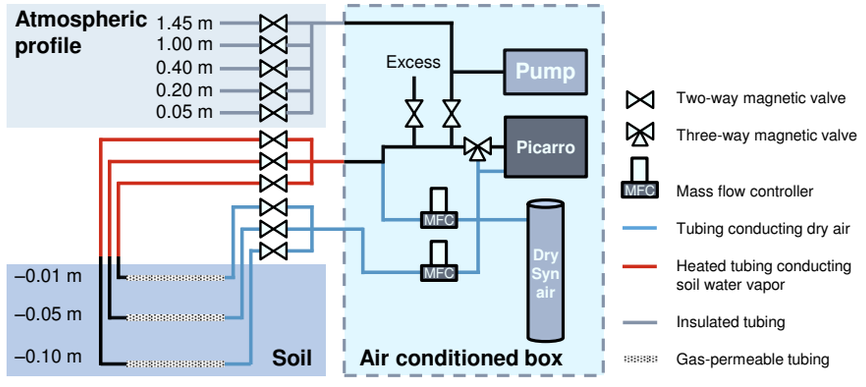

Figure 3.1
Field experimental setup

Differences between Equations (3.2a) and (3.2b) and those of, e.g., Majoube (1971) were explained to be due to the specific conditions prevailing during sampling and potentially proton exchange between soil water and the polypropylene material (Rothfuss et al. 2013). Soil temperature is therefore the only explanatory factor and points to the prevalence of thermodynamic conditions. In a recent study, where the method of Rothfuss et al. (2013) was applied to soil and sediment samples, Oerter et al. (2017) showed that clay and water gravimetric contents statistically explained the variability of δ_s^l for a given soil temperature. This was, however, not tested here, as new evidence showed the opposite during a series of laboratory experiments using the same silt loam soil, i.e., soil water content values in the range of 0.21- 0.45 m^3 m^{-3} did not have an impact on the value of δ_s^l (Quade et al. (2018).

Water vapor was sampled sequentially from the soil and the atmosphere in the following order (with duration given in minutes): soil at –0.01 m (30); atmosphere at 1.50 m (6); atmosphere at 1.00 m (6); atmosphere at 0.45 m (6); atmosphere at 0.20 m (6); atmosphere at 0.01 m (6); soil at –0.05 m (30); atmosphere at 1.50 m (6); atmosphere at 1.00 m (6); atmosphere at 0.45 m (6); atmosphere at 0.20 m (6); atmosphere at 0.01 m (6); soil at –0.1 m (30).

3.2.3 Destructive measurements for isotopic analysis

Soil from the surface layer (between –0.01 and –0.05 m depth) and aboveground plant material were collected destructively in triplicate at 13:30 UTC on D1, and 12:00 UTC on D2. On D3, soil and plant samples were collected every 3 h, again each time in triplicate. The collected samples were stored in the

air-conditioned box in the field for a few hours, and then transported on the same day to the laboratory where they were kept at –18 °C until cryogenic water extraction. Green tissue (e.g., outer leaf) was discarded from the base of the plant and only white (i.e., non-transpiring) tissue was kept for extraction and determination of δ_x. Plant and soil samples were extracted for 3 h and 4 h at 105 °C, respectively, while the evaporated water was trapped in liquid nitrogen. Finally, the extracted water was measured with a second cavity ring-down spectrometer set in liquid injection modus (L2120-*i*, Picarro, Inc.). Organic compounds (e.g., alcohol) in these samples were removed in-line by a Micro-Combustion Module™ (Picarro, Inc.).

3.2.4 Determination of the end-members of the isotopic mixing equation

δ_{ET} was determined from the intercept of the linear regression of the isotopic composition of the atmospheric water vapor (δ_a) with the inverse of the water vapor mixing ratio ($1/MR_a$) measured across heights (Keeling 1958):

$$\delta_a = \frac{1}{MR_a}\left[MR_{bg}\left(\delta_{bg} - \delta_{ET}\right)\right] + \delta_{ET} \quad (3.3)$$

where MR_{bg} and δ_{bg} are the mixing ratio and isotopic composition of the background (i.e., local) atmospheric water vapor. Statistically significant δ_{ET} results with a coefficient of determination $R^2 > 0.6$ and a p-value < 0.05 were kept for computing *T*/*ET* ratios.

δ_E was estimated both from destructive and non-destructive measurements of δ_s^l by use of the Craig and Gordon (1965) model (Good et al. 2014):

$$\delta_E = \frac{(\delta_{EF}^l + 1)/\alpha_{eq} - h'\left(\delta_{bg} + 1\right)}{1 - h'}\frac{1}{\alpha_K} - 1 \quad (3.4)$$

where α_{eq} and α_K are the equilibrium (Majoube 1971) and kinetic fractionation factor (Dongmann et al. 1974), respectively, and h' is the relative humidity normalized to the saturated vapor pressure at the respective soil temperature. The isotopic composition of soil water at the evaporation front (δ_{EF}^l) was either defined as (i) the soil water isotopic composition that was measured at the depth of strongest isotopic gradient (following the recommendation of Rothfuss et al. 2015), and as (ii) the isotopic composition value measured in the extracted water samples. α_{eq} was determined according to Majoube (1971), while α_K was determined by using the formulation of Dongmann et al. (1974) and Mathieu and Bariac (1996):

$$\alpha_{\mathrm{K}}^{\mathrm{i}} = \left(\frac{D}{{}^{\mathrm{i}}D}\right)^{n} \tag{3.5}$$

$$n = \frac{(\theta_{\mathrm{EF}} - \theta_{\mathrm{res}})n_{\mathrm{a}} + (\theta_{\mathrm{sat}} - \theta_{\mathrm{EF}})n_{\mathrm{s}}}{\theta_{\mathrm{sat}} - \theta_{\mathrm{res}}} \tag{3.6}$$

where D and ${}^{\mathrm{i}}D$ are the molecular diffusivities of $^{1}H_2{}^{16}O$ and of either i = $^{1}H^{2}H^{16}O$ or $^{1}H_2{}^{18}O$, θ_{EF} (m^3 m^{-3}) is the water content at the evaporating front, θ_{sat} = 0.35 m^3 m^{-3} is the saturated soil water content, θ_{res} = 0 m^3 m^{-3} is the residual soil water content, with n_s = 1, when evaporation is controlled by the soil (i.e., soil at residual soil water content) and n_a = 0.5, when evaporation is controlled by the atmosphere (i.e., soil is water-saturated).

The third and last end-member of the mixing equation, namely δ_T, was finally inferred from the isotopic composition value measured in the water extracted from the plant xylem tissue, assuming that isotopic steady-state conditions prevailed during sampling, i.e., $\delta_T = \delta_x$.

The standard error of *T/ET* $\left(\sigma_{T/ET}^2\right)$ depends on the standard errors of δ_E, δ_T and δ_{ET} $\left(\sigma_{\delta_E}^2,\ \sigma_{\delta_T}^2,\ \sigma_{\delta_{ET}}^2\right)$. $\sigma_{\delta_T}^2$ was assumed to be equal to the standard deviation of the three δ_x replicates, $\sigma_{\delta_{ET}}^2$ was determined by the linear regression model, and $\sigma_{\delta_E}^2$ was determined using the Gaussian error propagation (in detail in Rothfuss et al. 2010) under the assumption that all the errors of all measurements are independent. The error of *T/ET* was determined using the latter assumption as well:

$$\sigma_{T/ET}^2 = \left(\frac{\partial(T/ET)}{\partial(\delta_T)}\right)^2 \sigma_{\delta_T}^2 + \left(\frac{\partial(T/ET)}{\partial(\delta_{ET})}\right)^2 \sigma_{\delta_{ET}}^2 + \left(\frac{\partial(T/ET)}{\partial(\delta_E)}\right)^2 \sigma_{\delta_E}^2 \tag{3.7}$$

3.2.5 Micro-lysimeters and eddy covariance measurements

At the beginning of every field measurement, micro-lysimeters were installed at four different locations in 15 m distance to the EC station (one in each wind direction) to measure soil evaporation. For each micro-lysimeter, a PVC ring with an inner diameter of 20 cm, wall thickness of 0.5 cm, and a depth of 11 cm was pushed carefully into the ground to obtain an undisturbed soil monolith. After retrieving the soil column and cleaning the outside of the PVC ring, the bottom of each lysimeter was sealed with an acrylic glass disc preventing percolation and capillary rise out of or into the micro-lysimeter. Then, the micro-lysimeters were weighed initially and placed back into their original location, making sure that the lysimeters were level with the soil surface, laterally fully surrounded by soil, and shielded by sugar beet leaves, thus, representing the general conditions and characteristics of the field site (especially regarding heat flux and shading). Subsequently, the micro-lysimeters were repeatedly collected, cleaned, weighed, and placed back to their original location every 60 to 90 min. To avoid divergence of lysimeters,

and subsequently their evaporation, from undisturbed soil, monoliths were freshly taken at the beginning of each field measurement and never used longer than the second day after installation (Boast and Robertson 1982). A scale with a precision of 0.1 g (equivalent to 0.0032 mm evaporation) was used, which had to be enclosed in a box to avoid wind effects. By considering the mean lysimeter surface area, the time periods between weighing and the latent heat of vaporization, the measured lysimeter weight differences were converted to W m^{-2}. The abovementioned scale resolution equals a latent heat flux resolution ≤ 2.2 W m^{-2}. For D1 three, for D2 four, for the first day of D3 five and for the second day of D3 nine weight differences were obtained for each micro-lysimeter.

Total *ET* was quantified with the EC technique, which is continuously in operation at the station (Sect. 2.1), based on 20 s^{-1} raw data measurements of an ultrasonic anemometer (CSAT3, Campbell Scientific, Logan, UT, USA) and an open-path gas analyzer (LI7500, Li-Cor, Lincoln, NE, USA) mounted at 2.43 m above ground level. Data were processed with the software TK3, including corrections for density fluctuations and system spectral response as well as a three-class quality flagging scheme following the Spoleto agreement and random error estimation (Mauder et al. 2013). Here, we used latent heat flux results of the high and intermediate quality class. Typical random errors of these classes for our site are 10 % and 30 %, respectively (Mauder et al. 2013). The unknown systematic error of EC measurements can be roughly indicated by the energy balance closure gap (Mauder et al. 2013), which is on average 15 % for the season (spring/summer 2017) (Eder et al. 2015, Ney and Graf 2018).

Finally, *T*/*ET* results obtained from the isotope-based approach were used to calculate the latent heat flux of E (L_E) from the latent heat flux of ET (L_{ET}) measured by the EC station using the following relationship: $L_E = 1 - T/ET * L_{ET}$.

3.4 Results

3.4.1 Soil and atmospheric measurements

Mean values of soil temperature (T_s) and water content (θ) measured at –0.01 m as well as those of the air temperature (T_a) and relative humidity (h) measured at 2 m above the soil surface for the different field days are listed in Table 1. $\delta_s^{l}{}^{2}H$ and $\delta_s^{l}{}^{18}O$ values measured in the water extracted from the soil samples (S) and inferred non-destructively from the soil water vapor sampled in the tubing profile (P) are reported also in Table 1.

During D1, the weather was sunny with weak northeasterly wind. T_a increased from 27.5 °C to 30.7 °C, while h decreased from 53 % to 33 %, respectively. θ (–0.01 m) remained constant (0.17 m^3 m^{-3}) and $T_s(-0.01\ \mathrm{m})$ increased from 31.4 °C to 35.7 °C. A comparison between δ_s^l(S) and δ_s^l(P) for ^2H and ^{18}O was not possible. Exemplary Keeling plots for δ^2H and $\delta^{18}O$ are shown for the period 11:00–11:30 UTC in Figure 3.2c and 3.2d. On D1, significant linear regressions for the calculation of $\delta_{ET}{}^2H$ and $\delta_{ET}{}^{18}O$ were always found.

The weather conditions on D2 were fair, with some clouds and weak wind from north to northwest. T_a (T_s) increased from 12.6 to 16.1 °C (from 14.0 °C to 16.6 °C), whereas h decreased from 84 % to 47 %. $\delta_s^{l\,2}H$ (P) was slightly higher (1.1 ‰) than the value obtained from S, while $\delta_s^{l\,18}O$ (P) was significantly (1.7 ‰) lower than $\delta_s^{l\,18}O$ (S). During the first atmospheric measurements (08:30–9:00 UTC), a statistically significant linear relationship was found for δ^2H only, while during the second atmospheric measurements period (10:30–11:00 UTC) this was the case for both isotopic compositions.

Also, during D3, weather conditions were fair with some clouds and weak wind from south to southwest. An inversion with dewfall developed during the night from August 21 to 22. On 21 August 2017, T_a increased from 17.6 °C to a maximum of 21.2 °C at 17:30 UTC. The following day, the temperature increased up to 19.6 °C at 13:00 UTC. During the night, the maximum h value was measured at 98 % on 22 August 2017. $T_s(-0.01\ \mathrm{m})$ varied in a diurnal cycle from 13.8 °C (22 August 2017, 08:00 UTC) to 18.4 °C (21 August 2017, 17:00 UTC). θ decreased continuously from 0.23 (21 August 2017, 11:00 UTC) to 0.21 m^3 m^{-3} (22 August 2017, 11:00 UTC).

$\delta_s^{l\,2}H$(P) values were systematically lower than $\delta_s^{l\ 2}H$(S) (Table 1). On 21 August 2017, they were lower by 6.9, 3.9 and 6.0 ‰ than $\delta_s^{l\,2}H$(S) at 12:00, 15:00, and 18:00 UTC, respectively. The $\delta_s^{l\ 2}H$(S) mean value was characterized by high standard deviation, reflecting the high natural heterogeneity of isotopic composition of soil surface water in the field. In the period before sunset (21 August 2017, 10:30 to 18:41 UTC), $\delta_s^{l\,18}O$(P) and $\delta_s^{l\,18}O$(S) values were in good agreement (within 0.2 to 0.3 ‰). On the next day after sunrise (22 August 2017, 04:33 to 13:30 UTC), the difference between $\delta_s^{l\,18}O$(P) and $\delta_s^{l\,18}O$(S) values increased significantly (to 0.7 to 0.8 ‰). The decrease in air temperature and the occurrence of dewfall led to inaccurate values for $\delta_s^{l\,2}H$(P) and $\delta_s^{l\,18}O$(P) during nighttime (21 August 2017, 18:41 UTC, to 22 August 2017, 04:33 UTC) due to condensation within the soil tubing system. Similar problems were observed for the Keeling plot analyses. Data collected before sunset and after sunrise yielded significant linear regressions, whereas significant relationships could not be derived from nighttime data.

Table 3.1

Overview of experimental conditions prevailing during the three days (D1-D3) of the field campaign: soil temperature (T_s) and soil water content (θ) measured at –0.01 m as well as the air temperature (T_a) and relative humidity (h) measured 2 m above the soil surface. The hydrogen and oxygen isotopic composition values of the soil liquid water (δ_s^l) determined from the soil destructive sampling and cryogenic extraction (S) and inferred from the on-line monitoring of the soil isotopic profile (P) as well as the measured value of the xylem water (δ_x) are also reported.

Sampling date and time	$T_s(-0.01\ \mathrm{m})$ [°C]	$\theta(-0.01\ \mathrm{m})$ [m³/m³]	$T_a(2\ \mathrm{m})$ [°C]	$h_a(2\ \mathrm{m})$ [%]	$\delta_s^{l\,2}$H (S) [‰]	$\delta_s^{l\,18}$O (S) [‰]	$\delta_s^{l\,2}$H (P) [‰]	$\delta_s^{l\,18}$O (P) [‰]	$\delta_x{}^2$H [‰]	$\delta_x{}^{18}$O [‰]
D1 29.05.2017 11:30	33.6	0.17	29.1	43	–39.3 ± 1.7	–3.8 ± 0.6	NA	NA	–50.5 ± 1.0	-6.1 ± 0.1
D2 13.07.2017 12:00	15.2	0.20	14.2	73	–44.8 ± 2.6	–5.5 ± 0.3	–45.9 ± 1.7	–3.8 ± 0.2	–54.2 ± 0.1	–7.9 ± 0.1
D3 21.08.2017 12:00	16.3	0.22	18.6	53	–32.8 ± 0.2	–4.1 ± 0.2	–25.9 ± 1.6	–4.4 ± 0.2	–39.4 ± 0.3	–5.2 ± 0.1
21.08.2017 15:00	19.2	0.22	20.4	50	–31.3 ± 3.5	–4.1 ± 0.6	–27.3 ± 1.5	–4.3 ± 0.2	–39.1 ± 0.2	–5.0 ± 0.1
21.08.2017 18:00	18.4	0.21	20.7	50	–35.5 ± 1.6	–4.7 ± 0.5	–29.5 ± 1.7	–4.5 ± 0.2	–41.2 ± 0.8	–5.5 ± 0.1
21.08.2017 21:00	17.1	0.21	17.8	67	–36.8 ± 1.0	–5.2 ± 0.3	NA	NA	–39.1 ± 0.2	–5.3 ± 0.1
22.08.2017 00:00	15.4	0.21	13.6	88	–36.4 ± 5.8	–4.5 ± 1.4	NA	NA	NA	NA
22.08.2017 03:00	14.2	0.21	11.5	94	–37.7 ± 1.9	–4.8 ± 0.5	NA	NA	–41.3 ± 0.5	–5.5 ± 0.1
22.08.2017 06:00	13.3	0.21	10.2	97	–33.0 ± 3.1	–4.5 ± 0.4	NA	NA	–40.5 ± 0.4	–5.4 ± 0.1
22.08.2017 09:00	14.4	0.21	13.5	87	–31.7 ± 2.3	–4.7 ± 0.2	NA	–3.9 ± 0.4	-38.3 ± 0.2	4.6 ± 0.1
22.08.2017 12:00	16.9	0.21	19.1	65	–33.4 ± 1.9	*–4.6 ± 0.2*	NA	–3.9 ± 0.3	-40.7 ± 0.3	5.3 ± 0.1

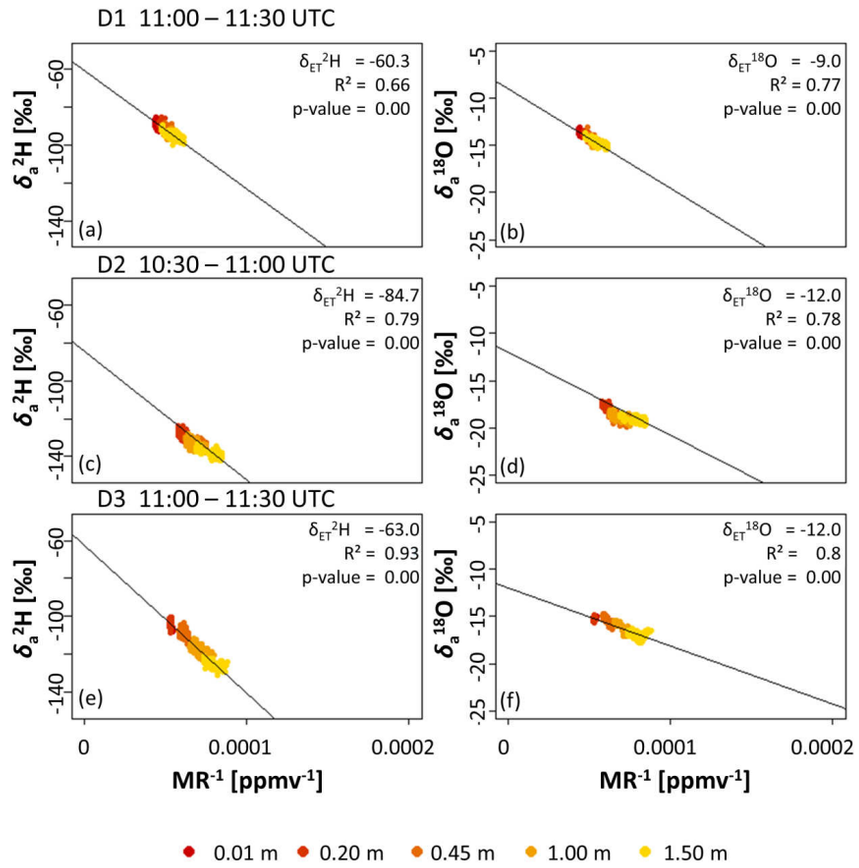

Figure 3.2
Exemplary Keeling plots of $\delta_a{}^2H$ (a,c,e) and $\delta_a{}^{18}O$ (b,d,f) of water vapor measured at different heights (0.01-1.50 m) within and above the canopy on D1 (29 May 2017, 11:00–11:30 UTC), D2 (13 July 2017, 10:30–11:00 UTC) and D3 (21 August 2017, 11:00–11:30 UTC). The value of the y-intercept (δ_{ET}), the coefficient of determination (R^2) and p-value are reported.

3.4.2 *ET* partitioning

The hydrogen stable isotopic composition of *E*, *T*, and *ET*, as well as the corresponding calculated values for *T*/*ET* are shown in Figure 3. The light blue area indicates nighttime periods. During the first two campaign days, $\delta_{ET}{}^2$H spanned between –60.3 ± 1.1 ‰ (D1, 11:15 UTC) and –102.6 ± 0.8 ‰ (D2, 08:45 UTC). On D3, the highest values were observed before sunset (–29.1 ± 1.8 ‰) and after sunrise (–40.5 ± 2.8 ‰); the lowest recorded value was –77.9 ± 1.0 ‰ at 09:15 UTC. $\delta_T{}^2$H (= $\delta_x{}^2$H) ranged between –54.2 ± 0.1 ‰ (D1) and –38.3 ± 0.2 ‰ (D3, 08:45 UTC). $\delta_E{}^2$H(S) (calculated with Eq. (2)) varied from –81.2 ± 11.1 ‰ (D2, 08:45 UTC) to –127.8 ± 3.5 ‰ (D1, 12:15 UTC). Due to occurrence of dewfall on D3, a nighttime increase of $\delta_E{}^2$H was observed between 19:15 and 03:15 UTC. $\delta_E{}^2$H values derived from the soil profiles were only available on the two last campaign days. Higher $\delta_E{}^2$H values were calculated on the basis of destructive sampling (S) than determined from the monitoring of the soil profile (P) (with a mean absolute difference of 3.2 ‰ on D2). During D3, $\delta_E{}^2$H(S) values were in average 10.0 ‰ higher than $\delta_E{}^2$H(P).

On D2 at 08:45 UTC, on D3 at 18:15 UTC (i.e., shortly before sunset) and 05:15 UTC (shortly after sunrise), it occurred that $\delta_{ET} < \delta_E$ or $\delta_{ET} > \delta_T$, leading to *T*/*ET* ratio estimates smaller than 0 or greater than 1. The discrepancies in $\delta_E{}^2$H between S and P caused only slightly different results for *T*/*ET*. Against our expectations, we did not observe an increase in *T*/*ET* with increasing LAI. During D1, the soil water content near the surface was considerably lower than during D2 and D3 (Table 1) which could have caused a low evaporation rate. Plant transpiration can use water from deeper soil layers (θ (–0.10 m) = 0.21 m^3 m^{-3}) than soil evaporation, which could explain the comparably high *T*/*ET* during D1. The low value for δ_x (Table 1) also supports this assumption.

Analogous results for oxygen stable isotopic composition are shown in Figure 3.4. During D1 and D2, $\delta_{ET}{}^{18}$O varied between –9.0 ± 0.1 ‰ (D1, 11:15 UTC), and –12.0 ± 0.1 ‰ (D2, 10:45 UTC). On D3, the highest values were observed before sunset (6.9 ± 0.4 ‰) and after sunrise (–2.5 ± 0.3 ‰), and the lowest (–12.0 ± 0.1 ‰) at 09:15 UTC. $\delta_T{}^{18}$O ranged between –4.6 ± 0.1 ‰ on D3 (08:45 UTC) and –7.9 ± 0.1 ‰ on D2. $\delta_E{}^{18}$O(S) varied from –7.9 ± 1.9 ‰ (D3, 05:15 UTC, influence of the dewfall) to –28.9 ± 1.8 ‰ (D3, 6:15 UTC). Values for $\delta_E{}^{18}$O(P) were available on D2 and D3. The largest discrepancies between $\delta_E{}^{18}$O(S) and $\delta_E{}^{18}$O(P) were observed on D2, with a mean difference of 5.6 ‰, while on D3 the mean observed difference was only 1.1 ‰. The calculated *T*/*ET* values were within the theoretical range, except for the values of D3 between 17:15 and 05:15 UTC. Similar to hydrogen isotopic composition measurements, the observed differences between $\delta_E{}^{18}$O(S) and $\delta_E{}^{18}$O(P) had a minor impact on the

calculated *T/ET* values. All δ^{18}O-based *T/ET* estimates were higher than those based on δ^{2}H (D1 by 0.06, D2 by 0.36 and D3 by 0.08).

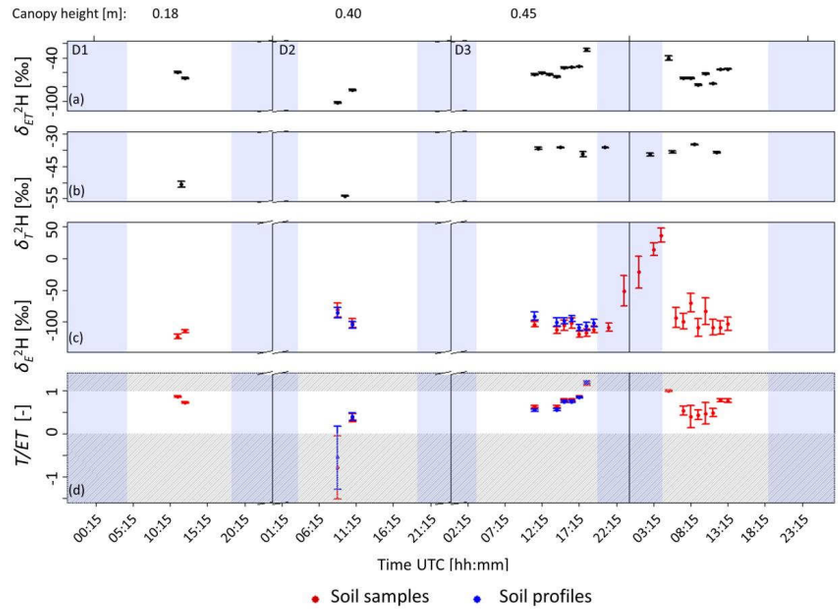

Figure 3.3
(a) Hydrogen isotopic composition of the evapotranspiration flux ($\delta_{ET}{}^{2}$H in ‰), determined with the Keeling plot approach (only results with $R^2 > 0.6$ are shown); (b) hydrogen isotopic composition of the transpiration flux ($\delta_{T}{}^{2}$H in ‰) inferred from that of the water extracted from the plant xylem sap ($\delta_{x}{}^{2}$H in ‰) and assuming isotopic steady-state conditions ($\delta_{T}{}^{2}\mathrm{H} = \delta_{x}{}^{2}\mathrm{H}$); (c) hydrogen isotopic composition of the evaporation flux ($\delta_{E}{}^{2}$H in ‰) calculated with Equation (3.3) on basis of either destructive (sampling of soil down to 5 cm depth, red symbols) or non-destructive (monitoring system with the tubing profiles, blue symbols) determination of δ_{s}^{l}; (d) transpiration fraction (*T/ET*) calculated with Equation (3.1) on the basis of destructive (red) and non-destructive determination of δ_{s}^{l} (blue). Grey shaded areas indicate values outside the theoretical range, and blue shaded areas represent nighttime periods.

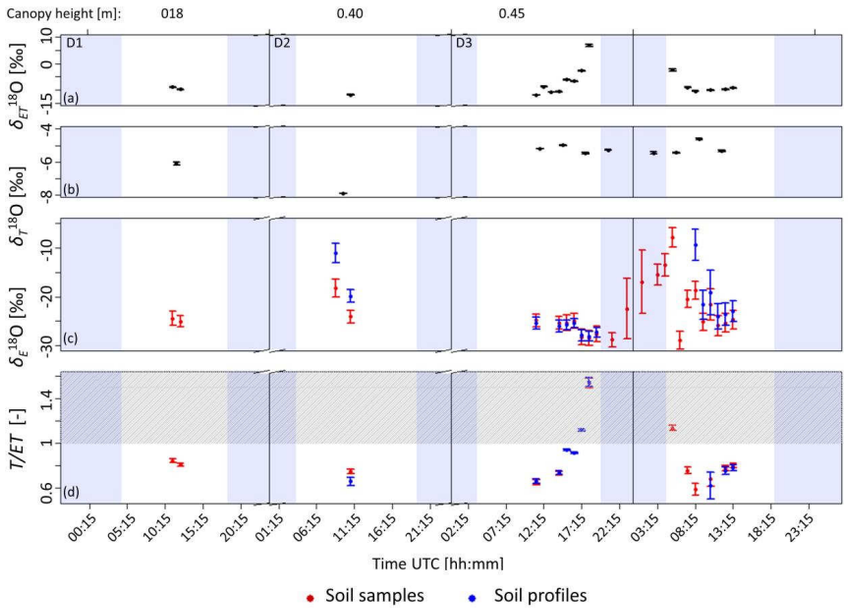

Figure 3.4
(a) Oxygen isotopic composition of the evapotranspiration flux ($\delta_{ET}{}^{18}O$ in ‰), determined with the Keeling plot approach (results with $R^2 > 0.6$ are shown); (b) oxygen isotopic composition of the transpiration flux ($\delta_{T}{}^{18}O$ in ‰) inferred from that of the water extracted from the plant xylem sap ($\delta_{x}{}^{18}O$ in ‰) and assuming isotopic steady-state conditions ($\delta_{T}{}^{18}O = \delta_{x}{}^{18}O$); (c) oxygen isotopic composition of the evaporation flux ($\delta_{E}{}^{18}O$ in ‰) calculated with Equation (3.3) on the basis of either destructive (sampling of soil down to 5 cm depth, red symbols) or non-destructive (monitoring system with the tubing profiles, blue symbols) determination of δ_s^l; (d) transpiration fraction (*T/ET*) calculated with Equation (3.1) on the basis of destructive (red) and non-destructive determination of δ_s^l (blue). Grey shaded areas indicate values outside the theoretical range, and blue shaded areas represent nighttime periods.

3.4.3 Latent heat flux of *E* and *ET*

The latent heat fluxes corresponding to *ET* (L_{ET}, W m^{-2}) measured by the EC station, together with the latent heat flux corresponding to *E* (L_E) obtained from the micro-lysimeter measurements, and the isotope-based *T/ET* estimates are shown in Figure 3.4. L_{ET} increased with increasing LAI. Generally, discrepancies between the L_E estimates based on the different methods (δ^2H, δ^{18}O and micro-lysimeters) were found. During D1, the estimates based on δ^2H(S) showed the lowest L_E with, e.g., 28.6 W m^{-2} at 11:15 UTC, δ^{18}O(S)-based estimates were slightly higher with a value of 33.3 W m^{-2} at 11:15 UTC, whereas the lysimeter estimates showed a higher value of 80.5 W m^{-2} at 11:45 UTC. On D2, the lowest L_E was again estimated on the basis of δ^{18}O measurements, with, e.g., L_E(S) = 71.5 W m^{-2} and L_E(P) = 96.6 W m^{-2} at 10:45 UTC. L_E(S) values inferred from δ^2H were higher (e.g. L_E(S) = 180.3 W m^{-2} and L_E(P) = 171.7 W m^{-2}). The lysimeter-derived estimate was 165.5 W m^{-2}, close to the range of the δ^2H estimates.

On D3, a diurnal variation of L_E was observed. On 21 August 2017, the L_E estimates derived from δ^2H were slightly lower than the values obtained with the lysimeter method. On average, L_E(lysimeter) was 12.9 W m^{-2} higher than L_E(S) and 7.0 W m^{-2} higher than L_E(P). L_E estimates derived from δ^{18}O(P) (δ^{18}O(S)) measurements were lower than L_E(lysimeter), with a mean absolute difference of 32.4 W m^{-2} (31.8 W m^{-2}). At the beginning of 22 August 2017, both isotope-based estimates for L_E showed higher values compared to the lysimeter method until 11:15 UTC. From this point onward, isotope-based estimates were lower than those of the lysimeter approach, i.e., δ^2H-based L_E(S) by 25.1 W m^{-2}, δ^{18}O-based L_E(S) by 29.2 W m^{-2} and δ^{18}O-based L_E(P) by 24.3 W m^{-2}.

Based on the L_{ET} measurements, weighted mean daily *T/ET* ratios were calculated (Table 2). Negative L_{ET} values as well as *T/ET* >1 and *T/ET* < 0 were excluded. In general, δ^{18}O-based estimates following both destructive (S) and non-destructive (P) sampling were higher than those obtained from δ^2H or micro-lysimeter measurements. δ^2H- and micro-lysimeter-based estimates agreed better (especially on D3.1 before sunset), with a RMSE of 0.178 (*T*/*ET* (S) vs. *T*/*ET* (micro-lysimeter)) and 0.099 (*T*/*ET* (P) vs. *T*/*ET* (micro-lysimeter))

Table 3.2

Weighted mean *T/ET* ratios ($= \sum(L_{ET} * T/ET) / \sum(L_{ET})$, cases where negative L_{ET} values or *T/ET* >1 and *T/ET* < 0 were discarded from the analysis) for the micro-lysimeter estimates as well as δ^2H and δ^{18}O estimates obtained from the soil sampling (S) and the soil profiles (P).

T/ET	**Micro-lysimeter**	**δ^2H**		**δ^{18}O**	
		(S)	(P)	(S)	(P)
D1	0.54	0.79	NA	0.82	NA
D2	0.53	0.36	0.39	0.75	0.66
D3.1 (before sunset)	0.64	0.69	0.63	0.77	0.78
D3.2 (after sunset)	0.75	0.57	NA	0.72	0.71

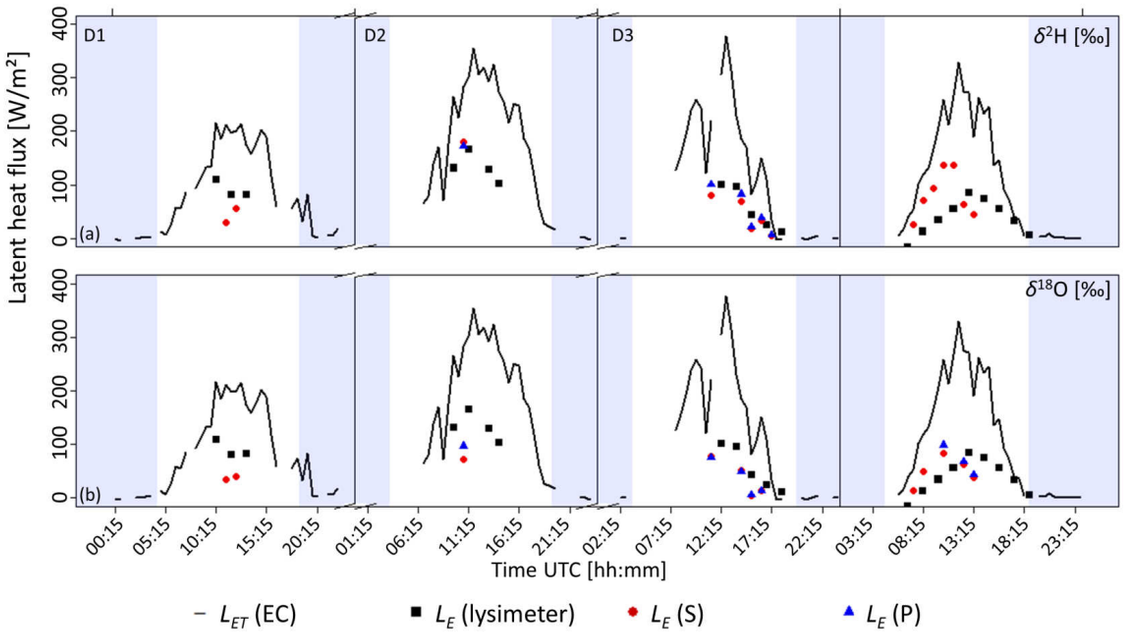

Figure 3.5

Latent heat flux (W m^{-2}) of evapotranspiration measured by the eddy covariance station (L_{ET}(EC), black line) and partitioning results for the latent heat flux of evaporation obtained from single measurements with micro-lysimeters (L_E(lysimeter), black squares), from the soil samples (L_E(S), red dots) and soil profiles (L_E(P), blue triangles) for (a) δ^2H and (b) δ^{18}O**.** Blue shaded areas represent the nighttime period. L_E(S) and L_E(P) were calculated on basis of isotope-derived *T*/*ET* ratios and L_{ET}(EC) using the following relationship: $L_E = 1 - T/ET * L_{ET}$.

3.5 Discussion

3.5.1 Differences between destructive and non-destructive methods

In this study we compared measurements of the isotopic composition obtained from destructive soil sampling and non-destructive soil profile measurements. The former method is widely used in source-partitioning studies (Walker and Brunel 1990, Williams et al. 2004, Dubbert et al. 2013). However, it involves the time-consuming and labor-intensive extraction of water by, e.g., vacuum distillation (Orlowski et al. 2013) or direct vapor equilibration (Wassenaar et al. 2008). Destructive sampling also has a strong impact when soil availability is limited, e.g., in mesocosms experiments. However, this is usually not a problem under field conditions.

The method used in the present study, which was previously developed by Rothfuss et al. (2013), and successfully applied in the laboratory by Gangi et al. (2015), Rothfuss et al. (2015) and Quade et al. (2018), enables long-term monitoring of the soil water vapor isotopic composition in a non-destructive manner. It only requires a temperature correction of the isotopic values of the sampled water vapor to obtain the soil liquid water isotopic composition over a wide range of soil water content values, without the need to account for additional (kinetic) fractionation effects (Rothfuss et al. 2013). One limitation of the monitoring approach is its non-applicability in case of water vapor condensation in the tubing between the sampling location and the laser spectrometer. It is therefore mandatory to insulate (and ideally to heat) the tubing to reduce temperature gradients between the soil and the atmosphere, and thereby to avoid condensation.

Orlowski et al. (2016a), (2018) showed that there were significant differences in water isotopic composition of soil waters determined with different water extraction methods and that these differences were significantly correlated to soil texture and soil water content. In their study, Orlowski et al. (2016a) did not benchmark our sampling method together with the traditionally used ones. Among the examined methods, the one resembling our monitoring method the most in terms of design and modus operandi was the direct vapor equilibration method. Considering their findings for this method, we should have observed higher values for $\delta_S(P)$ than for $\delta_S(S)$. This was almost always the case (Figure 3.3c and 3.4c), although differences between $\delta^2H(P)$ and $\delta^2H(S)$ were larger than between $\delta^{18}O(P)$ and $\delta^{18}O(S)$ when taking the standard deviations into account.

Errors in the estimation of δ_S values lead to inaccurate estimates of the isotopic composition of the evaporated water vapor when using the Craig and Gordon (1965) model, and ultimately will affect the *T/ET* estimates. However, not only the value of δ_E has consequences for the calculation of *T/ET*, but also

the relative distribution of the two end-members of Equation (3.1) (Rothfuss et al. 2010). A significant difference of δ_E has relatively low impact on the final *T/ET* value, when the difference between δ_E and δ_T is large. When considering the values within the theoretical range (i.e., $0 \leq T/ET \leq 1$), the highest observed *T/ET* difference between the soil samples and the soil profiles (0.09) resulted from a difference of 12.7 ‰ in δ^2H_E(S) and δ^2H_E(P) (D3, 8:45 UTC). The *T/ET* estimates derived from $\delta^{18}O$ were even less sensitive. Here, the highest difference of *T/ET* (0.08) was caused by a difference of 4.0 ‰ between $\delta_E{}^{18}$O(P) and $\delta_E{}^{18}$O(S) (D3, 10:45 UTC). Outliers in the transpiration fraction (*T/ET* > 1 or < 0) during D3 can be explained by low wind conditions and beginning dewfall (sunset) or dew evaporation (sunrise).

A quantitative comparison of the *T/ET* estimates by the different isotope-based methods is shown in Figure 3.6. The greatest discrepancies were found by comparing δ^2H- and δ^{18}O-based estimates. Here the mean differences (*T/ET*(δ^2H) – *T/ET*(δ^{18}O)) were equal to –0.15 for the soil samples and –0.22 for the soil profiles. The mean *T/ET* differences between S- and P-based estimates were smaller by a factor of more than 10, i.e., –0.01 for δ^2H and –0.02 for δ^{18}O.

The discrepancies between *T/ET*(S) and *T/ET*(P) derived from both isotopologues are directly linked to the discrepancies between δ_E(P) and δ_E(S), which could be partly explained by the natural heterogeneity of δ_s^l in an agricultural field. Additionally, the underlying measurement principles are different, leading to a distinct spatial and temporal representativeness of each method. While δ_s^l(S) is the mean value of the isotopic composition of the soil water sampled in a few minutes in different locations across the test site, δ_s^l(P) is inferred from the mean value of the isotopic composition of the soil water vapor sampled at one single depth from the vicinity of the gas-permeable tubing over a longer time period (i.e., in our case 10 min). While it appears more or less straightforward to calculate the volume of soil sampled destructively during the experiments, it is certainly more difficult to estimate the volume of soil from which the water vapor was sampled non-destructively. Under near-saturated conditions, for instance, this would correspond to a representative soil volume of approx. 42 cm^3 assuming that the soil water vapor originated from a maximum distance of 1 cm from the tubing walls. On the other hand, water vapor transport distance is larger under dry conditions, leading to a much greater sampling volume (e.g., 526 cm^3, assuming a maximum sampling distance of 5 cm around the tube). The destructively sampled water volume was less variable, ranging from approx. 65 cm^3 under saturated soil conditions and 19 cm^3 under dry soil conditions (for a soil sample weight of 300 g at field bulk density). One way to further increase the spatial representativeness of the non-destructive sampling would be to increase the length of the gas-permeable tubing. However, this could lead to a greater loss of sampling air through the walls

of the gas-permeable tubing, especially under dry conditions, and therefore limit the applicability of the method itself.

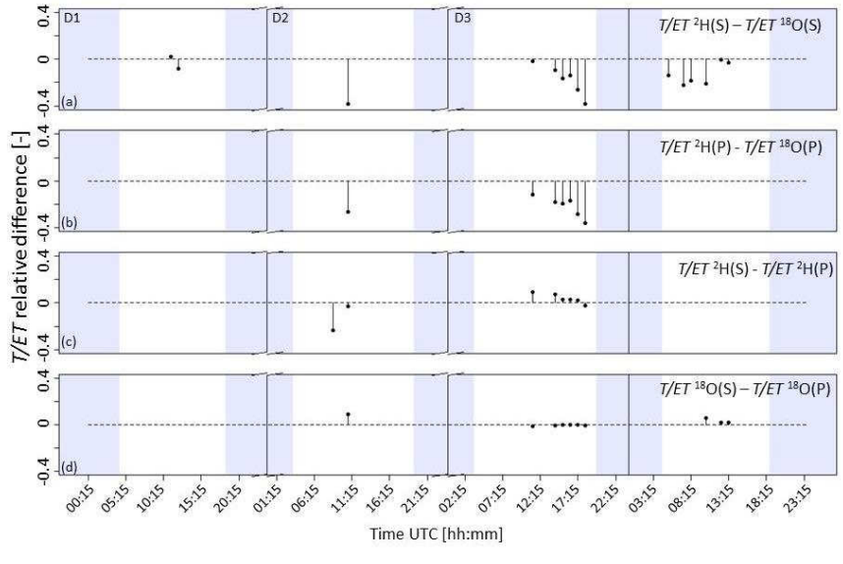

Figure 3.6
Relative differences in transpiration fraction (*T/ET*) derived from (a) soil samples (S) (δ^2H-estimates – δ^{18}O-estimates), (b) soil profiles (P) (δ^2H-estimates – δ^{18}O-estimates), (c) δ^2H-estimates (S – P), and (d) δ^{18}O-estimates (S – P). Blue shaded areas represent nighttime periods.

3.5.2 Sensitivity of *T/ET* estimates to uncertainty of δ_E, δ_T, and δ_{ET} values

The calculation of the isotope-based *T/ET* values also depends on two other sensitive variables, namely δ_{ET} and δ_T. δ_{ET} was estimated by the Keeling plot approach (Keeling 1958), which was used previously in a number of studies (Wang and Yakir 2000, Xu et al. 2008, Aouade et al. 2016). Obtaining δ_{ET} requires the assumption that δ_E and δ_T do not change over the measurement period. Good et al. (2012) showed that a sampling period of 30 min (which was also chosen in the present study) resulted in the highest accuracy of their δ_{ET} estimates. In the present study, the Keeling plot technique, based on vertical gradients of atmospheric MR and isotopic composition measured in and above the canopy (Williams et al. 2004, Wang et al. 2010, Aouade et al. 2016), was favored over that based on temporal changes of MR and isotopic composition observed at one or two heights over the canopy (Good et al. 2014, Wei et al. 2015, Wang et al. 2016). The precision of Keeling-plot-derived δ_{ET} estimates, i.e., the standard error of the calculated water vapor isotopic composition value when the inverse of MR theoretically equals zero,

relies on the spread of both MR and isotopic composition values. Even though the temporal resolution of δ_{ET} estimates can be significantly increased, obtaining a precise estimate of δ_{ET} on the basis of vertical gradients rather than temporal changes of MR and isotopic compositions is much more challenging. Therefore, the explanatory power and the significance of the results were carefully evaluated by means of the coefficient of determination (R^2) and the p-value, respectively. Values below the thresholds of $R^2 > 0.6$ and $p < 0.05$ were systematically excluded from the analysis.

δ_E values were estimated following the model of Craig and Gordon (1965), which is based on a transfer resistance analogy and initially describes water vapor isotopic transport from a freely evaporating surface. It was applied in the present study to the evaporation of soil water, leaving δ_E sensitive to changes of relative humidity, soil and air temperature as well indirectly to soil water content (according to the model of Mathieu and Bariac 1996). However, fast changes of either one of these variables within 30 min caused by unstable weather conditions were not observed during our campaign days.

δ_T was obtained from measurements of the extracted xylem (x) water of the sugar beets' root crown, assuming isotopic steady state of the transpiration flux ($\delta_T = \delta_x$). Leaf water reaches isotopic steady state at a constant transpiration rate, i.e., when leaf transpiration losses are exactly compensated by inflow of xylem water. Isotopic steady state occurs when weather conditions and water availability for root water uptake remain stable long enough over the course of the experiment. How fast isotopic steady state is reached within the leaf also depends on the water turnover time in the leaf (i.e., the ratio of transpiration rate and water volume contributing to transpiration; Dubbert et al. 2017). During none of three campaign days we observed visible plant water stress, which would have indicated stomata closure and possible departure from isotopic steady state. Sugar beet develops a central root system of up to 2 m depth, enabling access to deep soil water when necessary. The lowest soil water content at 1 m depth was 0.35 $m^3\ m^{-3}$ in our study, observed on 22 August 2017 at 13:30 UTC, suggesting sufficient water availability for sugar beet during the whole study period.

Furthermore, the relatively large water volume of a sugar beet leaf involved in transpiration could lead to significant temporal changes of leaf water turnover rates when transpiration rate is low and could therefore lead to departure from or delayed arrival at isotopic steady state. However, although we did not determine the water volume of the sugar beet leaves in-situ as done in other studies (e.g. Hu et al. 2014), we did not observe low transpiration rates which would have invalidated our assumption of isotopic steady state. Another problem that can occur during destructive determination of δ_T from δ_x is the possible contamination of the xylem water with enriched water from the base of the leaves that has already undergone isotopic fractionation during transpiration. However, this was accounted for in our

study by systematically removing any green tissue and sampling the central (white) part of the root crown, which is not exposed to the ambient air conditions.

3.5.3 From *T/ET* to ecosystem latent heat fluxes

Finally, *T*/*ET* results obtained from the isotope-based approach were used to calculate the latent heat flux of E (L_E) from the latent heat flux of ET (L_{ET}) measured by the EC station using the following relationship: $L_E = 1 - T/ET * L_{ET}$. This allowed the comparison of the isotope-derived results of L_E with those obtained from the micro-lysimeter measurements. In case of the micro-lysimeter measurements, soil evaporation was determined by small weight changes of the undisturbed soil monoliths with the exclusion of drainage and plant water uptake from and capillary rise to the lysimeters. The micro-lysimeters were only installed for one or two days to minimize discrepancies with the general field conditions (as suggested by e.g., Boast and Robertson 1982, Evett et al. 1995, Kool et al. 2014). However, the surface of the lysimeter monoliths dried out faster than the surrounding soil surface (most notably during D1). Possible causes include slightly less shading by the surrounding plants than experienced by the undisturbed soil surface on average, and less than perfect thermal contact between lysimeter and surrounding soil. During a typical daytime situation in the growing season, the latter would lead to increased heating and thus an overestimation of evaporation (Evett et al. 1995). On the other hand, the blocking of upward water (vapor) movement by the lysimeter bottom could lead to an underestimation especially later during the day. Accidental loss or addition of soil during weighing of the lysimeters as well as wind and temperature effects on the scale could lead to additional random, but no systematic errors. Shawcroft and Gardner (1983) started that accurate evaporation measurements via lysimeters depend on a number of compensating errors, while Kool et al. (2014) implied micro-lysimeters as the most reliable measurement method for soil evaporation. The deviation between the four micro-lysimeters was small for D1, D3 and the last three measurements on D2, suggesting a high accuracy under the assumption of homogeneous field conditions.

Assuming that micro-lysimeters are more likely to over- than underestimate soil evaporation fits well to the isotope-based partitioning results. On the other hand, the isotope-based evaporation estimates could be underestimated due to multiplication of the evaporation fraction with the EC-based latent heat flux. EC fluxes are subject to the energy balance closure problem, which may indicate an underestimation of the turbulent sensible and/or latent heat flux (Foken et al. 2011). The Selhausen site is no exemption and shows on average an energy balance closure gap of 15 % (Eder et al. 2015, Ney and Graf 2018).

The δ^2H and δ^{18}O estimates of the latent heat flux of *E* led to different results. For δ^2H, estimates were more variable and less precise than those derived from δ^{18}O. One reason might be the lower precision of

the laser analyzer regarding analysis of δ^2H due to the much lower abundance of ^{2}H compared to ^{18}O, associated with a much weaker absorption line for ^{2}H than for ^{18}O in the near-infrared spectral region of the analyzer. Another reason could be related to a small effect of the tubing system on the hydrogen isotopic composition of the water vapor by exchange of protons between the water vapor and the tubing material, which would only affect δ^2H, but not δ^{18}O. This, together with the fact that lysimeters may overestimate the latent heat flux, suggests that the δ^{18}O-derived *T/ET* estimates were the most reliable.

3.6 Conclusion

In this study, we tested the non-destructive continuous method (P) of Rothfuss et al. (2013) for partitioning of *ET* of a sugar beet (*Beta vulgaris*) field into *E* and *T*, and compared its outcome with traditional destructive sampling (S) of soil water. Only small discrepancies (on average 0.01 for δ^2H and 0.02 for δ^{18}O) were found between *T/ET* values derived with the two isotopic methods for determination of soil liquid water isotopic composition, even though differences of computed δ_E values were significant (maximum differences were 12.7 ‰ for δ^2H and 9.3 ‰ for δ^{18}O).

Furthermore, it was possible to compare the isotope-derived *T/ET* estimates to those of the EC and micro-lysimeter techniques. Mean absolute deviations of isotope-based from micro-lysimeter-based estimates of latent heat flux of evaporation (L_E) were lower than 38.9 W m^{-2} and were maximal for δ^2H(S) measurements. These differences were more than three times higher than the mean absolute differences between L_E(P) and L_E(S) derived from both hydrogen and oxygen stable isotopic compositions of soil water. The latter discrepancy is in line with recent findings on the systematic offsets of water isotopic compositions values between existing methods for extraction of water from soil samples for isotope analysis, and partly highlight the need for further investigation of these offsets for accurate separation of *E* from *T* in the field.

Chapter 4

Progress and Challenges of Isotope Based Source Partitioning of Evapotranspiration

Based on a document prepared for submission:

Quade, M. Dubbert, M. Brüggemann, N. Graf, A. Vereecken, H. and Rothfuss, Y.: Progress and Challenges of Isotope Based Source Partitioning of Evapotranspiration (in preparation)

4.1 Introduction

The atmospheric water vapor is an important contributor to the greenhouse effect of the Earth's atmosphere. For reliable predictions of meteorological and hydrological forecasting models, a good knowledge of the single sources (e.g., evaporation, *E*, and transpiration, *T*) within the atmospheric water budget is crucial. Flux measurement stations (e.g., Terrestrial Environmental Observations (TERENO), http://teodoor.icg.kfa-juelich.de) usually measure the net flux of the atmospheric water vapor above the land surface (evapotranspiration, *ET*) via the eddy covariance (EC) technique. Disentangling the net *ET* flux into its raw components *E* and *T* is performed by source partitioning methods. These methods can be divided into instrumental approaches (Kool et al. 2014) and correlation-based modelling approaches (Scanlon and Kustas 2010). The instrumental approaches include additional measurements, e.g. soil-flux chamber measurements (Raz-Yaseef et al. 2010, Lu et al. 2017), micro-lysimeter measurements (Kelliher et al. 1992) or atmospheric profile measurements (Ney and Graf 2018).

Another powerful instrumental method to partition ET is using the difference of properties of heavier stable isotopologues of water ($^{1}H^{2}H^{16}O$ and $^{1}H_{2}{}^{18}O$) relative to $H_{2}{}^{16}O$. The evaporation process of a water body is affected by equilibrium and kinetic fractionation, which lead to an isotopically depleted isotopic composition of the evaporated water vapor (δ_E) compared to that the liquid soil water (Craig and Gordon 1965). On the other hand, the isotopic composition of the transpired water vapor (δ_T) usually equals that of the soil water source used by the plants due to the fact that plants transpire mostly at isotopic steady state (Yakir and Sternberg 2000). Even when steady-state conditions are not reached for leaf water, the magnitude of the isotopic depletion of leaf transpiration is lower than for evaporation. In most cases, therefore, the mixture of water vapor from both sources, i.e., *ET*, has an isotopic composition (δ_{ET}) value $\delta_E < \delta_{ET} < \delta_T$. By considering only two sources (*E* and *T*) contributing to ET, the transpiration fraction (*T/ET*) is obtained by inverting the isotopic mass balance equation $\delta_{ET} = (1 - T/ET)\delta_E + (T/ET)\delta_T$:

$$T/ET = \frac{\delta_{ET} - \delta_E}{\delta_T - \delta_E} \quad (4.1)$$

Thus, *T/ET* can be obtained from measurements of the hydrogen and oxygen stable isotopic composition ($\delta^{2}H$ and $\delta^{18}O$) of the single components *ET*, *E* and *T*.

The aim of this study is to give a literature overview of the progress and challenges of the different measuring/modeling methods for determining of δ_E, δ_T and δ_{ET} and partitioning *ET* both in the field and in the laboratory. In total, 31 studies were analyzed, a detailed overview of the studies is given in Appendix E, Table E2.

43 % of the reviewed studies (Fig. 4.1d) estimates δ_{ET} via the atmospheric Keeling (1958) plot approach (see section 4.2). For this, measurements of the water vapor concentration and isotopic composition at different heights within and above the canopy are required. In the first studies (e.g. Wang and Yakir 2000, Yepez et al. 2003), water vapor was collected by a cryogenic trapping system, which was time-consuming, labor-intensive and expensive to deploy in the field. The water is sampled at different heights by a pump into a small trap cooled with dry ice. With the development of laser absorption analyzers, online measurements of the isotopic composition of water vapor became possible. First, Lee et al. (2007) applied tunable diode laser spectroscopy successfully in the field for partitioning evapotranspiration in a mixed forest in Connecticut, USA. Since 2007, isotope-based partitioning studies increased rapidly (Fig. 4.1a) to approx. 1.3 publications per year (1990-2006: 0.4 publications per year). Chamber measurements have also been common for the estimation of δ_{ET}, 17 % of the reviewed studies used chambers in a similar way as for the estimation of δ_E. Other methods are the flux gradient technique (18 %) and EC measurements (3 %). The former uses vertical gradients of the gas concentration, e.g. water vapor in two heights and is mathematically nearly identical to the Keeling (1958) plot approach (section 4.2). The EC technique is the standard method to measure vertical turbulent fluxes of carbon, water and energy from the atmospheric boundary layer into the free atmosphere and is established in a worldwide network (FLUXNET, http://fluxnet.fluxdata.org). Griffis et al. (2010) successfully used the EC technique to calculate δ_{ET} by assuming that the usually used total water vapor flux equation (Equation 4.5 in section 4.2.1) is valid for the isotopic composition of the water vapor flux.

74 % of the analyzed studies (e.g. Walker and Brunel 1990, Wang et al. 2010, Sun et al. 2014) determined δ_E via the Craig and Gordon (1965) model (Fig. 4.1b). The Craig and Gordon (1965) model equation is presented in detail in section 4.3 and describes the enrichment process of an open water body during evaporation into the unsaturated atmosphere. To calculate δ_E, the model requires simultaneous measurements of meteorological variables (air and soil temperature, relative humidity and soil water content) as well as measurements of liquid soil water isotopic composition at the evaporation front (δ_{EF}) and the background isotopic composition of the atmosphere (δ_a). δ_{EF} is determined either following destructive soil sampling (e.g. Walker and Brunel 1990, Xu et al. 2008, Wei et al. 2018) or via the recently developed non-destructive sampling of the soil atmosphere (Rothfuss et al. 2013, Volkmann and Weiler 2014, Gaj et al. 2016). Measurements of δ_a are obtained from sampling atmospheric water vapor with commercial isotopic laser spectroscopy above the canopy. Another common measurement technique uses closed soil chambers. 17 % of the reviewed studies (e.g. Ferretti et al. 2003, Dubbert et al. 2013, Lu et al. 2017) used bare soil chambers in combination with the Keeling (1958) plot or mass-balance approach to obtain δ_E. The former method estimates δ_E via alternating measurements of the in- and outflowing water vapor in a dynamically flushed chamber by considering mass-balance (described

in detail in section 4.3), while the latter (Keeling 1958) estimates δ_E via a linear regression line of the isotopic composition plotted against the corresponding inverse of the water vapor concentration in a closed system (described in detail in section 4.2).

The Craig and Gordon (1965) model is also applied to determine δ_T values under non-steady state conditions (53% of the reviewed studies, Fig. 4.1c, detailed in section 4.4). This approach requires additional measurements, e.g. isotopic composition of leaf water (δ_L) and root zone source water (δ_{source}). 61 % of the analyzed studies which estimated δ_T under non-steady state (NSS) conditions were published in year 2014 or later. The first studies (e.g. Walker and Brunel 1990, Brunel et al. 1997, Wang and Yakir 2000) assumed isotopic steady-state (ISS) conditions (47 % of the reviewed studies, section 4.4), in which $\delta_{T,ISS} = \delta_{source}$, where source water equals the xylem water (Yakir and Sternberg 2000). However, more recent evidence (Dubbert et al. 2013) showed that this assumption is only valid during midday, which explains the trend of recent studies (published in year 2014 or later) using the Craig and Gordon (1965) model to estimate δ_T under NSS.

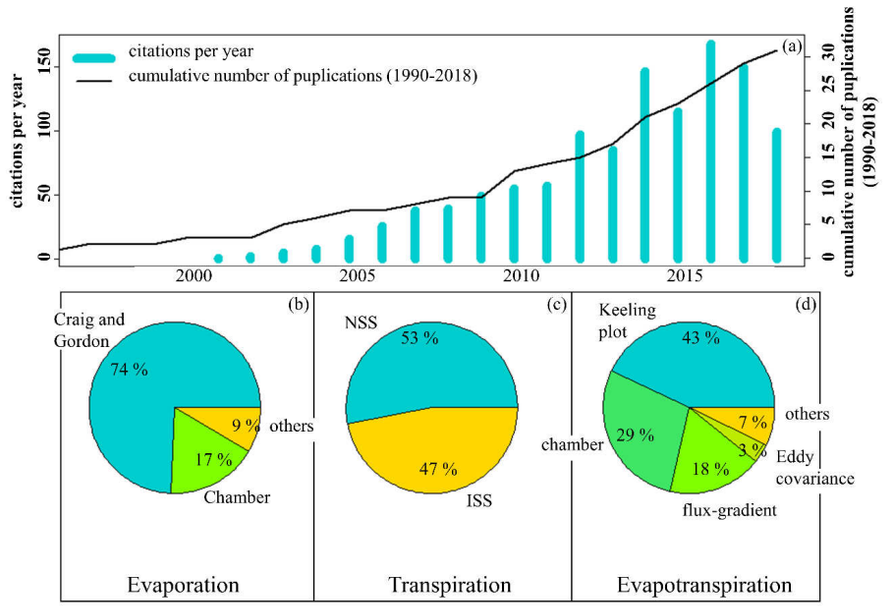

Figure 4.1
Results of the literature review (a): Evolution of the number of citations per year (blue bars) and cumulative number of publications (1990-2018, black line); (b): percentage of methods for determination of δ_E (c): percentage of methods which were used to determine δ_T; (d): percentage of methods which were used to determine δ_{ET}.

4.2 Isotopic composition of evapotranspiration

4.2.1 Methods

43 % of the reviewed studies estimated the isotopic composition of ET via the atmospheric Keeling (1958) approach. The approach assumes that the concentration of the water vapor in the atmosphere (C_a in g m^{-3}) above an ecosystem is a mixture of the background (of concentration C_b in g m^{-3}) and of the emitting source, here evapotranspiration (of concentration C_{ET} in g m^{-3}):

$$C_a = C_b + C_{ET} \tag{4.2}$$

The isotopic composition of these components can be expressed from the mass balance of the water stable isotopologues:

$$\delta_a C_a = \delta_b C_b + \delta_{ET} C_{ET} \tag{4.3}$$

with δ_b being the isotopic composition of the background air. Combining equation (4.1) and (4.2) leads to a simple linear mixing model:

$$\delta_a = \frac{1}{C_a}[C_b(\delta_b - \delta_{ET})] + \delta_{ET} \tag{4.4}$$

Repeated measurements of C_a and δ_a allow for applying a linear regression between both variables:

$$\delta_a = S\frac{1}{C_a} + I \tag{4.5}$$

where $S = [C_b(\delta_b - \delta_s)]$ is the slope and $I = \delta_{ET}$ the y-intercept of the linear regression line (Fig. 4.2).

The atmospheric Keeling (1958) plot approach is based on two assumptions. First, the isotopic compositions of the source and background air are constant over the measurement period. Second, there is no loss of water vapor from the ecosystem, e.g. during dewfall.

Chamber measurements are the second common method to determine δ_{ET} (29 % of the reviewed studies). Technical and mathematical methods are as described in section 4.3.1. Unlike for δ_E, measurements for δ_{ET} are performed with a chamber that covers a soil spot that is covered by vegetation in a representative way.

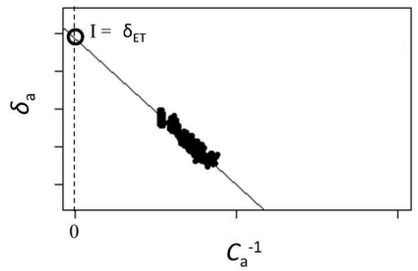

Figure 4.2

Exemplary Keeling (1958) plot.

18 % of the reviewed studies used the flux gradient method based on vertical gradients of the gas concentration, e.g. water vapor measurements at two heights. The water vapor flux from evapotranspiration (F_{ET} in mmol m^{-2} s^{-1}) is proportional to the changes in the mixing ratio of the water vapor ($\Delta\chi_a$ in mol(H_2O) mol(dry air)$^{-1}$) with height Δz [m]:

$$F_{\mathrm{ET}} = -K \frac{\rho_a}{M_a} \frac{\Delta\chi_a}{\Delta z} \tag{4.6}$$

with ρ_a [kg m^{-3}] being the density of dry air, M_a [kg mol^{-1}] the molecular weight of dry air and K [m^2 s^{-1}] the eddy diffusivity of water vapor. Assuming that K is constant at the regarded height over short time scales (< 1 h), the flux ratio of abundant (i = $^1H_2{}^{16}O$) and rare (j = $^1H^2H^{16}O$ or $^1H_2{}^{18}O$) isotopologue can be rewritten as:

$$R_{ET} = {}^iF_{ET}/{}^jF_{ET} \approx \Delta^i\chi_a/\Delta^j\chi_a \tag{4.7}$$

which can also be expressed in δ-notation as:

$$\delta_{ET} = \frac{\Delta^i\chi_a/\Delta^j\chi_a}{R_{std}} - 1 \tag{4.8}$$

R_{ET} is also equal to the slope of the regression line between ${}^i\chi_a$ and ${}^j\chi_a$:

$${}^i\chi_a = R_{ET}\,{}^j\chi_a + C \tag{4.9}$$

with C [-] being the y-intercept. Dividing Equation (4.9) by ${}^j\chi_a R_{std}$ with $\delta_a = \frac{\Delta^i\chi_a/\Delta^j\chi_a}{R_{std}} - 1$ results in:

$$\delta_a = \delta_{ET} + C/R_{std}\frac{1}{{}^j\chi_a} \tag{4.10}$$

By assuming ${}^{j}\chi_{\mathrm{a}} \approx \chi_a$, the approach is nearly identical with the Keeling (1958) plot approach.

Griffis et al. (2010) found a good agreement in water vapor mixing ratios and fluxes (F_{ET}) when comparing traditional eddy-covariance measurements and data processing with a spectral analysis of simultaneous measurements with a tunable diode laser:

$$F_{\mathrm{ET}} = \bar{\rho}_a \overline{\omega' \chi_a'} + S = \bar{\rho}_a \int C_{\omega\chi_a}(f) df + S \qquad (4.11)$$

with ω [m s^{-1}] being the vertical wind velocity (primes indicate instantaneous values, the overbar indicates averaged values over a time period, e.g. 30 min). The term $\overline{\omega' \chi_a'}$ designates the covariance and is equal to the term $\int C_{\omega\chi_a}(f) df$ which is the integrated cospectral density of the fluctuations in the vertical wind velocity and water vapor mixing ratios at the frequency f [Hz]. S [Δ(mol(H_2O) mol(dry air)$^{-1}$)) Δ(m)$^{-1}$] is defined as the storage term which is the rate of change in the atmospheric water molar mixing ratio between the ground and the eddy-covariance instrument height.

Equation 4.11 can be rewritten for the rare (i) and the abundant (j) isotopologue similar as for equation 4.6. The ratio of both isotopic flux equations R_{ET} is than defined as:

$$R_{ET} = {}^{i}F_{ET} / {}^{j}F_{ET} \approx C^{i}_{\omega\chi_\omega}(f) / C^{j}_{\omega\chi_\omega}(f) \qquad (4.12)$$

or expressed in δ-notation:

$$\delta_{ET}(f) = \frac{C^{i}_{\omega\chi_\omega}(f) / C^{j}_{\omega\chi_\omega}(f)}{R_{std}} - 1 \qquad (4.13)$$

4.2.2 Progress and challenges

The Keeling (1958) plot approach can be used in two different ways, either by measuring δ_{a} and C_{a} at one height above the canopy over a certain time interval or at several heights within and above the canopy over shorter time intervals. Three of the studies reviewed here (Good et al. 2014, Wei et al. 2015, Wei et al. 2018) used measurements performed at one single height above the canopy, while the remaining 28 studies used measurements of several heights within and above the canopy. Good et al. (2012) compared these two different methods with a third method which uses the mean values of the isotopic composition of the atmospheric water vapor from each height. After a detailed uncertainty analysis, they concluded that the use of mean values increased the uncertainty of the final value of δ_{ET}, whereas for the other two methods (which used all data points) the uncertainty of δ_{ET} was comparably small. However, they found different δ_{ET} values for the measurements at a single height vs. several measuring heights during the same time interval. The authors could not conclude which value was the most representative.

In addition, they found a good agreement between the Keeling (1958) plot approach, applied at different heights, and the flux gradient method due to the similarity of Equation 4.5 and 4.10. The Keeling (1958) plot approach was also successfully applied to closed chamber measurements by Yepez et al. (2005) and Wang et al. (2013). However, chamber measurements have the disadvantage of creating non-natural conditions. The temperature and relative humidity inside the chamber can be significantly higher than *h*' and T_a. In addition, water vapor can condense on the inside of the chamber or within the tubing system, resulting in isotopic fractionation and leading to unstable and unreliable isotopic results.

Dynamic chamber measurements, which are based on the mass-balance approach, may reduce the problem of condensation inside the chamber. It is also possible to flush the dynamic chamber with dry air, so that the sampled water vapor only originates from the source(s) inside the chamber. Stable measurements over a certain time period would indicate ISS, and δ_{ET} can be directly measured without any further calculations. However, dry air can stress the plants due to an unnaturally high water vapor concentration gradient between the stomata and the atmosphere, which can result in NSS conditions.

Both the atmospheric Keeling (1958) plot approach and the flux-gradient technique suffer from the need of significant differences (high spatial gradients) in the water vapor mixing ratio and isotopic composition between the soil/canopy surface and the free atmosphere to obtain precise values of δ_{ET}. A portable, elevator-based facility as developed by Ney and Graf (2018) and designed for atmospheric CO_2 and water vapor concentration measurements, allows to measure highly vertically resolved water vapor isotopic profiles to infer *ET* and δ_{ET}. Such profile measurements, however, need high throughput analyzers to provide reliable information on ecosystem fluxes. Commercially available cavity ring-down laser spectrometers operate in low-flow mode at low frequency (e.g. 35 ml min^{-1} and 1.3 Hz for the L2120-*i*, Picarro, Inc., Santa Clara, CA, USA) and are, thus, not suitable for such measurements. To our knowledge only two instruments are able to monitor water vapor stable isotopic compositions at higher flow rate (φ) and higher frequency (*f*): the lead-salt tunable diode laser spectrometer TGA200 (Campbell Scientific, Inc., Logan, Utah, USA; φ = 1.7 l min^{-1} at f = 10 Hz) and the Quantum Cascade Laser (QCL) Trace Gas Monitor (Aerodyne, Inc., Billerica, MA, USA; $\varphi \leq 250$ l min^{-1} and f = 10 Hz), although for the latter no published results are available.

These instruments could be used for isotopic eddy covariance measurements, which are not common yet within the isotopic source-partitioning community. Only one study (Griffis et al. (2010)) demonstrated till date that water vapor mixing ratio and fluxes measured with the traditional eddy covariance technique (with infrared gas analyzer) agreed well with the combined eddy-covariance/TGA200 measurements, which suggests that the measured ET isofluxes should be realistic. This measurement brings the advantage of providing δ_{ET} values on a half-hourly basis. The actual disadvantage is that these

instruments are quite large and usually need stable environmental conditions (especially temperature) during field deployment.

4.3 Isotopic composition of evaporated water vapor

4.3.1 Methods

74 % of the analyzed studies (Appendix A, Table A2) determined δ_E by using the Craig and Gordon (1965) model equation:

$$\delta_E = \frac{1}{\alpha_K(1-h')}\left(\frac{\delta_{EF}+1}{\alpha_{eq}} - (\delta_a + 1)h'\right) - 1 \quad (4.14)$$

with δ_{EF} being the isotopic composition of the liquid water at the evaporation front (EF) and h' [%] the relative humidity of the air normalized to the saturated vapor pressure (P_{sat} in Pa) at the temperature of the evaporation front T_{EF} [°C]:

$$h' = h\frac{P_{sat}(T_a)}{P_{sat}(T_{EF})} \quad (4.15)$$

where h [%] is the relative humidity.

The value of δ_E results from the cumulative effect of equilibrium and kinetic fractionation processes. The equilibrium fractionation factor (α_{eq} [-]) was first empirically determined by Majoube (1971) and depends on the surface temperature (T_s in K) of the water body:

$$\alpha_{eq}(T_s) = exp\left(\frac{A}{T_s^2} + \frac{B}{T_s} + C\right) \quad (4.16)$$

with constants A = 1137, B = –0.4156 and C = –0.0020667 for the fractionation of oxygen isotopologues of water, and A = 24844, B = –76.248 and C = 0.052612 for the hydrogen isotopologues of water.

The kinetic fractionation factor (α_K) is defined as the ratio of the transport resistances from the evaporating water surface to the ambient air of the most abundant isotopologue i = $^1H_2{}^{16}O$ and less abundant isotopologues (j = $^1H^2H^{16}O$ or $^1H_2{}^{18}O$). This term was introduced in the Craig and Gordon (1965) model as inversely proportional to the ratio of the molecular diffusivities of $^1H_2{}^{16}O$ (D) and of either $^1H^2H^{16}O$ or $^1H_2{}^{18}O$ (D_i). Later Dongmann et al. (1974) et al. proposed the following expression:

$$\alpha_K = \left(\frac{D_j}{D_i}\right)^n \quad (4.17)$$

where n [-] describes the aerodynamic regime above the liquid-vapor interface. Dongmann et al. (1974) et al. proposed that n ranges from 0.5 (fully turbulent) to 1 (fully diffusive), with a value of 2/3 corresponding to laminar flow conditions. Later Mathieu and Bariac (1996) adapted the definition of n to the case of evaporation from soil and proposed a formulation which includes the soil water content (θ, in $m^3\ m^{-3}$):

$$n = \frac{(\theta_{EF} - \theta_{res})n_a + (\theta_{sat} - \theta_{EF})n_s}{\theta_{sat} - \theta_{res}} \quad (4.18)$$

with θ_{EF}, θ_{res} and θ_{sat} the soil water content at the evaporation front, the residual and saturated water content values. Equation (4.18) therefore states that $n = 1$ when $\theta_{EF} = \theta_{sat}$ and n = 0.5 when $\theta_{EF} = \theta_{res}$.

Like for the estimation of δ_{ET}, bare soil chamber measurements wer used to obtain δ_E (17% of the reviewed studies). Two different types of chambers exist for this purpose. A closed chamber is placed over the bare soil plot and measures the increasing water vapor concentration over a time interval in a closed lope. The y-intercept of the linear regression line of the inverted increasing water vapor concentration against the corresponding isotopic composition estimates δ_E via the Keeling (1958) plot approach (see section 4.2.1, Equation 4.5). Dynamic chambers have an inlet and an outlet where the incoming and outcoming ecosystem water vapor concentration and isotopic composition are measured alternately. With these measurements δ_E is estimated by a mass-balance approach (Dubbert et al. 2013, 2014):

$$\delta_E = \frac{w_{out}\delta_{out} - w_{in}\delta_{in}}{w_{out} - w_{in}} - \frac{w_{in}w_{out}(\delta_{out} - \delta_{in})}{w_{out} - w_{in}} \quad (4.19)$$

with δ_{in} and δ_{out} being the isotopic composition of the water vapor and w_{in} and w_{out} the mole fraction of water [mol(H_2O) mol(air)$^{-1}$] entering the chamber (in) and the mixed sample air (out). It is also possible to flush the dynamic chamber with dry air, so that the sampled water vapor only originates from the source inside the chamber. Stable measurements over a certain time period would indicate steady-state conditions and δ_E is directly measured without any further calculations.

4.3.2 Progress and challenges

The calculation of δ_E via the Craig and Gordon (1965) model depends on simultaneous measurements of h, T_{EF}, θ_{EF} δ_a and δ_{EF}. The measurements of h, T_{EF} and θ_{EF} are usually done via classical temperature and humidity (e.g. capacitive) sensors. Measurements of δ_a are obtained from measurements of the

atmospheric water vapor above the canopy. The most challenging variable to estimate is δ_{EF}. In 26 % of the reviewed studies (e.g. Walker and Brunel 1990, Brunel et al. 1997, Ferretti et al. 2003, Yepez et al. 2003) soil samples were only collected from the soil surface. Subsequently, soil water was extracted in the laboratory (e.g. by distillation, cryogenic vacuum extraction, CO_2 equilibrium, high pressure mechanical squeezing, microwave extraction) and finally measured via an isotope ratio mass spectrometer or an infrared laser absorption analyzer. Studies on the development of soil water stable isotopic profiles during the evaporation process at unsaturated soil conditions (e.g. Barnes and Allison 1988, Barnes and Walker 1989) showed that the decreasing water content during the evaporation process leads to an isotopic maximum at the evaporation front. The evaporation front is possibly located in deeper soil layers, depending on the soil water content. Thus, sampling soil at the soil surface does not provide precise estimates of the evaporated water vapor. In 61 % of the reviewed studies (e.g. Williams et al. 2004, Yepez et al. 2005, Zhang et al. 2011, Dubbert et al. 2013) soil profiles were partially or entirely sampled. As the soil layer with the highest isotopic enrichment is associated with the location of the evaporation front, the spatial resolution of the soil layers should be as high as possible (preferably layer thicknesses of 2 cm or smaller). Especially in arid regions, where rain events are rare, the evaporation front is located in deeper soil layers, which makes an exact estimation of the evaporation front quite challenging. In addition, the subsequent cryogenic extraction of the liquid soil water can influence the measured isotopic composition of the liquid soil water due to soil physicochemical properties which affect the isotopic composition of the extracted soil water (Orlowski et al. 2016b). But also other soil water extraction methods (e.g. high pressure mechanical squeezing, microwave extraction) influence the final value of δ_{EF} (Orlowski et al. 2016a).

Recently, Rothfuss et al. (2013), Volkmann and Weiler (2014) and Gaj et al. (2016) developed non-destructive methods to measure the isotopic composition of the soil water vapor (δ_s^v) in different depths over long periods of time by flushing gas permeable tubing/membranes (e.g., Accurel® PP V8/2HF, Membrana GmbH, Germany; Rothfuss et al. (2013) installed in the soil with dry synthetic air and thereby sampling water vapor in the vicinity of tubing. A subsequent dilution of the sampled water vapor might be necessary to provide water vapor mixing ratio values within the range of highest accuracy of the stable isotope analyzer (e.g., 10,000 –15,000 ppmv for Picarro L2120-*i*). Rothfuss et al. (2013) investigated the dependencies of the soil water vapor water isotopic composition on both soil temperature (T_{soil}) and soil water content (θ_s). The method was successfully applied during laboratory experiments with sand (Gangi et al. 2015, Rothfuss et al. 2015) and silt loam (Quade et al. 2018). Volkmann and Weiler (2014) developed a soil water vapor probes with a rigid hydrophobic microporous polyethylene (Porex Technologies, Aachen, Germany) probe head. They tested the method in two different modi operandi. In the “advection dilution” sampling method, soil water vapor is collected from the head of the probe

with a vacuum pump. Subsequently, the sample air is diluted with nitrogen gas (N_2) and measured with a commercial laser spectroscopic instrument. In the "diffusion dilution" method, N_2 is directed into the probe head at a flow rate set by a mass-flow controller. The N_2 carrier gas equilibrates with soil water in a similar way as for the method of Rothfuss et al. (2013). Volkmann and Weiler (2014) tested the probe under field conditions and presented isotopic soil water profiles with high accuracy and precision for both methods. Gaj et al. (2016) used a commercially available soil gas probe (BGL-30, METER Group, Munich, Germany) with the same modus operandi as the "diffusion dilution" method by Volkmann and Weiler (2014) for a field study in central Namibia. The results of both studies indicate that sampling of soil water vapor via gas-permeable membranes is a highly promising approach for high resolution and long-term monitoring of soil water isotopic profiles in the field. Oerter et al. (2017) compared δ_s estimates of the monitoring method of Rothfuss et al. (2013) on the one hand and the direct equilibrium and vacuum extraction methods on the other hand. They showed a good agreement between the vacuum-extracted liquid water and the gas-permeable tubing method (root mean square error, RMSE: 1.7 ‰ for δ^2H and 0.62 ‰ for $\delta^{18}O$) or the direct equilibrium method (RMSE: 3.1 ‰ δ^2H_l and 0.62 ‰ for $\delta^{18}O_l$). However, Oerter et al. (2017) found a dependency of the isotopic composition of the liquid soil water on the texture (clay content) and gravimetric content of the soil, which was not considered in the initial studies of Rothfuss et al. (2013), Volkmann and Weiler (2014) and Gaj et al. (2016). Therefore, this dependency should be investigated further to provide accurate estimates of the isotopic composition of the soil liquid water.

Another important factor that influences the precision of δ_E estimates is the choice of the value of α_K. Only a handful studies tried to estimate or model α_K for soil evaporation. Braud et al. (2009a) simulated α_K values during long-term laboratory experiments with the soil-vegetation-atmosphere transfer model SiSPAT-Isotope. They found a decreasing trend of α_K values from saturated to unsaturated soil conditions, which contradicts the model of Mathieu and Bariac (1996). Similar results to the study by Braud et al. (2009a) were obtained by Rothfuss et al. (2015) during a long-term soil column laboratory experiment. Quade et al. (2018) were able to estimate α_K values during bare soil evaporation with a soil column experiment under semi-controlled conditions. They showed that α_K could not be considered as a constant value solely depending on flow conditions as proposed by Dongmann et al. (1974). They found the best model-to-data fit compared to the values of Mathieu and Bariac (1996) when the soil was fully saturated, but not for non-saturated conditions. They concluded that turbulent transport still played a major role during the evaporation process, especially under non-saturated conditions. These studies show that further sensitivity analyses of α_K to environmental conditions are needed to provide realistic estimates of δ_E.

To weight the influence of α_K, the Craig and Gordon (1965) model assumes 100% relative humidity within the soil pore space at the evaporation front. This is expressed with the "kinetic effect" term $\alpha_K(1-h')$ in Equation 4.14. However, this assumption is not valid for dry soils. Under very dry conditions the Kelvin equation estimates a relative humidity within the soil pore space below 100%:

$$h' = \exp\left(\frac{p_w m_w}{\rho_w R T_s}\right) \quad (4.20)$$

with p_w (hPa) the pressure of the liquid water phase, m_w the molar weight of water ($1.8*10^{-2}$ kg), ρ_w the density of water (1000 kg m^{-3}) and R the universal gas constant (8.3144 J mol^{-1} K^{-1}). Under isothermal conditions (T_s= 20°C) the value of δ_E decreases by 1‰ in δ^2H and $\delta^{18}O$ when assuming only 99.9% (field capacity: pF = 5.1), and already by 8‰ when assuming only 99.2% (pF = 6.0) relative humidity within the soil pore space (1‰ per 0.1%). This linear relationship has a large effect on the final *T/ET* results, especially for $\delta^{18}O$, for which the difference $\delta_T - \delta_E$ is usually smaller than for δ^2H.

4.4 Isotopic composition of transpired water vapor

4.4.1 Methods

Leaves are thin, well-mixed and isotopically uniform water sources which can be described with the Craig and Gordon (1965) model (Eq. 2). During the transpiration process the isotopic composition of the transpired water vapor is only partly affected by fractionation processes. In turn, the observed δ_L is lower than predicted by Eq. 2 (Dongmann et al. 1974). Farquhar and Lloyd (1993) proposed an equation incorporating the transpiration rate (T_{rate}, in mmol $m^{-2}s^{-1}$) and the effective anatomical dimension (L, in m):

$$\delta_L = \delta_{source} + (\delta_{ss} - \delta_{source})\frac{1-e^{-p}}{Pe} \quad (4.21)$$

with δ_{source} the isotopic composition of the unfractionated root zone source water (equal to the isotopic composition of the soil water), Pe the Péclet number:

$$Pe = \frac{T_{rate} * L}{C * D^i} \quad (4.22)$$

with C the mole fraction of water ($5.56 \cdot 10^4$ mol m^{-3}), D^i the vapor diffusivity of either $^1H^2H^{16}O$ or $^1H_2{}^{18}O$ and

$$\delta_{ss} = \frac{1}{\alpha_K(1-h')}\left(\frac{\delta_{source}+1}{\alpha_{eq}} - (\delta_a + 1)h'\right) - 1 \,. \qquad (4.23)$$

The kinetic fractionation factor for leaf transpiration differs from the one used for soil evaporation and is defined as (Cernusak et al. 2005):

$$\alpha_K = 1 - \frac{32r_s+21r_b}{r_a+r_s+r_b} \qquad \text{for } \delta^{18}O \qquad (4.24a)$$

and

$$\alpha_K = 1 - \frac{16.4r_s+10.09r_b}{r_a+r_s+r_b} \qquad \text{for } \delta^{2}H \qquad (4.24b)$$

With r_a the aerodynamic (a), r_s the leaf stomatal (s) and r_b the boundary layer (b) resistance (r, in s m^{-1}).

Dubbert et al. (2013) proposed an equation based on the method of Cuntz et al. (2007). They assumed that environmental conditions which change the isotopic composition to a new value at time t are constant over a time period dt (Dongmann et al. 1974, Cuntz et al. 2007):

$$\delta_L(t+dt) = \delta_C + (\delta_L(t) - \delta_x)\exp\left(-\frac{g_t w_i}{\alpha_K \alpha_{eq} V_m} dt\right) \qquad (4.25)$$

with $\delta_L(t)$ and $\delta_L(t+dt)$ being the isotopic composition of the leaf water at the site of evaporation at time t and $t+dt$, g_t [mol m^{-2} s^{-1}] the total stomatal conductance, w_i [mol(H_2O) mol(air)$^{-1}$] the humidity in the stomatal cavity, and V_m [mol m^{-3}] the mesophyll water volume. δ_C is the Craig and Gordon steady-state isotopic ratio at the evaporation site:

$$\delta_C = \frac{1}{(\delta_x+1)\alpha_K\alpha_{eq}(1-h)} + \alpha_{eq}h(\delta_a + 1) \qquad (4.26)$$

with δ_x and δ_a being the isotopic compositions of the xylem water (x) and of ambient water vapor (a).

Farquhar and Cernusak (2005) proposed an equation for the evaporative isotopic enrichment in leaves ($\Delta_{L,e}$) depending on the isotopic enrichment of the bulk leaf water ($\Delta_{L,b}$):

$$\Delta_{L,e} = \Delta_{L,s} - \frac{\alpha_K\alpha_{eq}}{g\, w_i}\frac{d(W\Delta_{L,b})}{dt} \qquad (4.27)$$

where g [mol m^{-2} s^{-1}] is the leaf stomatal conductance and W [mol m^{-2} leaf] the water concentration within the leaf. The isotopic fractionation enrichment that occurs within the leaf ($\Delta_{L,s}$) is defined as:

$$\Delta_{L,s} = (\varepsilon_{eq} + \varepsilon_K + (\Delta_v - \varepsilon_K)h \quad (4.28)$$

where Δ_v is the isotopic enrichment of the atmospheric water vapor.

Under stable environmental conditions for a sufficient period of time, no fractionation of the water occurs when it is extracted by the roots and, thus, no change in the isotopic composition of xylem sap water, which is known as isotopic steady state (ISS) (Yakir and Sternberg 2000):

$$\delta_T \text{ (ISS)} = \delta_x \quad (4.29)$$

with δ_x being the isotopic composition of the xylem (x) water. For the assumption of ISS to hold true, the amount of water transpired by the plant must be equal to the amount of water which is taken up by the root system from the soil (no drought stress). While the study of Walker and Brunel (1990) suggested that this assumption is reasonable on longer timescales (>24 h), Sutanto et al. (2014) in their review claimed that the assumption of ISS is only valid during midday.

4.4.2 Progress and challenges

The isotopic composition of transpired water vapor is directly measured via plant chambers, either at the leaf level or using custom-built branch chambers. Most studies used custom-made chambers, only a few studies (e.g. Wang et al. 2010) used commercially available leaf chambers (e.g. LICOR-6400, Nebraska, USA). Chamber measurements have several disadvantages as discussed in section 4.2.2, but are essential to monitor δ_T directly without relying on additional modelling steps from either δ_x or δ_L to δ_T. Volkmann et al. (2016) developed an in-situ method for the monitoring of the isotopic composition of tree xylem water: a xylem water isotopic probe with a gas-permeable head (microporous hydrophobic polyethylene, Porex Technologies, Aachen, Germany) was horizontally inserted into the tree. N_2 was led through the gas-permeable probe for isotopic equilibration with the xylem water. Subsequently, the sample air was measured with an infrared laser cavity ring-down spectrometer. The probe obtained direct, continuous and high-resolution measurements of the tree xylem water which is usable for automatable field measurements.

While in-situ techniques, e.g. coupling plant gas-exchange chambers to laser spectrometers, have the advantage of directly measuring the transpiration signature, all destructive sampling techniques as well as in-situ monitoring of xylem water as described by Volkmann et al. (2016) observe xylem or leaf isotopic signatures, eventually involving a modelling step to obtain δ_T. While a number of studies (e.g. Wei et al. 2015, Aouade et al. 2016, Volkmann et al. 2016, Zhou et al. 2018) assume ISS and hence argue that $\delta_x = \delta_T$, there is growing evidence that plants rarely reach ISS throughout the day (Simonin et

al. 2013, Dubbert et al. 2014, 2017). Moreover, the leaf water turnover time, which can effectively be described by stomatal conductance, vapor pressure deficit and leaf water volume, is extremely species-specific and ranges from several minutes to several hours (Song et al. 2015). As the leaf water turnover time describes the necessary time for a leaf to reach ISS (see exponent in equation 4.25), ISS can either be observed for large parts of the day (e.g. in many herbaceous species) or not at all (e.g. in plant species strongly controlling their stomatal conductance, see Dubbert et al. (2017) and Dubbert and Werner (2018) for an overview). Therefore, the validity of assuming ISS for the purpose of *ET* partitioning will largely depend on the desired temporal scale (considering NSS necessary at sub-diurnal to diurnal scale but unimportant at larger time scales). In case NSS is likely to occur, δ_T can be modeled using a Dongmann version of the Craig and Gordon equation as shown in section 4.4.1 (Dongmann et al. 1974). However, this complicates the partitioning approach considerably in comparison to direct chamber measurements of δ_T, as a large number of additional observations are necessary. In particular, g_t and the canopy temperature (T_C) are important input parameters. Therefore, the use of chamber measurements is highly recommended in any event.

The choice of an appropriate method for sampling unfractionated xylem water isotopic signatures is crucial for a correct determination of δ_T. For example, herbaceous, grass or crop species do not have suberized stems, thus destructive sampling would have to rely on leaf water sampling or sampling the plant culm belowground, which is highly destructive and not possible on plots of common size. Moreover, while the majority of studies still provide evidence for an unfractionated uptake and transport of xylem water through plants, there is growing evidence of fractionation of xylem water during times with low transpiration rate (drought condition, see e.g. Martin-Gomez et al. (2017) for deciduous species).

4.5 Conclusion and outlook

Since 2007 the number of source partitioning studies of evapotranspiration (*ET*) has increased to an average 1.3 publications per year (1990-2006 average: 0.4 publications per year). 54 % of the reviewed studies focus on semi-arid and arid ecosystems, where water availability is low and water scarcity is a major problem. Therefore, especially irrigation should be optimized in these ecosystems to minimize water losses. *ET* partitioning studies provide crucial background information, however, up to now only indirect methods (based on Scanlon and Kustas 2010) might be able to provide continuous and sub-daily estimates of the transpiration fraction (*T/ET*). Water stable isotopologues are powerful tracers, but isotope-based methods to partition ET need to be further developed for continuous long-term monitoring.

For continuous isotope-based *ET* partitioning in the field, automatized non-destructive measurements are mandatory. To calculate the isotopic composition of evaporation (δ_E) via the Craig and Gordon (1965) model, the isotopic composition of the soil liquid water (δ_s) should be measured online either with soil probes based on gas-permeable tubing or membranes, as proposed by Rothfuss et al. (2013), Volkmann and Weiler (2014), or Gaj et al. (2016). These measurement techniques are easy to install and apply, but require a lot of additional material, such as mass flow controllers and dry air. The main advantage of the measurement technique of Rothfuss et al. (2013) is the long-term monitoring of δ_s at different depths at one location. The soil gas probes of Volkmann and Weiler (2014) or Gaj et al. (2016) are more suitable to provide spatially distributed δ_s measurements because they only need a small hole in the soil for installation.

Another major challenge in isotope-based ET partitioning studies are long-term measurements of the isotopic composition of plant transpiration (δ_T). To our knowledge, the xylem water isotope probe by Volkmann et al. (2016) is the only promising method to obtain non-destructive measurements of δ_T. It avoids the problem of non-natural environmental conditions inside plant chambers, but due to the relatively large probe head (10 cm in outer diameter) this method can only be applied to trees. In future studies, the diameter of the probe head should be decreased in order for this technique to be usable for medium-sized plants like maize and, on longer term, thin-stem (cereal) plants.

Half-hourly values of the isotopic composition of evapotranspiration (δ_{ET}) could be practicably obtained from eddy covariance measurements and high-flow laser spectroscopy. The technique is already available and Griffis et al. (2010) proved the high potential of this measurements, but the majority of the reviewed studies (30 out of 31) use other techniques (e.g. Keeling (1958) plot approach or chamber measurements) instead. The main reason for this is that high-flow laser spectroscopy instruments are expensive and still under development. Nevertheless, for further studies this method is the most promising approach for automatized measurements of δ_{ET}.

Chapter 5

5.1 Synopsis

The aim of this thesis was to improve the understanding of water vapor ecosystem fluxes by the use of stable isotopologues with the main focus on the use of the gas-permeable tubing for non-destructive long-term monitoring of the isotopic composition of soil water vapor. Additionally, we evaluated actual measurement techniques which are used in isotope-based *ET* partitioning studies. For this, the results of three work packages, which resulted in three publications, were presented in chapters 2 to 4.

First, we presented the results of three semi-controlled bare soil laboratory experiments to investigate the kinetic fractionation factor (α_K) in Chapter 2. The soil water isotopic composition was monitored non-destructively by the use of gas-permeable tubing (Rothfuss et al. 2013). The soil column experiments differed in their soil water content (Experiment 1: $\theta = \theta_{sat} = 0.45$ m^3 m^{-3}, Experiment 2: $\theta = 0.25$ to 0.22 m^3 m^{-3}, Experiment 3: $\theta = 0.38$ to 0.32 m^3 m^{-3}) and aerodynamic conditions (Experiment 1 and 2: laboratory air, Experiment 3: laboratory air + ^2H_2O vapor labeling pulse). In combination with meteorological measurements we were able to determine α_K from the Craig and Gordon (1965) model with two different approaches. The first approach used the Keeling (1958) plot for the determination of the isotopic composition of the evaporated water vapor (δ_E). With this, the rearrangement of the well-known Craig and Gordon (1965) model equation for the determination of α_K, derived from δ_E, was possible (CG65). The second approach was independent of the determination of δ_E. Here the α_K values were fitted against the slope of the soil evaporation line in a dual isotopic coordinate system (G71). The results of CG65 showed that the application of the Keeling (1958) plot in the laboratory was related to high uncertainties which finally resulted in a higher accumulated uncertainty of the α_K values compared to G71. Especially the estimates for α_K^{2H} were outside the theoretical range proposed by Dongmann et al. (1974) or Mathieu and Bariac (1996), which could be explained by greater analytical memory effects (depending on the combination of flow rate and tubing length) of δ^2H compared to δ^{18}O. The C71 approach is independent of the estimation of δ_E and showed a good agreement with the values from Mathieu and Bariac (1996). The small discrepancies between these two estimates indicate that the turbulent transport of water vapor still plays an important role during the evaporation process, even at soil water content below saturation.

The non-destructive gas-permeable tubing enables continuous long-term experiments in the laboratory to better characterize α_K. This method can also be used in the field for long-term monitoring during *ET* partitioning studies. Chapter 3 presents the application of this non-destructive on-line method, based on microporous gas-permeable tubing by Rothfuss et al. (2013), during a field *ET* partitioning campaign in sugar beet. Until then, this method was only applied in the laboratory, whereas other studies (Volkmann

and Weiler 2014, Gaj et al. 2016) already applied similar methods (using gas-permeable material in soil gas probes) in the field. The measurements were conducted on three different days (D1: 29th of May 2017, D2: 13th of July 2017 and D3: 21st-22nd of August 2017) at the TERENO research site Selhausen (North Rhine-Westphalia, Germany) on an agricultural field. To evaluate the method, we compared *T/ET* estimates from the non-destructive soil profiles with the commonly used destructive soil sampling, and to a combination of micro-lysimeter and EC measurements. The results showed that only small differences were found between transpiration fraction (*T/ET*) estimates obtained from the gas-permeable tubing or soil sampling (on average 0.01 for δ^2H and 0.02 for δ^{18}O) despite the significant differences of the computed δ_E (maximum differences were 12.7 ‰ for δ^2H and 9.3 ‰ for δ^{18}O). This discrepancy is in line with the results of Orlowski et al. (2016a) and (2018), where differences between measurement techniques and water extraction methods were analyzed. However, the mean absolute deviations of the isotope-based *T/ET* estimates to those of the EC and micro-lysimeter techniques were more than three times higher. During the measurement days we observed that the soil surface from the micro-lysimeters dried faster than the surrounding soil surface, which indicates a slight overestimation of the evaporation flux. Therefore, the *T/ET* estimates obtained from the isotope-based partitioning appeared more plausible.

As already mentioned, similar methods also used microporous gas-permeable material to measure the isotopic composition of the soil water vapor. To discuss the actual progress and challenges within isotope-based *ET* partitioning studies, we presented a review of 31 publications in Chapter 4. From the literature review we concluded that microporous gas-permeable material is currently the most promising approach for continuous long-term measurements of δ_E. The measurement technique is easy to install but requires extensive additional equipment (e.g. mass-flow controller and dry air). One recent study (Volkmann et al. 2016) already demonstrated that this material is also suitable to measure the isotopic composition of xylem water in trees, which is equal to the isotopic composition of the transpired water vapor (δ_T) under steady-state conditions (Yakir and Sternberg 2000). But both methods are still under development and need more evaluation in the laboratory as well as under field conditions. Continuous measurements of the isotopic composition of the evapotranspiration water vapor flux (δ_{ET}) are currently possible by using a high-frequency laser spectrometer in combination with EC measurements. Griffis et al. (2010) already proved that this method has a great potential for long-term monitoring at meteorological flux stations. Unfortunately, up to now only two companies provide high-frequency laser spectrometers, which are expensive and still under development. These new measurement techniques are costly but have the potential to provide sub-daily isotopic flux data.

5.2 Synthesis

76 % of the reviewed studies presented in Chapter 4 use the Craig and Gordon (1965) model for the calculation of the isotopic composition of evaporated water vapor. This model requires simultaneous measurements of many different variables, such as soil temperature, relative humidity, isotopic composition of the atmospheric water, isotopic composition of the liquid soil water, and the choice of the kinetic fractionation factor. While the meteorological measurements (temperature, relative humidity) are easy to obtain, especially the measurement of the isotopic composition of the liquid soil water is subject to higher uncertainties. One important aspect is a correct estimate of the depth of the evaporation front. For this the soil is usually sampled with a soil auger to obtain isotopic soil profiles, but soil sampling is a destructive method and therefore not suitable for long-term monitoring.

The gas-permeable tubing of Rothfuss et al. (2013) allows the measurement of the isotopic composition of the liquid soil water in a non-destructive manner and was already successfully applied during laboratory experiments by Gangi et al. (2015), Rothfuss et al. (2015) and during the laboratory experiment presented in Chapter 2 (Quade et al. 2018). Other studies (Volkmann and Weiler 2014, Gaj et al. 2016) developed similar methods, using soil water probes with gas-permeable material as probe heads. The review presented in Chapter 4 suggests that these methods are the most promising approaches for the field long-term monitoring. First, Rothfuss et al. (2013) tested the gas-permeable tubing in sand and provided a temperature-dependent correction for the conversion of the isotopic composition of the vapor to that of the liquid water phase. They also tested the method for a possible soil water content dependency but did not observe any. Oerter et al. (2017) tested the same gas-permeable tubing with a different set-up in different soil types and showed a dependency of the method on soil water and clay content (discussed in Chapter 2.4). During the laboratory experiment presented in Chapter 2 we could neglect a clay content dependency because the clay content was the same across all soil layers in the soil column as well as in the two soil standards which were used for calibration. Neglecting the clay content during the field study presented in Chapter 3 is also reasonable. Due to the fact that the farmer cultivates the field regularly with a chisel plough to a depth of 15 cm, differences in the clay content between different soil depths in this range are negligible. The soil standards used for calibration were filled with soil sampled at the test site from the upper 10 cm, which agrees with the deepest measurement depth. Volkmann and Weiler (2014) as well as Gaj et al. (2016) showed that their method allowed measurement of soil water vapor with high accuracy and precision. They did not evaluate the method in the laboratory and did not provide a correction for clay content or soil water content in their studies. Furthermore, they used the formulation of Majoube (1971) for the conversion of the vapor to the liquid isotopic

composition, whereas Rothfuss et al. (2013) already showed that the method needs a specific temperature correction which is in turn related to Majoube (1971).

The results in Chapter 3 show that the application of the gas-permeable tubing by Rothfuss et al. (2013) is challenging under field conditions. Temperature differences between the soil and the atmosphere can cause condensation problems, which usually result in biased measurements. Compared to the soil probes by Volkmann and Weiler (2014) or Gaj et al. (2016), the tubing system has the great advantage that measurements at different depths are performed at one location. However, for long-term measurements the tubing connected from the buried, permeable tubes to the analyzer should be heated and insulated to avoid condensation. In addition, the tubing system should be flushed regularly with dry air to remove remaining water vapor from previous measurements.

The choice of α_K is another challenge in evapotranspiration partitioning studies. The laboratory experiment presented in Chapter 2 indicated that this factor is not a constant as assumed in the first studies by Craig and Gordon (1965) and Barnes and Allison (1983). Also, the factor does not only depend on the flow conditions as proposed by Dongmann et al. (1974). The results presented in Chapter 2 indicate that α_K depends on the soil water content as proposed by Mathieu and Bariac (1996) and on turbulent transport processes. During the first experiment presented in Chapter 2 α_K estimates based on G71 ($\alpha_K^{2H} = 1.0132 \pm 0.0011$, $\alpha_K^{18O} = 1.0149 \pm 0.0012$) varied without any significant trend in accordance with the values of Mathieu and Bariac (1996) ($\alpha_K^{2H} = 1.0129 \pm 0.0003$, $\alpha_K^{18O} = 1.0146 \pm 0.0003$) under saturated soil conditions. During the second experiment (non-saturated conditions) mean α_K estimates ($\alpha_K^{2H} = 1.0132 \pm 0.0015$, $\alpha_K^{18O} = 1.0149 \pm 0.0012$) were identical (without their standard deviation) to the first experiment and differ slightly from the values of Mathieu and Bariac (1996) ($\alpha_K^{2H} = 1.0185 \pm 0.0003$, $\alpha_K^{18O} = 1.0209 \pm 0.0003$). However, a linear increase of 0.0001 per day was observed which indicated the influence of the drying soil surface on α_K, but additionally the turbulent transport of water vapor plays an important role at soil water content below saturation. For the field study presented in Chapter 3, the α_K values of Mathieu and Bariac (1996) were chosen because the results of the laboratory experiment presented in Chapter 2 indicated α_K values close to those reported by Mathieu and Bariac (1996) under non-saturated soil conditions.

45 % of the reviewed studies presented in Chapter 4 used the Keeling (1958) plot approach for the estimation of the isotopic composition of water vapor from evapotranspiration. This approach uses the linear regression of the isotopic composition of the atmospheric water vapor against the inverse water vapor mixing ratio to estimate the isotopic composition of water vapor from evapotranspiration. Without any representative vegetation, the Keeling (1958) plot approach estimates the isotopic composition of

the water vapor from soil evaporation. This was the case during the laboratory experiment presented in Chapter 2. However, using the Keeling (1958) plot approach with the laboratory set-up was challenging due to a compromise between the sampling duration of the atmospheric water vapor and flow rate. A greater sampling duration and flow rate minimized memory effects of the tubing system and instrument but could also lead to an overlap of neighboring sampling heights. To avoid an overlap in sampling, the optimal flow rate for a sampling duration of 15 min was calculated as 200 ml min^{-1} (by assuming a cylindrical air layer at each sampling height). However, measurements of δ^2H suffered from stronger memory effects of the laser spectrometer than δ^{18}O (Schmidt et al. 2010), which resulted in a systematic overestimation of $\alpha_K^{^2H}$ obtained from CG65 compared to the theoretical range of Mathieu and Bariac (1996). During the field study presented in Chapter 3, the air layer was always mixed by the wind which allowed for a short sampling sequence (here 6 min per height) at a high flow rate (3 l min^{-1}).

5.3 Conclusions and Outlook

5.3.1 Perspective of the gas-permeable tubing

The results from the laboratory experiment in Chapter 2, the field campaign in Chapter 3 and the literature review in Chapter 4 showed that the gas-permeable material is the most promising approach for non-destructive long-term monitoring of the soil water vapor. However, for further applications more tests are necessary. Oerter et al. (2017) showed a dependency of the method on the soil water and clay content, the former of which was not observed by Rothfuss et al. (2013). Additional studies should be conducted in which the gas-permeable tubing by Rothfuss et al. (2013) is tested in different soil types differing in their clay and soil water content to prove or disprove the findings of Oerter et al. (2017). Furthermore, the method should be compared to other measurement techniques as described in Orlowski et al. (2016a) and Orlowski et al. (2018) to investigate the offsets between the different measurement techniques and to enhance comparability to other studies. Finally, the influence of roots which are growing around the tubing system should be investigated to be sure that that the sampled water vapor originates from the soil at this depth and not from the root which might have access to deeper soil layers.

5.3.2 Investigation of the kinetic fractionation factor

The results of the laboratory experiments with bare soil presented in Chapter 2 indicate that further investigations of the temporal dynamics of α_K are urgent. More bare soil laboratory experiments under

controlled atmospheric conditions should be conducted. For this, closed chambers like in Braud et al. (2009a) and Rothfuss et al. (2010) could be used. Using a chamber has the advantage of a controlled input of the isotopic composition of the atmospheric water vapor. By this, the fast changes in the isotopic composition of the atmospheric water vapor observed in the semi-controlled experiments in Chapter 2 can be avoided. This would decrease the uncertainty of the Keeling (1958) plot approach within the laboratory set-up and improve the α_K values obtained from CG65. In a second experiment, fast changes of the isotopic composition of the atmospheric water vapor could be simulated to identify the influence on α_K. Finally, similar experiments should be conducted in the field under natural conditions to compare the results with the laboratory experiments and identify other influencing factors of α_K (e.g., wind).

5.4 Acknowledgements

This thesis would not have been possible without Youri Rothfuss who always had an open door for me, even in stressful times, my project coordinator Alexander Graf who always shared his opinion and my doctoral thesis supervisor Nicolas Brüggemann who always came up with new ideas! Additionally, I would like to thank my project PhD mates Anne Klosterhalfen and Patrizia Ney for motivating me and each other and making the field work always enjoyable.

Thanks to Magdalena Landl for a various number of vegetarian cooking evenings and to Michael Stockinger for always taking care of my plants, my bird and my garden as well as Shurong Liu for funny conversations about the German language and being a good office mate. Thanks to all the “Düren” PhD students at the IBG-3 for being good friends.

I would also like to show my gratitude to Virginia Leffke who will always stay my best friend even with more than 600 km distance between us. To Anne Walter for various conversations about our PhD theses and exciting as well as relaxing holidays far far away! To my family for always supporting me in my ambitious dreams and especially to my niece who is always teaching me that life can be tough but there is no reason not to be happy. Finally, I would like to thank Alexei Richter for always making me laugh and being my shoulder to lean on!

Appendix A. Example of measuring sequence

An example of one measuring sequence (performed on day of experiment – DoE 14) is shown in Fig. A1. The isotopic compositions were measured in the vapor stream collected from soil across depths (–0.57 to –0.01 m), of both standards ("STD1" and "STD2"), and in the atmosphere column across heights (0.01 to 1.00 m). To avoid overlapping sampling inside the atmosphere column measuring time fast set to a maximum of 15 minutes. Figure A1 highlights the steady behavior of soil water vapor measurements and, in contrast, the fluctuations of the atmospheric vapor measurements.

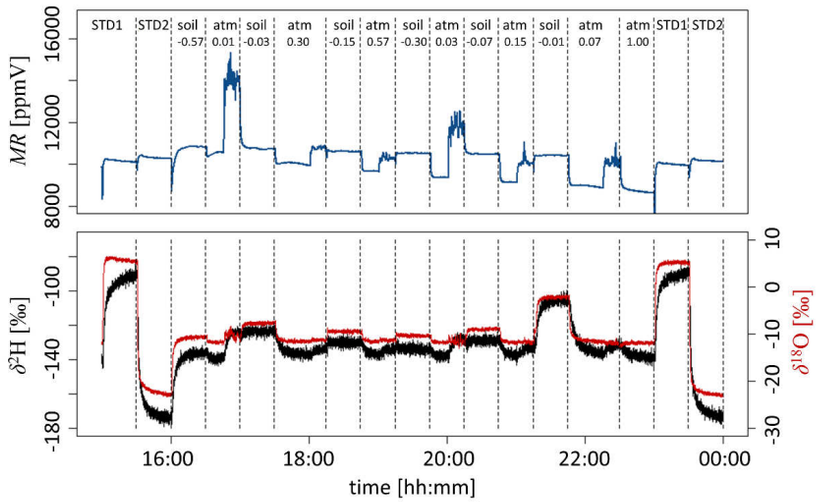

Figure A1
Water vapor mixing ratio (in ppmV) and isotopic composition (δ^2H and $\delta^{18}O$ in ‰) of the water vapor sampled on Day of Experiment 14 from the ambient air "atm", both standards ("STD1" and "STD2") and soil depths ("soil"), the numbers representing the depth/high regarded to the soil surface

Appendix B. Example of Keeling plot regression lines on DoE 73

An exemplarily Keeling plot is shown in Figure B1 where measurements of the mixing ratio (*MR*) and isotopic composition (δ^2H and $\delta^{18}O$) of the soil water vapor sampled inside the air column are plotted against each other. The isotopic composition of Evaporation (δ_E) is obtained from the value of the y-intercept of the linear regression (δ_{col} vs. $1/MR_{col}$).

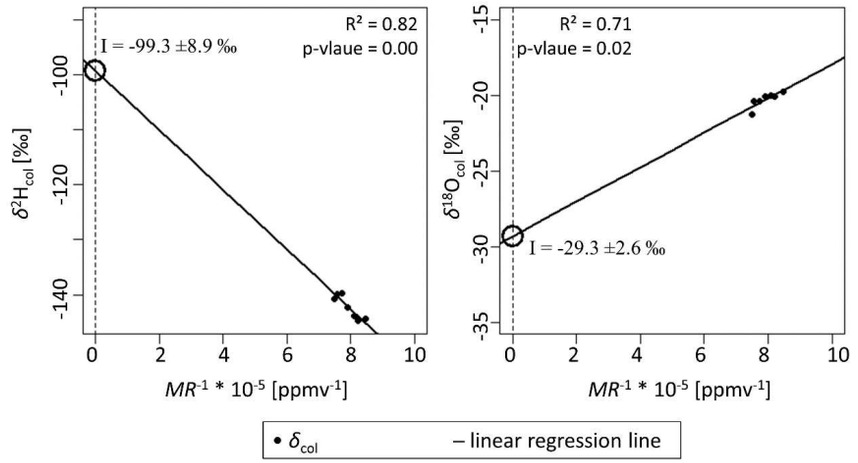

Figure B1

Linear Regression line (Keeling plot) of δ^2H (left) and $\delta^{18}O$ (right) against the inverse MR on Day of Experiment 73, values for the y-Intercept (I), the coefficient of determination (R^2) and the p-value are reported.

Appendix C: Error calculation on the kinetic fractionation factor α_K

The value for the kinetic fractionation factor α_{K} is given by:

$$\alpha_K = \frac{(\delta_{\mathrm{s}}^{\mathrm{l}}+1)/\alpha_{\mathrm{eq}}^{\mathrm{i}} - h'(\delta_{\mathrm{a}}+1)}{(1-h')\,(\delta_E+1)} \qquad \text{(C1)}$$

The kinetic fractionation factor α_k depends on errors made in the determination of the following variables: relative air humidity h' normalized to the saturated vapor pressure (P_{sat} [Pa]) (Soderberg et al. 2012) at the temperature of the evaporation front T_{EF} and temperature T_a, as well as the isotopic compositions of soil evaporation δ_E , atmospheric water vapor δ_{a} and soil water at the evaporation front $\delta_{\mathrm{s}}^{\mathrm{l}}$. The equations for h' and $\alpha_{\mathrm{eq}}^{\mathrm{i}}$ are given below:

$$h' = h\frac{\exp\left(13.7-\frac{5120}{T_a}\right)}{\exp\left(13.7-\frac{5120}{T_{\mathrm{EF}}}\right)} \qquad \text{and} \qquad \text{(C2)}$$

$$\alpha_{\mathrm{eq}}^{\mathrm{i}} = \exp\left[-\left(\frac{A}{T_{\mathrm{EF}}^2}+\frac{B}{T_{\mathrm{EF}}}+C\right)\right] \qquad \text{(C3)}$$

with constants $A = 1137, B = -0.4156\ and\ C = -0.0020667$ for i = ^{18}O and $A = 24844, B = -76.25\ and\ C = 0.05261$ for i = ^{2}H.

We assumed that the errors of all measurements are independent so the standard error $\sigma_{\alpha_k}^2$ can be calculated as:

$$\sigma_{\alpha_{\mathrm{K}}}^2 = \left(\frac{\partial\alpha_{\mathrm{K}}}{\partial h}\right)^2\sigma_h^2 + \left(\frac{\partial\alpha_{\mathrm{K}}}{\partial T_{\mathrm{a}}}\right)^2\sigma_{T_a}^2 + \left(\frac{\partial\alpha_{\mathrm{K}}}{\partial T_{\mathrm{EF}}}\right)^2\sigma_{T_{\mathrm{EF}}}^2 +$$

$$\left(\frac{\partial\alpha_K}{\partial\,\delta_{\mathrm{E}}}\right)^2\sigma_{\delta_{\mathrm{E}}}^2 + \left(\frac{\partial\alpha_{\mathrm{K}}}{\partial\,\delta_{\mathrm{a}}}\right)^2\sigma_{\delta_a}^2 + \left(\frac{\partial\alpha_{\mathrm{K}}}{\partial\,\delta_{\mathrm{s}}^{\mathrm{l}}}\right)^2\sigma_{\delta_{\mathrm{s}}^{\mathrm{l}}}^2 \qquad \text{(C4)}$$

The first three partial derivate terms can be obtained using the chain rules:

$$\frac{\partial \alpha_{\mathrm{K}}}{\partial h} = \frac{\partial \alpha_{\mathrm{K}}}{\partial h'} \frac{\partial h'}{\partial h} \tag{C5}$$

$$\frac{\partial \alpha_{\mathrm{K}}}{\partial T_{\mathrm{a}}} = \frac{\partial \alpha_{\mathrm{K}}}{\partial h'} \frac{\partial h'}{\partial T_{\mathrm{a}}} \tag{C6}$$

$$\frac{\partial \alpha_{\mathrm{K}}}{\partial T_{\mathrm{EF}}} = \frac{\partial \alpha_{\mathrm{K}}}{\partial \alpha_{\mathrm{eq}}} \frac{\partial \alpha_{\mathrm{eq}}}{\partial T_{\mathrm{EF}}} + \frac{\partial \alpha_{\mathrm{K}}}{\partial h'} \frac{\partial h'}{\partial T_{\mathrm{EF}}} \tag{C7}$$

with:

$$\frac{\partial \alpha_{\mathrm{K}}}{\partial h'} = \frac{(-\delta_{\mathrm{a}} - 1)}{(1-h')(\delta_E + 1)} + \frac{\frac{\delta_{\mathrm{S}}^{\mathrm{l}} + 1}{\alpha_{\mathrm{eq}}} - h'(\delta_{\mathrm{a}} + 1)}{(1-h')^2(\delta_E + 1)} \tag{C5-1}$$

$$\frac{\partial h'}{\partial h} = \frac{\exp\left(13.7 - \frac{5120}{T_{\mathrm{a}}}\right)}{\exp\left(13.7 - \frac{5120}{T_{\mathrm{EF}}}\right)} \tag{C5-2}$$

$$\frac{\partial h'}{\partial T_{\mathrm{a}}} = h \, \frac{5120}{(T_{\mathrm{a}})^2} \frac{\exp\left(13.7 - \frac{5120}{T_{\mathrm{a}}}\right)}{\exp\left(13.7 - \frac{5120}{T_{\mathrm{EF}}}\right)} \tag{C6-1}$$

$$\frac{\partial \alpha_{\mathrm{K}}}{\partial \alpha_{\mathrm{eq}}} = \frac{\delta_{\mathrm{S}}^{\mathrm{l}} + 1}{(h'-1)\,(\delta_E + 1)\,\alpha_{\mathrm{eq}}^{\mathrm{l}\,2}} \tag{C7-1}$$

$$\frac{\partial \alpha_{eq}}{\partial T_{\mathrm{EF}}} = \alpha_{eq} \left(\frac{2A}{T_{\mathrm{EF}}^3} + \frac{B}{T_{\mathrm{EF}}^2} \right) \tag{C7-2}$$

$$\frac{\partial h'}{\partial T_{\mathrm{EF}}} = -h \, \frac{5120}{(T_{\mathrm{EF}})^2} \frac{\exp\left(13.7 - \frac{5120}{T_{\mathrm{a}}}\right)}{\exp\left(13.7 - \frac{5120}{T_{\mathrm{EF}}}\right)} \tag{C7-3}$$

Combining equation C4-1 to C6-3 leads to

$$\frac{\partial \alpha_{\mathrm{K}}}{\partial h'} = \frac{\exp\left(13.7 - \frac{5120}{T_a}\right)}{\exp\left(13.7 - \frac{5120}{T_{\mathrm{EF}}}\right)} \left(\frac{(-\delta_a^v - 1)}{(1-h')(\delta_E^v + 1)} + \frac{\frac{\delta_S^l + 1}{\alpha_{eq}} - h'(\delta_a^v + 1)}{(1-h')^2(\delta_E^v + 1)} \right) \tag{C8}$$

$$\frac{\partial \alpha_{\mathrm{K}}}{\partial T_a} = h\ \frac{5120}{(T_a)^2}\frac{\exp\left(13.7-\frac{5120}{T_a}\right)}{\exp\left(13.7-\frac{5120}{T_{\mathrm{EF}}}\right)}\left(\frac{(-\delta_a^v-1)}{(1-h')(\delta_E^v+1)}+\frac{\frac{\delta_s^l+1}{\alpha_{eq}}-h'(\delta_a^v+1)}{(1-h')^2(\delta_E^v+1)}\right) \tag{C9}$$

$$\frac{\partial \alpha_{\mathrm{K}}}{\partial T_{\mathrm{EF}}} = \frac{\delta_{\mathrm{s}}^{\mathrm{l}}+1}{(h'-1)\,(\delta_E+1)\,\alpha_{\mathrm{eq}}^{\mathrm{i}\ 2}}\ \alpha_{eq}\left(\frac{2A}{T_{\mathrm{EF}}^3}+\frac{B}{T_{\mathrm{EF}}^2}\right)-$$

$$\frac{\exp\left(13.7-\frac{5120}{T_{\mathrm{a}}}\right)}{\exp\left(13.7-\frac{5120}{T_{\mathrm{EF}}}\right)}\left(\frac{(-\delta_{\mathrm{a}}-1)}{(1-h')(\delta_E+1)}+\frac{\frac{\delta_{\mathrm{s}}^{\mathrm{l}}+1}{\alpha_{\mathrm{eq}}^{\mathrm{i}}}-h'(\delta_{\mathrm{a}}+1)}{(1-h')^2(\delta_E+1)}\right)\ h\ \frac{5120}{(T_{\mathrm{EF}})^2}\frac{\exp\left(13.7-\frac{5120}{T_{\mathrm{a}}}\right)}{\exp\left(13.7-\frac{5120}{T_{\mathrm{EF}}}\right)} \tag{C10}$$

The last first three partial derivate terms are given below:

$$\frac{\partial \alpha_{\mathrm{K}}}{\partial\ \delta_E} = \frac{(\delta_{\mathrm{s}}^{\mathrm{l}}+1)/\alpha_{\mathrm{eq}}^{\mathrm{i}}-h\prime(\delta_{\mathrm{a}}+1)}{(1-h')\,(\delta_E+1)^2} \tag{C11}$$

$$\frac{\partial \alpha_{\mathrm{K}}}{\partial\ \delta_{\mathrm{a}}} = \frac{-h\prime}{(1-h')\,(\delta_E+1)} \tag{C12}$$

$$\frac{\partial \alpha_{\mathrm{K}}}{\partial\ \delta_{\mathrm{s}}^{\mathrm{l}}} = \frac{1/\alpha_{\mathrm{eq}}^{\mathrm{i}}}{(1-h')\,(\delta_E+1)} \tag{C13}$$

Appendix D: Calibration with the two standard vessels

Figure D1 shows the dependencies of δ^2H and δ^{18}O raw readings (blue points) to water vapor mixing ratio (MR) of the laser spectrometer (L2120-i, Picarro, Inc.). Figure A1 also illustrates that these MR-dependencies change with respect to the values of δ^2H and δ^{18}O raw readings. These relationships were determined by sampling and measuring from both soil water vapor standards (st1 and st2) and by fitting second order polynomial functions (black line) in the form "$a \cdot MR^2 + b \cdot MR + c$" to the δ^2H and δ^{18}O raw readings (i.e., $\boldsymbol{\delta^2 H^v_{st1,raw}}$ and $\boldsymbol{\delta^{18} O^v_{st1,raw}}$, $\boldsymbol{\delta^2 H^v_{st2,raw}}$ and $\boldsymbol{\delta^{18} O^v_{st2,raw}}$). In table A1 are reported the values of a, b, and c parameters for each polynomial function.

Corrected isotopic composition values in some soil water vapor or atmospheric water vapor sample ($\boldsymbol{\delta^v_{sample,corr}}$) were computed from raw isotopic composition values ($\boldsymbol{\delta^v_{sample,raw}}$) using Eq. (A1):

$$\boldsymbol{\delta^v_{sample,corr} = \delta^v_{sample,raw} + \frac{1}{2}\left(\delta^v_{st1}(10,000) - \delta^v_{st1}(MR) + \delta^v_{st2}(10,000) - \delta^v_{st2}(MR)\right)} \quad \text{(A1)}$$

Equation (A1) makes the simple assumption that the dependency of $\boldsymbol{\delta^v_{sample,raw}}$ to water vapor mixing ration is the average of those observed for standard $\boldsymbol{\delta^v_{st1}}$ and $\boldsymbol{\delta^v_{st2}}$.

Table D1
Values of the parameters a, b, and c of the fitted second order polynomial equations (i.e., in the form "$a \cdot MR^2 + b \cdot MR + c$")

parameter	$\boldsymbol{\delta^2 H^v_{st1,raw}}$	$\boldsymbol{\delta^{18} O^v_{st1,raw}}$	$\boldsymbol{\delta^2 H^v_{st2,raw}}$	$\boldsymbol{\delta^{18} O^v_{st2,raw}}$
a [‰ ppmV^{-2}]	-1.53*10-8	1.18*10-10	-5.45*10-9	2.42*10-9
b [‰ ppmV^{-2}]	-5.71*10-4	-1.66*10-5	2.27*10-4	9.31*10-5
c [‰ ppmV^{-2}]	-151.00	4.93	-85.02	-23.58

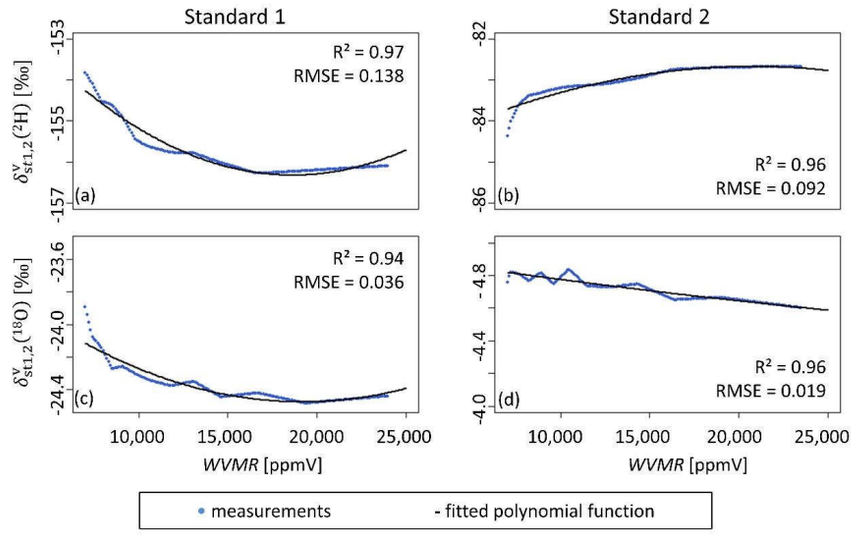

Figure D1
Observed (blue points) and fitted (black lines) relationships between the hydrogen (panels a-b) and oxygen (panels c-d) isotopic compositions of the water vapor sampled from the soil standards 1 (panels a-c) and 2 (panels b-d) (δ_{st1}^{v} and δ_{st2}^{v}) with water vapor mixing ratio (MR).

Appendix E: Overview on the reviewed studies

In total 31 published studies were reviewed. These studies were found by entering the term: ((“evapotranspiration” or “transpiration” or “evaporation”) and partition* and isotop*) into the ISI Web of Science search engine (www.webofknowledge.com).

Table E1

List of Symbols and Abbreviations used in Table E2

Symbol	Description	Unit	Abbrevia-tions	Description
T_y	temperature of the y = a: atmosphere s: soil c: canopy w: water l: leaf	°C	AWV (X)	atmospheric water vapor at X m height
e	vapor pressure	Pa	S_S (X)	soil samples at X cm depth
rh	relative humidity	%	X_S	xylem-samples
θ_s	soil volumetric water content	m3/m3	ST_S	stem-samples
θ_L	leaf water content	Vol%	W_S	water samples
v	wind speed	m s^{-1}	P_S	precipitation samples
v_d	wind direction	°	I_S	irrigation samples
P	Precipitation	mm m^{-2}	L_S	leaf samples
p	pressure	hPa	T	transpiration
R_n	net radiation	W m^{-2}	E	evaporation
R_s	solar radiation	W m^{-2}	ET	evapotranspiration
R_d	radiation flux density	W m^{-2}		
L_{ET}	latent heat flux of evapotranspiration	W m^{-2}		
Q_s	sensible heat flux	W m^{-2}		
F	sap-flux	m^3 m^{-2} s^{-1}		
E_{Lys}	soil evaporation (micro-lysimter)	mm d^{-1}		
E_{pot}	potential evaporation	mm d^{-1}		
T_{rate}	transpiration rate	mmol $m^{-2}s^{-1}$		
PPFD	photosynthetic photon flux density	µmol s^{-1} m^{-2}		
LAI	leaf area index	m^2 m^{-2}		
P_c	plant cover fraction	-		
EC	electrical conductivity	S m^{-1}		
g_l	leaf stomatal conductance	-		
NEE	net ecosystem exchange	-		
δ_y	isotopic composition of y = a: atmospheric water vapor L: leaf water x: xylem water s: source water st: stem water sw: soil water w: surface water *P*: precipitation water I: irrigation water	‰		
T/ET	transpiration fraction	%		

Table E2

Overview of the reviewed studies that use water stable isotopologues for partitioning evapotranspiration. This set of studies can be found, and further progress monitored, by entering ((“evapotranspiration” or “transpiration” or “evaporation”) and partition* and isotop*) into the ISI Web of Science search engine (www.webofknowledge.com)

Author (Year)	**Journal**	**Aim**	**Field, Lab or Model**	**Region, Land**	**Ecosystem**	**Climate, T_a *P*-amount**	**Isotopic measure-ments**	**addition al measure-ments**	**Timescale**	**δ_{ET}**	**δ_T**	**δ_E**	***T/ET***
Walker and Brunel (1990)	Journal of Hydrology	examining the isotopic composition of water in the major parts in the soil-plant-atmosphere continuum	Field	Hincks Conservation Park, Australia,	Eucalyptus mallee, 69% veg. 31 % bare soil	semiarid, 30°C (Jan) 23.6 °C (Mar) 400 mm (annual)	AWV (2.25, 4.5, 9), S_S, L_S, ST_S,	T_S, *rh*, T_a, T_L, T_{rate}	Daily Jan 16-19 1988, Mar 7-15 1988,		Craig and Gordon (1965) model (NSS) and leaf and steam water (ISS)	Craig and Gordon (1965) model	T has the largest contribution to ET
Brunel et al. (1997)	Journal of Hydrology	- determine possible sources of water used by the vegetation - partition ET	Field	Sahel, Niger,	fallow bushland of woody shrubs, 20 % vegetation	semiarid	AWV (3, 6, 12), S_S (0-120, 10 cm intervals), P_S,ST_S	*F*, T_a, *rh*, T_s, θ_s	Daily Jul 18-30 92	mass-balance	stem water (ISS)	Craig and Gordon (1965) model	Mean: 21 %
Wang and Yakir (2000)	Hydrological Processes	using stable isotopes in ET studies	Field	Israel, arid	wheat,		AWV (0.8, 0.9, 1.7, 2.5, 3.4, 7) L_S,ST_S, S_S	T_S, *rh*, T_a	Feb 18, 20, Mar 23 1994	Keeling (1958) plot	stem water (ISS)	Craig and Gordon (1965) model	Maximum value: 98.5– 96.5 % during midday
Ferretti et al. (2003)	Plant and Soil	- influence of precipitation variations on E and T - evaluate if elevated CO_2 can reduce T	Field	Colorado, USA,	shortgrass steppe	semiarid, 15.6 °C (summer) 0.6 °C (winter), 320 mm (annual)	S_S (1, 3, 5, 7, 10, 25, 50), P_S	Bowen Ratio, T_a, T_s, θ_s, R_n	Monthly May to Jun 99, Feb to Oct 00 and Apr to Oct 01	chamber (mass-balance)	chamber (mass-balance, NSS)	chamber (mass-balance)	Range: 10 – 100 % 100 % in Nov 99, Jun – Aug 00, Jun 01, Sep 01, 10 % in Mar 00
Yepez et al. (2003)	Agricultural Forest Meteorology	partition ET into EV and T and test the validity of the approach	Field	Arizona, USA,	savanna woodland (mesquite, grass) *LAI*: 1.6 (Jul)	semiarid, 24.8 °C (Jul), 343 mm (annual)	AWV (0.1, 0.5, 1, 3, 4.6, 6, 8, 10, 12, 14), S_S (0-10), ST_S	T_a, *rh*, *v*, v_d, T_s, R_s, *LAI*	Sep 22 01	Keeling (1958) plot	stem water (ISS)	Craig and Gordon (1965) model	85 ±6 % (δ^2H) 88 ±5 % (δ^{18}O)

Author (Year)	Journal	Aim	Field, Lab or Model	Region, Land	Ecosystem	Climate, T_a *P*-amount	Isotopic measure-ments	addition al measure-ments	Timescale	δ_{ET}	δ_T	δ_E	*T/ET*
Williams et al. (2004)	Agricultural Forest Meteorology	- utility the Keeling plot for ET-partitioning - evaluate consequences of plant functional heterogeneity for upscaling sap flux	Field	Marrakech, Morocco,	Agdal olive orchard, 400 trees per ha	semiarid, 253 mm *P*	AWV (0.1, 1.2, 3.7, 6.4, 8.9), S_S (0-2, 20-30), ST_S	L_{ET}, Q_s, v, v_d, T_a, rh, R_s, T_s, F,	Twice daily Oct 27 – Nov 11 02	Keeling (1958) plot	stem water (ISS)	Craig and Gordon (1965) model	prior irrigation: 100% following irrigation: 69-85 %
Yepez et al. (2005)	Agricultural Forest Meteorology	- present a static, plot-scale gas exchange chamber - demonstrate applicability of the method	Field	Arizona, USA,	grassland *E.lehman-niana* LAI: 0.66, *H.contortus* LAI: 0.37	semiarid, irrigation pulse of 39 mm at Jun 12	AWV, S_S (0-2, 2-4, 4-6, 6-10, 10-20, 20-30), L_S	T_a, rh, *LAI*, T_c, g_l, e	twice Daily, Jun 12 – 27	chamber (Keeling 1958 plot)	Farquhar and Cernusak (2005) (NSS)	Craig and Gordon (1965) model	Day 1: 35 ±7 %, Day 3: 43 ±8 % (after irrigation), Day 7: 22 ±5 %
Lee et al. (2007)	Global Biogeochemi cal Cycles	- quantify how environmental variables influ-ence temporal variation of δ_T - investigate temporal dyna-mics of forest water use	Field	Connecticut, USA	mixed forest (red maple, eastern white pine, beech, hemlock)	7 °C (annual), 1330 mm (annual)	AWV (21.7, 30.7), P_S, W_S, S_S(0-5), ST_S	T_a, rh, L_{ET}, Q_s, E_{Lys}, v, v_d, P, R_s, R_n	Daily, May 20 – Oct 17,	flux gradient	Craig and Gordon (1965) model (NSS)	Craig and Gordon (1965) model	70 %
Xu et al. (2008)	Botanical Studies	determination of the relative contribution of EV and T to ET	Field	Balang Mountain China,	subalpine shrubland, *LAI*: 2.05	semiarid, 3°C (annual) 710 mm (annual)	AWV(0.1, 0.5, 1.5, 2.0, 3.0), S_S(0-10), ST_S	P, v, E_{pot}, $PPFD$, p, T_s, T_a, rh, *LAI*	Jun 21,24,25 06,	Keeling (1958) plot	steam water (ISS)	Craig and Gordon (1965) model	Jun 21: 74.5 ±9.9 % Jun 24: 65.6 ±8.3 % Jun 25: 96.9 ±2.0 %
Wenninger et al. (2010)	Physics and Chemistry of the Earth	- improve hydrological process under-standing of water transport and evaporation - quantify ground/canopy *T/ET*	Lab	Delft, Nether-lands	1. bare soil 1. Teff	–	S_S(1.7, 5.1, 9.4, 1.45, 2.2)	T_s, θ_s, EC	Daily Feb 2 – 26 09		mass-balance (ISS)	mass-balance	70 %
Wang et al. (2010)	Geophysical Research Letters	- develop and evaluate a new ET partitioning technique	Lab (Class-house)	Arizona, USA	mesquite tree (25 %, 50%, 75%, 100% woody cover)	–	AWV (0.5, 1.0, 2.0), I_S	T_a, rh, T_s	hourly, Sep – Oct 08 39°C	Keeling (1958) plot	1. custo-mized leaf chamber 2. standard leaf chamber (NSS)	Craig and Gordon (1965) model	Woody cover 25 % -100 %: 61 % – 83 %

Author (Year)	Journal	Aim	Field, Lab or Model	Region, Land	Ecosystem	Climate, T_a P-amount	Isotopic measure-ments	additional measure-ments	Timescale	δ_{ET}	δ_T	δ_E	T/ET
Rothfuss et al. (2010)	Hydrological Processes	- partition ET during the growth of tall fescue cover - establish bare soil steady state isotopic profiles	Lab, (Cham-ber)	Paris, France	fescue cover, *LAI* increased from 0 to 3.9	–	AWV, W_S, X_S	T_a, rh, θ_s, *LAI*	Apr 8, 20 Mai 2, 10, 17 25 °C	condensed water	xylem water (ISS)	input water	*LAI* 0: 0 %, *LAI* 0.4: 6 %, *LAI* 1.2: 17 %, *LAI* 1.6: 30 %, *LAI* 3.9: 95 %
Griffis et al. (2010)	Boundary-layer Meteorology	Determining δ_{ET} via EC meas.	Field	Minnesota, USA	corn (2008) soybean (2009)		AWV (0.1, 0.85, 1.85, 2.7) P_S, S_S, X_S, I_S	v, v_d, T_a, rh	Daily, Aug 08 – Sep 19 08, Jun 19 – Aug 31 09	Eddy covariance	xylem water (ISS)	Craig and Gordon (1965) model	
Zhang et al. (2011)	Journal of Hydrology	- first use of hybrid micrometeorological / isotopic approach in the North China Plain - quantifying soil water contribution to E and T	Field	North China Plain, China,	irrigated winter wheat, *LAI* 2.6	semiarid 12 °C (annual), 480 mm (annual)	AWV (0.1, 3, 10), S_S (20, 30, 40, 60, 80, 100) ST_S,P_S	θ_s, T_a, rh, L_{ET}, E_{Lys}, *LAI*, water table	6 days between: Mar 01 – Jun 04 09,	Keeling (1958) plot	stem water (ISS)	Craig and Gordon (1965) model	DOY 138: 83 % DOY 149: 60%
Sutanto et al. (2012)	Hydrology Earth System Sciences	partitioning ET into EV and T under consideration of interception	Lab Model	Delft, Netherlands	grass-covered lysimeter	–	S_S (3.5, 10, 16.5, 23, 36.5)	θ_s, *EC*, T_s rh, T_a, v, R_s, EV_{Lys} Percu-lation	hourly, Nov 06 10 – Jan 31 11		mass-balance (ISS)	mass-balance	isotope: 83% HYDRUS 1D: 67%
Wang et al. (2013)	Geochimica et Cosmochimica Acta	- evaluate isotope based ET partitioning methods - partition ET - asses influence of warming to ET flux	Field	Oklahoma, USA,	grassland 1. control treatment (CT) 2. warming treatment (WT),	semiarid, 16 °C (annual), 911 mm (annual)	AWV, S_S (0-2)	T_a, rh, T_s, θ_s	May 31, Jun 03, 05, 07, 08 11,	chamber (Keeling 1958 plot)	1. chamber (Keeling (1958) plot and mass-balance ,NSS) 2. source water (ISS)	1. bare soil chamber (Keeling (1958) plot and mass-balance) 2. Craig and Gordon (1965) model	chamber: CT 65%, WT 77 % Craig and Gordon (1965): CT 83% WT 86 %
Dubbert et al. (2013)	Journal of Hydrology	* testing the Craig and Gordon (1965) model against directly measured δ_{EV} * quantify *T/ET*	Field	Central Portugal	open cork-oak woodland	Mediterran ean, 15.9 °C (annual) 680 mm (annual)	AWV, S_S (0.5, 2, 5, 10, 15, 20, 40)	*PPFD*, *P*, T_a, rh, T_s, θ_s	hourly, Apr 08, 12, 18, 26, May 02 11	chamber (mass-balance)	modelled with Dongmann et al. (1974) and Craig and Gordon (1965) model from soil water (NSS)	1. Craig and Gordon (1965) model 2. chamber (mass-balance)	Apr 08 + 12: approx. 80 % Apr 18 + 26: approx. 50% (after rainfall event)

Author (Year)	Journal	Aim	Field, Lab or Model	Region, Land	Ecosystem	Climate, T_a *P*-amount	Isotopic measure-ments	addition al measure-ments	Timescale	δ_{ET}	δ_T	δ_E	*T/ET*
Sun et al. (2014)	Agricultural Forest Meteorology	- calculate δ_T under NSS - quantify *T/ET* - investigate influence of foreign vapor on ET partitioning	Field	Yellow River Xiaolangdi forest, China	Chinese cork oak, 96 % vegetation	13.4 °C (annual) 643 mm (annual)	AWV (0.1, 11, 18) S_S (0-5, 5-10), L_S, ST_S	T_a, *rh*, *v*, v_d, θ_s, T_L, g_L	Sep 11, 14, 17, 20	Keeling (1958) plot	Craig and Gordon (1965) model (NSS)	Craig and Gordon (1965) model	Sep 11 : 91.10 % Sep 14: 86.30 % Sep 20: 85.37 %
Good et al. (2014)	Water Resources Research	compare partitioning estimates to scaled leaf-level measurements of T as well as flux-variance similarity partitioning	Field	Mpala Research Center, Kenya	grassland 0% green leaf coverage on Feb 7, max approx. 10% on Feb 16	arid 30 mm Irrigation + 6.7 mm rain	AWV (0.4), S_S (1, 5, 10, 20), L_S, P_S, I_S	*LAI*, T_a, P_c, T_s, θ_s R_n, L_{ET}, Q_s	hourly Feb 7 – 21 2011	Keeling (1958) plot	leaf chamber (NSS)	Craig and Gordon (1965) model	29 ± 5 % (mean) 40 % (max)
Hu et al. (2014)	Journal of Geophysical Research: Biogeoscienc es	- compare traditional δ_T estimates of with new model from this study - diagnose effect of soil sampling at different depths - explore potential uncertainties in ET partitioning	Field	Mongolia, China	grassland, *LAI* ranged between 0.4 and 0.55 (approx.)	semiarid, 2.1 °C (annual) 18.9 °C (Jul) –17.5°C (Jan) 383 mm (annual)	AWV (0.7, 1.7) S_S (5, 15, 25), L_S, ST_S	L_{ET}, T_a, T_c, T_s, θ_s, *p*, *LAI*	hourly Jun 27, Jul 22, 26, Aug 7, 11, 12 2009	flux gradient	Craig and Gordon (1965) model (NSS) + *LAI* depending model	Craig and Gordon (1965) model	83 % (mean)
Dubbert et al. (2014)	Frontiers in Plant Science	disentangle vegetation effects on water and carbon fluxes, soil evaporation, and influence of vegetation on rain infiltration	Field	Central Portugal	open cork-oak woodland, *LAI* 1.05	Mediterran ean, 15.9 °C (annual) 680 mm (annual)	AWV (2), S_S (0-0.5, 2,5, 10, 15, 20, 40), P_S	*PPFD*, *P*, T_a, *rh*, T_s, θ_s, L_{ET}, NEE, *LAI*	daily 22 / 26 days between Apr 7 – Mai 5, May 23–Jun 6, Sep 11–23, Oct 23 – Nov 22 2011	chamber (mass-balance)	modelled with Dongmann et al. (1974) and Craig and Gordon (1965) model from soil water (NSS)	Craig and Gordon (1965) model	May: 68 % June: 84 % fall: 45 %
Wei et al. (2015)	Water Resources Research	- identify temporal characteristics - partition ET - explore potential uncertainties in ET partitioning	Field	Tsukuba, Japan	rice paddy field, *LAI* 0 (May 1) *LAI* 5.5 (Jul 15)	13.7 °C (annual) 1200 mm (annual)	AWV (2), W_S	T_a, *rh*, L_{ET}, *LAI*	hourly / daily Jun – Aug 2013 May – Jun 2014	Keeling (1958) plot	pone water (ISS)	Craig and Gordon (1965) model	range: 2 – 100 % 47 % (May) 79 % (Jun) 98 % (Jul) 94 % (Aug)

Author (Year)	Journal	Aim	Field, Lab or Model	Region, Land	Ecosystem	Climate, T_a *P*-amount	Isotopic measure-ments	addition al measure-ments	Timescale	δ_{ET}	δ_T	δ_E	*T/ET*
Wang et al. (2015)	Agricultural Forest Meteorology	- couple isotopic fractionation process in SPAC model . test performance of the ISO-SPAC model . examine validity of ET partitioning	Field Model	Tsukuba, Japan	grassland (mowed two times a year) LAI range: 0.01 – 2.58 mean: 1.38	14.1 °C (annual) 1159 mm (annual)	AWV (0.1, 0.5-0.7, 1.6-2.0), L_S, ST_S, S_S(5 depths)	θ_s, T_L, g_L, *LAI*, θ_L, R_n, R_s, L_{ET}, T_a, *rh*, T_s, Q_s	weekly, Apr – Sep 2011	Keeling (1958) plot	modelled from xylem and leaf water (NSS) with 3 different models	Craig and Gordon (1965) model	range: 2 – 99 % ISO-SPAC: 84 ± % Isotope: 84 %
Berkelhammer et al. (2016)	Global Bio-chemical Cycles	comparison of independent approaches to estimate *T/ET*	Field Model	Rocky Mountains National Park, USA	- subalpine mixed coniferous forest LAI 4.2 (US-NR1) - open canopy forest *LAI* 1.2 (MEF)	US-NR1: 14 °C (July), 884 mm (annual) MEF: 19 °C (July) 430 mm (annual)	US-NR1: AVW (10, 15, 20); MEF: AVW (12, 17.7, 25.1); S_S,X_S,L_S	Q_s, L_{ET}, VPD, T_a, θ_s, GPP, *LAI*	daily, US-NR1: fall 2011 MEF: May – Sep 2011	modified Keeling (1958) plot (Noone et al. 2013)	Craig and Gordon (1965) model (NSS)	Craig and Gordon (1965) model	MEF: 49 ±23% US-NR1: 62 ±27%
Aouade et al. (2016)	Agricultural Forest Meteorology	- partitioning of available energy - estimating the total amount of *EV*, *T* and *ET* with isotopic measurements	Field	Haouz plain, Marocco	irrigated winter wheat *LAI* 0 – 1.2	semiarid, 240 mm (annual)	AWV (0, 0.4/0.9, 2, 3m, S_S (0-10: 2cm interval, 10-70: 10 cm interval, ST_S	R_s, T_a, *p*, *v*, *P*, *rh*, P_c, *LAI*, T_s, θ_s	daily Feb 22, 23, 34 2012 Apr 11 12 2013	Keeling (1958) plot	stem water (ISS)	Craig and Gordon (1965) model	after irrigation: 69 % prior irrigation: 80 %
Wen et al. (2016)	Agricultural Forest Meteorology	- characterize the ecosystem water pools - characterize temporal dynamics of *EV*, *T*, *ET* and *T/ET*	Field	Heihe River Basin, China	spring maize, *LAI* 5.6 (max)	arid, 74. °C (annual), 129.7 mm (annual)	AWV (0.5,1.5), S_S (0-5,5-10,10-80: 10 cm interval), ST_S, L_S, W_S (rain, dew, irrigation)	T_a, *rh*, *v*, *P*, T_s, θ_s, E_{Lys}, L_{ET}, *LAI*	daily May 27 – Sep 22 2012	flux gradient	Craig and Gordon (1965) model (NSS) + *LAI* depending model	Craig and Gordon (1965) model	isotope-based : 87 ±5 % lysimeter-based: 86 ±6%
Lu et al. (2017)	Agricultural Water Management	use of customized *T*, *EV* and *ET* chambers to measure their δ-value and estimate *T/ET*	Field	California, USA	Dessert Valley: forage sorghum *LAI* 0.5 – 1.5	arid 22.4 °C (annual), 12.6 °C (Jan), 32.9 (Aug) 80.3 mm (annual)	AWV	R_s, *v*, T_a, *rh*, *P*, T_s, L_{ET}, *LAI*	daily Jul 24, 28, 30, Aug 4, 6, 7 2014	chamber (mass-balance)	chamber (NSS)	chamber (mass-balance)	46 ±5.6 %

Author (Year)	Journal	Aim	Field, Lab or Model	Region, Land	Ecosystem	Climate, T_a P-amount	Isotopic measure-ments	addition al measure-ments	Timescale	δ_{ET}	δ_T	δ_E	T/ET
Wu et al. (2017)	Journal of Hydrometeo-rology	- refine and verify flow-through chamber method - identify temporal characteristics - quantify *T/ET*	Field	China	University test field: maize *LAI* 0 – 4 1. T/ET = 0.52 $LAI^{0.32}$, 2. T/ET = 0.71 $LAI^{0.14}$	arid, 8 °C (annual) 164 mm (annual)	AWV (1,2,4), S_S (0-5,5-10), ST_S	L_{ET}, v, T_a, rh, T_s, E_{Lys}	hourly, 18 days between May 21 and Aug 22	chamber (mass-balance)	dynamic chamber measurements (NSS)	1. chamber (mass-balance) 2. Craig and Gordon (1965) model	1. 87 % (morning) 59 % (evening) 73 % (mean) 2. 88 % (morning) 72 % (evening) 85 % (mean)
Piayda et al. (2017)	Biogeoscienc es	- disentangle vegetation effects on soil water infiltration and distribution - dynamics of soil *EV* and grassland water use	Field	Central Portugal	open cork-oak woodland: oak and grass, *LAI* 1.1	Mediterran ean 15.9 °C (annual) 680 mm (annual)	AWV, S_S (0-0.5,2,5,10, 15,20,40)	P, T_a, rh, T_s, θ_s, *PPFD*, *LAI*	daily, May 26 – Jun 12 2012	chamber (mass-balance)	leaf samples + Craig and Gordon (1965) model (NSS)	Craig and Gordon (1965) model	36% (tree site) and 41% (open site)
Wei et al. (2018)	Agricultural Forest Meteorology	-develop two-source model - investigate daily variabilities of *T/ET* - model sensitivity analyses - compare different approaches	Field Model	1. Japan 2. China	1. rice field, *LAI* 0– 6 2. winter wheat and summer corn , *LAI* 0 – 4.7	13.7 °C (annual) 1200 mm (annual)	1: AWV(2), W_S, 2: AWV, S_S(0-5,15-20,40-45), L_S, ST_S	T_a, rh, v, v_d, T_s, L_{ET}, P, R_d, R_n, Q_s, T_w, momentum heat, E_{Lys}, *LAI*	rice: May – Sep 2014 wheat:; Apr – Jun 2008 corn: Jun – Sep 2008	1: Keeling plot 2: flux gradient	leaf and steam water (ISS) and Farquhar and Cernusak (2005) (NSS)	Craig and Gordon (1965) model	rice: 74%, wheat: 93% corn: 81%
Zhou et al. (2018)	Agricultural Forest Meteorology	- investigate seasonal variations in GPP, *ET*, VPD, uWUE and *T/ET* - evaluate uWUE against stable isotope, lysimeter/ eddy covariance and sap flow methods - better understanding of carbon-water interactions	Field	Heihe River Basin (HRB), China	3 sites: upper HRB: Alpine meadow, *LAI* 6.3 middle HRB: irrigated cropland (maize), *LAI* 3.8 lower HRB: Populus euphratica, *LAI* 0.8	upper HRB: –0.4 °C (annual) 438 mm (annual) middle HRB: 6.9 °C (annual) 147 mm lower HRB: 10.4 °C (annual) 26 mm (annual)	AWV (0.5,1.5), S_S (0-5,5-10,10-80: 10 cm interval), L_S, ST_S	*NEE*, L_{ET}, T_a, rh, v, v_d, p, P, T_s, θ_s R_n, Q_s, F, E_{Lys} *LAI*	upper HRB: 2013 – 2015 middle HRB: May 2012 – 2015 lower HRB: 2014 – 2015	flux gradient	xylem water (ISS)	Craig and Gordon (1965) model	upper HRB: 55 %, middle HRB: 63 %, lower HRB: 55 %

References

Aouade, G., J. Ezzahar, N. Amenzou, S. Er-Raki, A. Benkaddour, S. Khabba & L. Jarlan 2016. Combining stable isotopes, Eddy Covariance system and meteorological measurements for partitioning evapotranspiration, of winter wheat, into soil evaporation and plant transpiration in a semi-arid region. Agricultural Water Management 177: 181-192; https://doi.org/10.1016/j.agwat.2016.07.021.

Araguás-Araguás, L., K. Rozanski, R. Gonfiantini & D. Louvat 1995. Isotope effects accompanying vacuum extraction of soil water for stable isotope analyses. Journal of Hydrology 168: 159-171; https://doi.org/10.1016/0022-1694(94)02636-P.

Barnes, C. J. & G. B. Allison 1983. The Distribution of Deuterium and ^{18}O in Dry Soils .1. Theory. Journal of Hydrology 60(1-4): 141-156; https://doi.org/10.1016/0022-1694(83)90018-5.

Barnes, C. J. & G. B. Allison 1988. Tracing of water movement in the unsaturated zone using stable isotopes of hydrogen and oxygen. Journal of Hydrology 100: 143-176; https://doi.org/10.1016/0022-1694(88)90184-9.

Barnes, C. J. & G. R. Walker 1989. The Distribution of Deuterium and 18O during Unsteady Evaporation from a Dry Soil. Journal of Hydrology 112: 55-67; https://doi.org/10.1016/0022-1694(89)90180-7.

Berkelhammer, M., D. C. Noone, T. E. Wong, S. P. Burns, J. F. Knowles, A. Kaushik, P. D. Blanken & M. W. Williams 2016. Convergent approaches to determine an ecosystem's transpiration fraction. Global Biogeochemical Cycles 30(6): 933-951; https://doi.org/10.1002/2016gb005392.

Boast, C. W. & T. M. Robertson 1982. A Micro-Lysimeter Method for Determining Evaporation from Bare Soil - Description and Laboratory Evaluation. Soil Science Society of America Journal 46(4): 689-696; https://doi.org/10.2136/sssaj1982.03615995004600040005x.

Braud, I., T. Bariac, J. P. Gaudet & M. Vauclin 2005a. SiSPAT-Isotope, a coupled heat, water and stable isotope (HDO and (H2O)-O-18) transport model for bare soil. Part I. Model description and first verifications. Journal of Hydrology 309(1-4): 277-300; https://doi.org/10.1016/j.jhydrol.2004.12.013.

Braud, I., P. Biron, T. Bariac, P. Richard, L. Canale, J. P. Gaudet & M. Vauclin 2009a. Isotopic composition of bare soil evaporated water vapor. Part I: RUBIC IV experimental setup and results. Journal of Hydrology 369(1-2): 1-16; https://doi.org/10.1016/j.jhydrol.2009.01.034.

Braud, I., T. Bariac, P. Biron & M. Vauclin 2009b. Isotopic composition of bare soil evaporated water vapor. Part II: Modeling of RUBIC IV experimental results. Journal of Hydrology 369(1-2): 17-29; https://doi.org/10.1016/j.jhydrol.2009.01.038.

Brunel, J. P., H. J. Simpson, A. L. Herczeg, R. Whitehead & G. R. Walker 1992. Stable Isotope Composition of Water-Vapor as an Indicator of Transpiration Fluxes from Rice Crops. Water Resources Research 28(5): 1407-1416; https://doi.org/10.1029/91wr03148.

Brunel, J. P., G. R. Walker, J. C. Dighton & B. Monteny 1997. Use of stable isotopes of water to determine the origin of water used by the vegetation and to partition evapotranspiration. A case study from HAPEX-Sahel. Journal of Hydrology 189(1-4): 466-481; https://doi.org/10.1016/S0022-1694(96)03188-5.

Cappa, C. D., M. B. Hendricks, D. J. DePaolo & R. C. Cohen 2003. Isotopic fractionation of water during evaporation. Journal of Geophysical Research-Atmospheres 108(D16); https://doi.org/10.1029/2003jd003597.

Cernusak, L. A., G. D. Farquhar & J. S. Pate 2005. Environmental and physiological controls over oxygen and carbon isotope composition of Tasmanian blue gum, Eucalyptus globulus. Tree Physiology 25(2): 129-146; https://doi.org/DOI 10.1093/treephys/25.2.129.

Coenders-Gerrits, A. M. J., R. J. van der Ent, T. A. Bogaard, L. Wang-Erlandsson, M. Hrachowitz & H. H. G. Savenije 2014. Uncertainties in transpiration estimates. Nature 506(7487): E1-E2; https://doi.org/10.1038/nature12925.

Coplen, T. B. 2011. Guidelines and recommended terms for expression of stable-isotope-ratio and gas-ratio measurement results. Rapid Communications in Mass Spectrometry 25(17): 2538-2560; https://doi.org/10.1002/rcm.5129.

Craig, H. 1961. Isotopic Variations in Meteoric Waters. Science 133(346): 1702-&; https://doi.org/DOI 10.1126/science.133.3465.1702.

Craig, H. & L. I. Gordon 1965. Deuterium and oxygen 18 variations in the ocean and marine atmosphere. Stable Isotopes in Oceanographic Studies and Paleotemperatures, 1965, Spoleto, Italy. edited by E. Tongiogi: 9-130.

Cuntz, M., J. Ogee, G. D. Farquhar, P. Peylin & L. A. Cernusak 2007. Modelling advection and diffusion of water isotopologues in leaves. Plant Cell and Environment 30(8): 892-909; https://doi.org/10.1111/j.1365-3040.2007.01676.x.

Dongmann, G., H. W. Nurnberg, H. Forstel & K. Wagener 1974. Enrichment of $H_2^{18}O$ in Leaves of Transpiring Plants. Radiation and Environmental Biophysics 11(1): 41-52; https://doi.org/10.1007/Bf01323099.

Doswell, C. A., R. Daviesjones & D. L. Keller 1990. On Summary Measures of Skill in Rare Event Forecasting Based on Contingency-Tables. Weather and Forecasting 5(4): 576-585; https://doi.org/10.1175/1520-0434(1990)005<0576:OSMOSI>2.0.CO;2.

Dubbert, M., M. Cuntz, A. Piayda, C. Maguas & C. Werner 2013. Partitioning evapotranspiration - Testing the Craig and Gordon model with field measurements of oxygen isotope ratios of evaporative fluxes. Journal of Hydrology 496: 142-153; https://doi.org/10.1016/j.jhydrol.2013.05.033.

Dubbert, M., A. Piayda, M. Cuntz, A. C. Correia, F. C. E. Silva, J. S. Pereira & C. Werner 2014. Stable oxygen isotope and flux partitioning demonstrates understory of an oak savanna contributes up to half of ecosystem carbon and water exchange. Frontiers in Plant Science 5; https://doi.org/10.3389/fpls.2014.00530.

Dubbert, M., A. Kubert & C. Werner 2017. Impact of Leaf Traitson Temporal Dynamics of Transpired Oxygen Isotope Signatures and Its Impact on Atmospheric Vapor. Frontiers in Plant Science 8; https://doi.org/10.3389/fpls.2017.00005.

Dubbert, M. & C. Werner 2018. Water fluxes mediated by vegetation: emerging isotopic insights at the soil and atmosphere interfaces. New Phytologist; https://doi.org/10.1111/nph.15547.

Eder, F., M. Schmidt, T. Damian, K. Traumner & M. Mauder 2015. Mesoscale Eddies Affect Near-Surface Turbulent Exchange: Evidence from Lidar and Tower Measurements. Journal of Applied Meteorology and Climatology 54(1): 189-206; https://doi.org/10.1175/Jamc-D-14-0140.1.

Evett, S. R., A. W. Warrick & A. D. Matthias 1995. Wall Material and Capping Effects on Microlysimeter Temperatures and Evaporation. Soil Science Society of America Journal 59(2): 329-336; https://doi.org/10.2136/sssaj1995.03615995005900020009x.

Fang, G. & C. A. Ward 1999. Temperature measured close to the interface of an evaporating liquid. Physical Review E 59(1): 417-428; https://doi.org/10.1103/PhysRevE.59.417.

Farquhar, C. C. & J. Lloyd 1993. Carbon and oxygen isotope e}ects in the exchange of carbon dioxide between plants and the atmosphere. Stable Isotopes and Plant Carbon/Water Relationships, Ehleringer JR, Hall AE, Farquhar GD (eds), Academic Press: New York: 47-70.

Farquhar, G. D. & L. A. Cernusak 2005. On the isotopic composition of leaf water in the non-steady state. Functional Plant Biology 32(4): 293-303; https://doi.org/10.1071/Fp04232.

Ferretti, D. F., E. Pendall, J. A. Morgan, J. A. Nelson, D. LeCain & A. R. Mosier 2003. Partitioning evapotranspiration fluxes from a Colorado grassland using stable isotopes: Seasonal variations and ecosystem implications of elevated atmospheric CO2. Plant and Soil 254(2): 291-303; https://doi.org/10.1023/a:1025511618571.

Foken, T., M. Aubinet, J. J. Finnigan, M. Y. Leclerc, M. Mauder & K. T. P. U 2011. Results of a Panel Discussion About the Energy Balance Closure Correction for Trace Gases. Bulletin of the American Meteorological Society 92(4): Es13-Es18; https://doi.org/10.1175/2011bams3130.1.

Gaj, M., M. Beyer, P. Koeniger, H. Wanke, J. Hamutoko & T. Himmelsbach 2016. In situ unsaturated zone water stable isotope (^{2}H and ^{18}O) measurements in semi-arid environments: a soil water balance. Hydrology and Earth System Sciences 20(2): 715-731; https://doi.org/10.5194/hess-20-715-2016.

Gangi, L., Y. Rothfuss, J. Ogee, L. Wingate, H. Vereecken & N. Bruggemann 2015. A New Method for In Situ Measurements of Oxygen Isotopologues of Soil Water and Carbon Dioxide with High Time Resolution. Vadose Zone Journal 14(8); https://doi.org/10.2136/vzj2014.11.0169.

Garvelmann, J., C. Kulls & M. Weiler 2012. A porewater-based stable isotope approach for the investigation of subsurface hydrological processes. Hydrology and Earth System Sciences 16(2): 631-640; https://doi.org/10.5194/hess-16-631-2012.

Gat, J. R. 1971. Comments on Stable Isotope Method in Regional Groundwater Investigattions. Water Resources Research 7(4): 980-993; https://doi.org/10.1029/WR007i004p00980.

Gat, J. R. 1996. Oxygen and hydrogen isotopes in the hydrologic cycle. Annual Review of Earth and Planetary Sciences 24: 225-262; https://doi.org/10.1146/annurev.earth.24.1.225.

Gee, G. W., M. D. Campbell, G. S. Campbell & J. H. Campbell 1992. Rapid Measurement of Low Soil-Water Potentials Using a Water Activity Meter. Soil Science Society of America Journal 56(4): 1068-1070; https://doi.org/10.2136/sssaj1992.03615995005600040010x.

Gonfiantini, R. 1978. Standards for Stable Isotope Measurements in Natural Compounds. Nature 271(5645): 534-536; https://doi.org/10.1038/271534a0.

Good, S. P., K. Soderberg, L. X. Wang & K. K. Caylor 2012. Uncertainties in the assessment of the isotopic composition of surface fluxes: A direct comparison of techniques using laser-based water vapor isotope analyzers. Journal of Geophysical Research-Atmospheres 117; https://doi.org/10.1029/2011jd017168.

Good, S. P., K. Soderberg, K. Y. Guan, E. G. King, T. M. Scanlon & K. K. Caylor 2014. $\delta^{2}H$ isotopic flux partitioning of evapotranspiration over a grass field following a water pulse and subsequent dry down. Water Resources Research 50(2): 1410-1432; https://doi.org/10.1002/2013wr014333.

Good, S. P., D. Noone & G. Bowen 2015. Hydrologic connectivity constrains partitioning of global terrestrial water fluxes. Science 349(6244): 175-177; https://doi.org/10.1126/science.aaa5931.

Granier, A. 1987. Evaluation of Transpiration in a Douglas-Fir Stand by Means of Sap Flow Measurements. Tree Physiology 3(4): 309-319; https://doi.org/DOI 10.1093/treephys/3.4.309.

Griffis, T. J., S. D. Sargent, X. Lee, J. M. Baker, J. Greene, M. Erickson, X. Zhang, K. Billmark, N. Schultz, W. Xiao & N. Hu 2010. Determining the Oxygen Isotope Composition of Evapotranspiration Using Eddy Covariance. Boundary-Layer Meteorology 137(2): 307-326; https://doi.org/10.1007/s10546-010-9529-5.

Hölttä, T., T. Linkosalo, A. Riikonen, S. Sevanto & E. Nikinmaa 2015. An analysis of Granier sap flow method, its sensitivity to heat storage and a new approach to improve its time dynamics. Agricultural and Forest Meteorology 211: 2-12; https://doi.org/10.1016/j.agrformet.2015.05.005.

Horita, J., K. Rozanski & S. Cohen 2008. Isotope effects in the evaporation of water: a status report of the Craig-Gordon model. Isotopes in Environmental and Health Studies 44(1): 23-49; https://doi.org/10.1080/10256010801887174.

Hu, Z. M., X. F. Wen, X. M. Sun, L. H. Li, G. R. Yu, X. H. Lee & S. G. Li 2014. Partitioning of evapotranspiration through oxygen isotopic measurements of water pools and fluxes in a temperate grassland. Journal of Geophysical Research-Biogeosciences 119(3): 358-371; https://doi.org/10.1002/2013jg002367.

Iannone, R. Q., D. Romanini, O. Cattani, H. A. J. Meijer & E. R. T. Kerstel 2010. Water isotope ratio (δ^2H and δ^{18}O) measurements in atmospheric moisture using an optical feedback cavity enhanced absorption laser spectrometer. Journal of Geophysical Research-Atmospheres 115; https://doi.org/10.1029/2009jd012895.

Jasechko, S., Z. D. Sharp, J. J. Gibson, S. J. Birks, Y. Yi & P. J. Fawcett 2013. Terrestrial water fluxes dominated by transpiration. Nature 496(7445): 347-+; https://doi.org/10.1038/nature11983.

Keeling, C. D. 1958. The Concentration and Isotopic Abundances of Atmospheric Carbon Dioxide in Rural Areas. Geochimica Et Cosmochimica Acta 13(4): 322-334; https://doi.org/10.1016/0016-7037(58)90033-4.

Keeling, C. D. 1961. The Concentration and Isotopic Abundances of Carbon Dioxide in Rural and Marine Air. Geochimica Et Cosmochimica Acta 24(3-4): 277-298; https://doi.org/Doi 10.1016/0016-7037(61)90023-0.

Kelliher, F. M., B. M. M. Kostner, D. Y. Hollinger, J. N. Byers, J. E. Hunt, T. M. Mcseveny, R. Meserth, P. L. Weir & E. D. Schulze 1992. Evaporation, Xylem Sap Flow, and Tree Transpiration in a New-Zealand Broad-Leaved Forest. Agricultural and Forest Meteorology 62(1-2): 53-73; https://doi.org/10.1016/0168-1923(92)90005-O.

Klosterhalfen, A., A. F. Moene, M. Schmidt, T. M. Scanlon, H. Vereecken & A. Graf 2019. Sensitivity analysis of a source partitioning method for H2O and CO2 fluxes based on high frequency eddy covariance data: Findings from field data and large eddy simulations. Agricultural and Forest Meteorology 265: 152-170; https://doi.org/https://doi.org/10.1016/j.agrformet.2018.11.003.

Kool, D., N. Agam, N. Lazarovitch, J. L. Heitman, T. J. Sauer & A. Ben-Gal 2014. A review of approaches for evapotranspiration partitioning. Agricultural and Forest Meteorology 184: 56-70; https://doi.org/10.1016/j.agrformet.2013.09.003.

Kormann, R. & F. X. Meixner 2001. An analytical footprint model for non-neutral stratification. Boundary-Layer Meteorology 99(2): 207-224; https://doi.org/Doi 10.1023/A:1018991015119.

Lee, D., J. Kim, K. S. Lee & S. Kim 2010. Partitioning of catchment water budget and its implications for ecosystem carbon exchange. Biogeosciences 7(6): 1903-1914; https://doi.org/10.5194/bg-7-1903-2010.

Lee, X., K. Kim & R. Smith 2007. Temporal variations of the (18)O/(16)O signal of the whole-canopy transpiration in a temperate forest. Global Biogeochemical Cycles 21(3); https://doi.org/10.1029/2006gb002871.

Lin, Y. & J. Horita 2016. An experimental study on isotope fractionation in a mesoporous silica-water system with implications for vadose-zone hydrology. Geochimica Et Cosmochimica Acta 184: 257-271; https://doi.org/10.1016/j.gca.2016.04.029.

Lu, X. F., L. Y. L. Liang, L. X. Wang, G. D. Jenerette, M. F. McCabe & D. A. Grantz 2017. Partitioning of evapotranspiration using a stable isotope technique in an arid and high temperature agricultural production system. Agricultural Water Management 179: 103-109; https://doi.org/10.1016/j.agwat.2016.08.012.

Luz, B., E. Barkan, R. Yam & A. Shemesh 2009. Fractionation of oxygen and hydrogen isotopes in evaporating water. Geochimica Et Cosmochimica Acta 73(22): 6697-6703; https://doi.org/10.1016/j.gca.2009.08.008.

Majoube, M. 1971. Oxygen-18 and Deuterium Fractionation between Water and Steam. Journal De Chimie Physique Et De Physico-Chimie Biologique 68(10): 1423-+; https://doi.org/10.1051/jcp/1971681423.

Martin-Gomez, P., L. Serrano & J. P. Ferrio 2017. Short-term dynamics of evaporative enrichment of xylem water in woody stems: implications for ecohydrology. Tree Physiology 37(4): 511-522; https://doi.org/10.1093/treephys/tpw115.

Mathieu, R. & T. Bariac 1996. A numerical model for the simulation of stable isotope profiles in drying soils. Journal of Geophysical Research-Atmospheres 101(D7): 12685-12696; https://doi.org/10.1029/96jd00223.

Mauder, M., M. Cuntz, C. Drue, A. Graf, C. Rebmann, H. P. Schmid, M. Schmidt & R. Steinbrecher 2013. A strategy for quality and uncertainty assessment of long-term eddy-covariance measurements. Agricultural and Forest Meteorology 169: 122-135; https://doi.org/10.1016/j.agrformet.2012.09.006.

Merlivat, L. 1978. Molecular diffusivities of $H_2{}^{16}O$, $HD^{16}O$, and $H_2{}^{18}O$ in gases. Journal of Chemical Physics 69(6): 2864-2871; https://doi.org/10.1063/1.436884.

Merlivat, L. & J. Jouzel 1979. Global Climatic Interpretation of the Deuterium-Oxygen-18 Relationship for Precipitation. Journal of Geophysical Research-Oceans 84(Nc8): 5029-5033; https://doi.org/10.1029/JC084iC08p05029.

Mualem, Y. 1976. New Model for Predicting Hydraulic Conductivity of Unsaturated Porous-Media. Water Resources Research 12(3): 513-522; https://doi.org/DOI 10.1029/WR012i003p00513.

Ney, P. & A. Graf 2018. High-Resolution Vertical Profile Measurements for Carbon Dioxide and Water Vapour Concentrations Within and Above Crop Canopies. Boundary layer meteorology 166(3): 449–473; https://doi.org/10.1007/s10546-017-0316-4.

Noone, D., C. Risi, A. Bailey, M. Berkelhammer, D. P. Brown, N. Buenning, S. Gregory, J. Nusbaumer, D. Schneider, J. Sykes, B. Vanderwende, J. Wong, Y. Meillier & D. Wolfe 2013. Determining water sources in the boundary layer from tall tower profiles of water vapor and surface water isotope ratios after a snowstorm in Colorado. Atmospheric Chemistry and Physics 13(3): 1607-1623; https://doi.org/10.5194/acp-13-1607-2013.

Oerter, E. J., A. Perelet, E. Pardyjak & G. Bowen 2017. Membrane inlet laser spectroscopy to measure H and O stable isotope compositions of soil and sediment pore water with high sample throughput. Rapid Communications in Mass Spectrometry 31(1): 75-84; https://doi.org/10.1002/rcm.7768.

Orlowski, N., H.-G. Frede, N. Brüggemann & L. Breuer 2013. Validation and application of a cryogenic vacuum extraction system for soil and plant water extraction for isotope analysis. Journal of Sensors and Sensor Systems 2: 179-193; https://doi.org/10.5194/jsss-2-179-2013.

Orlowski, N., D. L. Pratt & J. J. McDonnell 2016a. Intercomparison of soil pore water extraction methods for stable isotope analysis. Hydrological Processes 30(19): 3434-3449; https://doi.org/10.1002/hyp.10870.

Orlowski, N., L. Breuer & J. J. McDonnell 2016b. Critical issues with cryogenic extraction of soil water for stable isotope analysis. Ecohydrology 9(1): 3-10; https://doi.org/10.1002/eco.1722.

Orlowski, N., L. Breuer, N. Angeli, P. Boeckx, C. Brumbt, C. S. Cook, M. Dubbert, J. Dyckmans, B. Gallagher, B. Gralher, B. Herbstritt, P. Herve-Fernandez, C. Hissler, P. Koeniger, A. Legout, C. J. Macdonald, C. Oyarzun, R. Redelstein, C. Seidler, R. Siegwolf, C. Stumpp, S. Thomsen, M. Weiler, C. Werner & J. J. McDonnell 2018. Inter-laboratory comparison of cryogenic water extraction systems for stable isotope analysis of soil water. Hydrology and Earth System Sciences 22(7): 3619-3637; https://doi.org/10.5194/hess-22-3619-2018.

Piayda, A., M. Dubbert, R. Siegwolf, M. Cuntz & C. Werner 2017. Quantification of dynamic soil-vegetation feedbacks following an isotopically labelled precipitation pulse. Biogeosciences 14(9): 2293-2306; https://doi.org/10.5194/bg-14-2293-2017.

Quade, M., N. Brüggemann, A. Graf, J. Vanderborght, H. Vereecken & Y. Rothfuss 2018. Investigation of Kinetic Isotopic Fractionation of Water During Bare Soil Evaporation. Water Resources Research 54; https://doi.org/10.1029/2018WR023159.

Raz-Yaseef, N., E. Rotenberg & D. Yakir 2010. Effects of spatial variations in soil evaporation caused by tree shading on water flux partitioning in a semi-arid pine forest. Agricultural and Forest Meteorology 150(3): 454-462; https://doi.org/10.1016/j.agrformet.2010.01.010.

Rothfuss, Y., P. Biron, I. Braud, L. Canale, J. L. Durand, J. P. Gaudet, P. Richard, M. Vauclin & T. Bariac 2010. Partitioning evapotranspiration fluxes into soil evaporation and plant transpiration using water stable isotopes under controlled conditions. Hydrological Processes 24(22): 3177-3194; https://doi.org/10.1002/hyp.7743.

Rothfuss, Y., I. Braud, N. Le Moine, P. Biron, J. L. Durand, M. Vauclin & T. Bariac 2012. Factors controlling the isotopic partitioning between soil evaporation and plant transpiration: Assessment using a multi-objective calibration of SiSPAT-Isotope under controlled conditions. Journal of Hydrology 442: 75-88; https://doi.org/10.1016/j.jhydrol.2012.03.041.

Rothfuss, Y., H. Vereecken & N. Bruggemann 2013. Monitoring water stable isotopic composition in soils using gas-permeable tubing and infrared laser absorption spectroscopy. Water Resources Research 49(6): 3747-3755; https://doi.org/10.1002/wrcr.20311.

Rothfuss, Y., S. Merz, J. Vanderborght, N. Hermes, A. Weuthen, A. Pohlmeier, H. Vereecken & N. Bruggemann 2015. Long-term and high-frequency non-destructive monitoring of water stable isotope profiles in an evaporating soil column. Hydrology and Earth System Sciences 19(10): 4067-4080; https://doi.org/10.5194/hess-19-4067-2015.

Rozanski, K., L. Araguás-Araguás & R. Gonfiantini 1993. Isotopic patterns in modern global precipitation. Climate Change in Continental Isotopic Records, Geophys. Monog. Ser., edited by P. K. Swart et al.: 1-36, AGU, Washington, D. C.

Scanlon, T. M. & W. P. Kustas 2010. Partitioning carbon dioxide and water vapor fluxes using correlation analysis. Agricultural and Forest Meteorology 150(1): 89-99; https://doi.org/10.1016/j.agrformet.2009.09.005.

Schmidt, M., K. Maseyk, C. Lett, P. Biron, P. Richard, T. Bariac & U. Seibt 2010. Concentration effects on laser-based del O-18 and del H-2 measurements and implications for the calibration of vapour measurements with liquid standards. Rapid Communications in Mass Spectrometry 24(24): 3553-3561; https://doi.org/10.1002/rcm.4813.

Shawcroft, R. W. & H. R. Gardner 1983. Direct Evaporation from Soil under a Row Crop Canopy. Agricultural Meteorology 28(3): 229-238; https://doi.org/10.1016/0002-1571(83)90028-6.

Simonin, K. A., A. B. Roddy, P. Link, R. Apodaca, K. P. Tu, J. Hu, T. E. Dawson & M. M. Barbour 2013. Isotopic composition of transpiration and rates of change in leaf water isotopologue storage in response to environmental variables. Plant, Cell & Enviroment 36: 2190-2206; https://doi.org/10.1111/pce.12129.

Soderberg, K., S. P. Good, L. X. Wang & K. Caylor 2012. Stable Isotopes of Water Vapor in the Vadose Zone: A Review of Measurement and Modeling Techniques. Vadose Zone Journal 11(3); https://doi.org/10.2136/vzj2011.0165.

Song, X., K. E. Loucos, K. A. Simonin, G. D. Farquhar & M. M. Barbour 2015. Measurements of transpiration isotopologues and leaf water to assess enrichment models in cotton. New Phytologist; https://doi.org/10.1111/nph.13296.

Sprenger, M., H. Leistert, K. Gimbel & M. Weiler 2016. Illuminating hydrological processes at the soil-vegetation-atmosphere interface with water stable isotopes. Reviews of Geophysics 54(3): 674-704; https://doi.org/10.1002/2015rg000515.

Sun, S., P. Meng, J. Zhang, X. Wan, N. Zheng & C. He 2014. Partitioning oak woodland evapotranspiration in the rocky mountainous area of North China was disturbed by foreign vapor, as estimated based on non-steady-state O-18 isotopic composition. Agricultural and Forest Meteorology 184: 36-47; https://doi.org/10.1016/j.agrformet.2013.08.006.

Sutanto, S. J., J. Wenninger, A. M. J. Coenders-Gerrits & S. Uhlenbrook 2012. Partitioning of evaporation into transpiration, soil evaporation and interception: A comparison between isotope measurements and a HYDRUS-1D model (vol 16, pg 2605, 2012). Hydrology and Earth System Sciences 16(9): 3261-3261; https://doi.org/10.5194/hess-16-3261-2012.

Sutanto, S. J., B. van den Hurk, P. A. Dirmeyer, S. I. Seneviratne, T. Rockmann, K. E. Trenberth, E. M. Blyth, J. Wenninger & G. Hoffmann 2014. HESS Opinions "A perspective on isotope versus non-isotope approaches to determine the contribution of transpiration to total

evaporation". Hydrology and Earth System Sciences 18(8): 2815-2827; https://doi.org/10.5194/hess-18-2815-2014.
Sverdrup, H. 1952. Evaporation from the Oceans. Compendium of Meteorology, American Meteorological Society, Boston: 1071-1081.
van Genuchten, M. T. 1980. A Closed-form Equation for Predicting the Hydraulic Conductivity of Unsaturated Soils. Soil Science Society of America Journal 44: 892-898; https://doi.org/10.2136/sssaj1980.03615995004400050002x.
Volkmann, T. H. M. & M. Weiler 2014. Continual in situ monitoring of pore water stable isotopes in the subsurface. Hydrology and Earth System Sciences 18(5): 1819-1833; https://doi.org/10.5194/hess-18-1819-2014.
Volkmann, T. H. M., K. Kuhnhammer, B. Herbstritt, A. Gessler & M. Weiler 2016. A method for in situ monitoring of the isotope composition of tree xylem water using laser spectroscopy. Plant Cell and Environment 39(9): 2055-2063; https://doi.org/10.1111/pce.12725.
Walker, C. D. & J. P. Brunel 1990. Examining Evapotranspiration in a Semiarid Region Using Stable Isotopes of Hydrogen and Oxygen. Journal of Hydrology 118(1-4): 55-75; https://doi.org/10.1016/0022-1694(90)90250-2.
Wang, L. X., K. K. Caylor, J. C. Villegas, G. A. Barron-Gafford, D. D. Breshears & T. E. Huxman 2010. Partitioning evapotranspiration across gradients of woody plant cover: Assessment of a stable isotope technique. Geophysical Research Letters 37; https://doi.org/10.1029/2010gl043228.
Wang, L. X., S. L. Niu, S. P. Good, K. Soderberg, M. F. McCabe, R. A. Sherry, Y. Q. Luo, X. H. Zhou, J. Y. Xia & K. K. Caylor 2013. The effect of warming on grassland evapotranspiration partitioning using laser-based isotope monitoring techniques. Geochimica Et Cosmochimica Acta 111: 28-38; https://doi.org/10.1016/j.gca.2012.12.047.
Wang, P., T. Yamanaka, X.-Y. Li & Z. Wei 2015. Partitioning evapotranspiration in a temperate grassland ecosystem: Numerical modeling with isotopic tracers. Agricultural and Forest Meteorology 208: 16-31; https://doi.org/10.1016/j.agrformet.2015.04.006.
Wang, P., X. Y. Li, Y. M. Huang, S. M. Liu, Z. W. Xu, X. C. Wu & Y. J. Ma 2016. Numerical modeling the isotopic composition of evapotranspiration in an arid artificial oasis cropland ecosystem with high-frequency water vapor isotope measurement. Agricultural and Forest Meteorology 230: 79-88; https://doi.org/10.1016/j.agrformet.2015.12.063.
Wang, X. F. & D. Yakir 2000. Using stable isotopes of water in evapotranspiration studies. Hydrological Processes 14(8): 1407-1421; https://doi.org/10.1002/1099-1085(20000615).
Wassenaar, L. I., M. J. Hendry, V. L. Chostner & G. P. Lis 2008. High Resolution Pore Water delta H-2 and delta O-18 Measurements by H2O(liquid)-H2O(vapor) Equilibration Laser Spectroscopy. Environmental Science & Technology 42(24): 9262-9267; https://doi.org/10.1021/es802065s.
Wei, Z., K. Yoshimura, A. Okazaki, W. Kim, Z. Liu & M. Yokoi 2015. Partitioning of evapotranspiration using high-frequency water vapor isotopic measurement over a rice paddy field. Water Resources Research 51(5): 3716-3729; https://doi.org/10.1002/2014wr016737.
Wei, Z. W., K. Yoshimura, A. Okazaki, W. Kim, Z. F. Liu & M. Yokoi 2015. Partitioning of evapotranspiration using high-frequency water vapor isotopic measurement over a rice paddy field. Water Resources Research 51(5): 3716-3729; https://doi.org/10.1002/2014wr016737.
Wei, Z. W., K. Yoshimura, L. X. Wang, D. G. Miralles, S. Jasechko & X. H. Lee 2017. Revisiting the contribution of transpiration to global terrestrial evapotranspiration. Geophysical Research Letters 44(6): 2792-2801; https://doi.org/10.1002/2016gl072235.
Wei, Z. W., X. H. Lee, X. F. Wen & W. Xiao 2018. Evapotranspiration partitioning for three agro-ecosystems with contrasting moisture conditions: a comparison of an isotope method and a two-source model calculation. Agricultural and Forest Meteorology 252: 296-310; https://doi.org/10.1016/j.agrformet.2018.01.019.

Wen, X. F., B. Yang, X. M. Sun & X. Lee 2016. Evapotranspiration partitioning through in-situ oxygen isotope measurements in an oasis cropland. Agricultural and Forest Meteorology 230: 89-96; https://doi.org/10.1016/j.agrformet.2015.12.003.

Wenninger, J., D. T. Beza & S. Uhlenbrook 2010. Experimental investigations of water fluxes within the soil-vegetation-atmosphere system: Stable isotope mass-balance approach to partition evaporation and transpiration. Physics and Chemistry of the Earth 35(13-14): 565-570; https://doi.org/10.1016/j.pce.2010.07.016.

Williams, D. G., W. Cable, K. Hultine, J. C. B. Hoedjes, E. A. Yepez, V. Simonneaux, S. Er-Raki, G. Boulet, H. A. R. de Bruin, A. Chehbouni, O. K. Hartogensis & F. Timouk 2004. Evapotranspiration components determined by stable isotope, sap flow and eddy covariance techniques. Agricultural and Forest Meteorology 125(3-4): 241-258; https://doi.org/10.1016/j.agrformet.2004.04.008.

Wu, Y. J., T. S. Du, R. S. Ding, L. Tong, S. E. Li & L. X. Wang 2017. Multiple Methods to Partition Evapotranspiration in a Maize Field. Journal of Hydrometeorology 18(1): 139-149; https://doi.org/10.1175/Jhm-D-16-0138.1.

Xiao, W., X. H. Lee, Y. B. Hu, S. D. Liu, W. Wang, X. F. Wen, M. Werner & C. Y. Xie 2017. An Experimental Investigation of Kinetic Fractionation of Open-Water Evaporation Over a Large Lake. Journal of Geophysical Research-Atmospheres 122(21): 11651-11663; https://doi.org/10.1002/2017jd026774.

Xiao, W., W. Zhongwang & X. Wen 2018. Evapotranspiration partitioning at the ecosystem scale using the stable isotope method—A review. Agricultural and Forest Meteorology 263: 346-361; https://doi.org/10.1016/j.agrformet.2018.09.005.

Xu, Z., H. Yang, F. Liu, S. An, J. Cui, Z. Wang & S. Liu 2008. Partitioning evapotranspiration flux components in a subalpine shrubland based on stable isotopic measurements. Botanical Studies 49(4): 351-361.

Xu, Z., H. B. Yang, F. D. Liu, S. Q. An, J. Cui, Z. S. Wang & S. R. Liu 2008. Partitioning evapotranspiration flux components in a subalpine shrubland based on stable isotopic measurements. Botanical Studies 49(4): 351-361; https://doi.org/10.5194/hess-16-2605-2012.

Yakir, D. & X. F. Wang 1996. Fluxes of CO2 and water between terrestrial vegetation and the atmosphere estimated from isotope measurements. Nature 380(6574): 515-517; https://doi.org/DOI 10.1038/380515a0.

Yakir, D. & L. D. L. Sternberg 2000. The use of stable isotopes to study ecosystem gas exchange. Oecologia 123(3): 297-311; https://doi.org/10.1007/s004420051016.

Yaseef, N. R., D. Yakir, E. Rotenberg, G. Schiller & S. Cohen 2010. Ecohydrology of a semi-arid forest: partitioning among water balance components and its implications for predicted precipitation changes. Ecohydrology 3(2): 143-154; https://doi.org/10.1002/eco.65.

Yepez, E. A., D. G. Williams, R. L. Scott & G. H. Lin 2003. Partitioning overstory and understory evapotranspiration in a semiarid savanna woodland from the isotopic composition of water vapor. Agricultural and Forest Meteorology 119(1-2): 53-68; https://doi.org/10.1016/s0168-1923(03)00116-3.

Yepez, E. A., T. E. Huxman, D. D. Ignace, N. B. English, J. F. Weltzin, A. E. Castellanos & D. G. Williams 2005. Dynamics of transpiration and evaporation following a moisture pulse in semiarid grassland: A chamber-based isotope method for partitioning flux components. Agricultural and Forest Meteorology 132(3-4): 359-376; https://doi.org/10.1016/j.agrformet.2005.09.006.

Zhang, Y. C., Y. J. Shen, H. Y. Sun & J. B. Gates 2011. Evapotranspiration and its partitioning in an irrigated winter wheat field: A combined isotopic and micrometeorologic approach. Journal of Hydrology 408(3-4): 203-211; https://doi.org/10.1016/j.jhydrol.2011.07.036.

Zhou, S., B. F. Yu, Y. Zhang, Y. F. Huang & G. Q. Wang 2018. Water use efficiency and evapotranspiration partitioning for three typical ecosystems in the Heihe River Basin, northwestern China. Agricultural and Forest Meteorology 253: 261-273; https://doi.org/10.1016/j.agrformet.2018.02.002.

Schriften des Forschungszentrums Jülich
Reihe Energie & Umwelt / Energy & Environment

Band / Volume 455
Entwicklung von thermischen Spritzprozessen für fortschrittliche Schutz- und Funktionsschichten
G. Mauer (2019), vi, 57 pp
ISBN: 978-3-95806-388-4

Band / Volume 456
Columnar Structured Thermal Barrier Coatings Deposited by Axial Suspension Plasma Spraying
D. Zhou (2019), VI, 126 pp
ISBN: 978-3-95806-391-4

Band / Volume 457
Modellierung zeitlich aufgelöster Ladeenergienachfragen von batterie-elektrischen Fahrzeugen und deren Abbildung in einem Energiesystemmodell
J. F. Linßen (2019), VIII, 189 pp
ISBN: 978-3-95806-395-2

Band / Volume 458
Synthesis and Analysis of Spinel Cathode Materials for High Voltage Solid-State Lithium Batteries
A. Windmüller (2019), iv, 142 pp
ISBN: 978-3-95806-396-9

Band / Volume 459
Monazite-type ceramics as nuclear waste form: Crystal structure, microstructure and properties
Y. Arinicheva (2019), 194 pp
ISBN: 978-3-95806-397-6

Band / Volume 460
Coupling a Solid Oxide Fuel Cell with a Biomass Gasifier: Degradation Mechanisms and Alternative Anode Materials
H. Jeong (2019), II, 112 pp
ISBN: 978-3-95806-398-3

Band / Volume 461
Model-based Source Partitioning of Eddy Covariance Flux Measurements
A. Klosterhalfen (2019), XVI, 132 pp
ISBN: 978-3-95806-401-0

Band / Volume 462
Entwicklung von großflächigen PECVD-Prozessen zur kontrollierten, homogenen Abscheidung dünner Siliziumschichten für die Photovoltaik
B. O. Grootoonk (2019), 154 pp
ISBN: 978-3-95806-402-7

Schriften des Forschungszentrums Jülich
Reihe Energie & Umwelt / Energy & Environment

Band / Volume 463
Simulation of Transport Processes through an Asymmetric Gas Separation Membrane
U. V. Unije (2019), xiv, 101 pp
ISBN: 978-3-95806-403-4

Band / Volume 464
Development, calibration and deployment of an airborne chemical ionization mass spectrometer for trace gas measurements
T. Khattatov (2019), 14, 125 pp
ISBN: 978-3-95806-404-1

Band / Volume 465
IEK-3 Report 2019 – Maßgeschneiderte Energieumwandlung für nachhaltige Kraftstoffe
D. Stolten, B. Emonts (Eds.) (2019), 171 pp
ISBN: 978-3-95806-410-2

Band / Volume 466
Initialinfrastruktur für Wasserstoffmobilität auf Basis von Flotten
F. Grüger (2019), V, 209 pp
ISBN: 978-3-95806-413-3

Band / Volume 467
Techno-ökonomische Analyse alternativer Wasserstoffinfrastruktur
M. E. Reuß (2019), 205 pp
ISBN: 978-3-95806-414-0

Band / Volume 468
Study on a miniaturized satellite payload for atmospheric temperature measurements
J. Liu (2019), 153 pp
ISBN: 978-3-95806-415-7

Band / Volume 469
Partitioning Water Vapor Fluxes by the Use of Their Water Stable Isotopologues: From the Lab to the Field
M. E. Quade (2019), XVI, 113 pp
ISBN: 978-3-95806-417-1

Weitere ***Schriften des Verlags im Forschungszentrum Jülich*** unter
http://wwwzb1.fz-juelich.de/verlagextern1/index.asp

Energie & Umwelt / Energy & Environment
Band / Volume 469
ISBN 978-3-95806-417-1

Mitglied der Helmholtz-Gemeinschaft

JÜLICH
Forschungszentrum